Alaska Department of Transportation & Public Facilities

Alaska University Transportation Center

Seismic Performance and Design of Bridge Foundations in Liquefiable Ground with a Frozen Crust
Final Report

Prepared By:

Zhaohui "Joey" Yang, Ph.D.

Xiaoyu Zhang

University of Alaska Anchorage, School of Engineering

December 2012

Prepared For:

Alaska University Transportation Center
Duckering Building Room 245
P.O. Box 755900
Fairbanks, AK 99775-5900

Alaska Department of Transportation
Research, Development, and Technology Transfer
2301 Peger Road
Fairbanks, AK 99709-5399

INE/AUTC 12.33

FHWA-AK-RD-12-19

REPORT DOCUMENTATION PAGE

Form approved OMB No.

1. AGENCY USE ONLY (LEAVE BLANK)	2. REPORT DATE	3. REPORT TYPE AND DATES COVERED
FHWA-AK-RD-12-19	December 2012	Final Report (08/01/2010-12/31/2012)

4. TITLE AND SUBTITLE

Seismic Performance and Design of Bridge Foundations in Liquefiable Ground with a Frozen Crust

5. FUNDING NUMBERS

AUTC#309010/410015
DTRT06-G-0011
T2-09-01/ T2-10-09

6. AUTHOR(S)
Zhaohui "Joey" Yang, Ph.D.
Xiaoyu Zhang

7. PERFORMING ORGANIZATION NAME(S) AND ADDRESS(ES)
Alaska University Transportation Center
P.O. Box 755900, Fairbanks, AK 99775-5900

8. PERFORMING ORGANIZATION REPORT NUMBER

INE/AUTC 12.33

9. SPONSORING/MONITORING AGENCY NAME(S) AND ADDRESS(ES)
Research and Innovative Technology Administration (RITA), U.S. Department of Transportation (USDOT)
1200 New Jersey Avenue, SE, Washington, DC 20590
Alaska Department of Transportation, Research, Development, and Technology Transfer
2301 Peger Road,Fairbanks, AK 99709-5399

10. SPONSORING/MONITORING AGENCY REPORT NUMBER

FHWA-AK-RD-12-19

11. SUPPLENMENTARY NOTES

12a. DISTRIBUTION / AVAILABILITY STATEMENT

No restrictions

12b. DISTRIBUTION CODE

13. ABSTRACT (Maximum 200 words)

Two major earthquakes in Alaska, namely 1964 Great Alaskan earthquake and 2002 Denali earthquake, occurred in winter season when the ground crust was frozen. None of the then-existing foundation types was able to withstand the force from the frozen crust overlying liquefied soils. This project aims to study how the frozen ground crust affects the performance of bridge pile foundations and how one can estimate the loads imposed by the frozen ground crust. A shake table experiment was conducted to gain in-depth understanding of the mechanism of frozen ground crust-pile foundation interaction and collect data to validate a solid-fluid coupled finite element (FE) model and a simplified method, i.e. the beam-on-nonlinear-Winkler-foundation (BNWF) or p-y approach. Loads imposed on pile foundations by the frozen crust were studied through solid-fluid coupled FE analyses of a typical Alaskan bridge foundation under two soil conditions–one with an unfrozen crust and the other with a frozen crust–and by comparison of results obtained from these two cases. The effectiveness of the p-y approach in predicting the response of piles subject to frozen ground lateral spreading in liquefiable soils was evaluated by comparing the analyses of results with those obtained from the FE modeling. Finally, guidelines were proposed for design practitioners to analyze the performance of pile foundations embedded in liquefiable soils subject to frozen ground crust lateral spreading with the p-y approach.

14- KEYWORDS: Earthquake engineering (Ttkfre), Foundation engineering (Ttkfh), Bridge foundations (Pdybbff)

15. NUMBER OF PAGES

138

16. PRICE CODE

N/A

17. SECURITY CLASSIFICATION OF REPORT	18. SECURITY CLASSIFICATION OF THIS PAGE	19. SECURITY CLASSIFICATION OF ABSTRACT	20. LIMITATION OF ABSTRACT
Unclassified	Unclassified	Unclassified	N/A

Notice

This document is disseminated under the sponsorship of the U.S. Department of Transportation in the interest of information exchange. The U.S. Government assumes no liability for the use of the information contained in this document.

The U.S. Government does not endorse products or manufacturers. Trademarks or manufacturers' names appear in this report only because they are considered essential to the objective of the document.

Quality Assurance Statement

The Federal Highway Administration (FHWA) provides high-quality information to serve Government, industry, and the public in a manner that promotes public understanding. Standards and policies are used to ensure and maximize the quality, objectivity, utility, and integrity of its information. FHWA periodically reviews quality issues and adjusts its programs and processes to ensure continuous quality improvement.

Author's Disclaimer

Opinions and conclusions expressed or implied in the report are those of the author. They are not necessarily those of the Alaska DOT&PF or funding agencies.

SI* (MODERN METRIC) CONVERSION FACTORS

APPROXIMATE CONVERSIONS TO SI UNITS

Symbol	When You Know	Multiply By	To Find	Symbol
		LENGTH		
in	inches	25.4	millimeters	mm
ft	feet	0.305	meters	m
yd	yards	0.914	meters	m
mi	miles	1.61	kilometers	km
		AREA		
in^2	square inches	645.2	square millimeters	mm^2
ft^2	square feet	0.093	square meters	m^2
yd^2	square yard	0.836	square meters	m^2
ac	acres	0.405	hectares	ha
mi^2	square miles	2.59	square kilometers	km^2
		VOLUME		
fl oz	fluid ounces	29.57	milliliters	mL
gal	gallons	3.785	liters	L
ft^3	cubic feet	0.028	cubic meters	m^3
yd^3	cubic yards	0.765	cubic meters	m^3
		NOTE: volumes greater than 1000 L shall be shown in m^3		
		MASS		
oz	ounces	28.35	grams	g
lb	pounds	0.454	kilograms	kg
T	short tons (2000 lb)	0.907	megagrams (or "metric ton")	Mg (or "t")
		TEMPERATURE (exact degrees)		
^oF	Fahrenheit	5 (F-32)/9 or (F-32)/1.8	Celsius	^oC
		ILLUMINATION		
fc	foot-candles	10.76	lux	lx
fl	foot-Lamberts	3.426	$candela/m^2$	cd/m^2
		FORCE and PRESSURE or STRESS		
lbf	poundforce	4.45	newtons	N
lbf/in^2	poundforce per square inch	6.89	kilopascals	kPa

APPROXIMATE CONVERSIONS FROM SI UNITS

Symbol	When You Know	Multiply By	To Find	Symbol
		LENGTH		
mm	millimeters	0.039	inches	in
m	meters	3.28	feet	ft
m	meters	1.09	yards	yd
km	kilometers	0.621	miles	mi
		AREA		
mm^2	square millimeters	0.0016	square inches	in^2
m^2	square meters	10.764	square feet	ft^2
m^2	square meters	1.195	square yards	yd^2
ha	hectares	2.47	acres	ac
km^2	square kilometers	0.386	square miles	mi^2
		VOLUME		
mL	milliliters	0.034	fluid ounces	fl oz
L	liters	0.264	gallons	gal
m^3	cubic meters	35.314	cubic feet	ft^3
m^3	cubic meters	1.307	cubic yards	yd^3
		MASS		
g	grams	0.035	ounces	oz
kg	kilograms	2.202	pounds	lb
Mg (or "t")	megagrams (or "metric ton")	1.103	short tons (2000 lb)	T
		TEMPERATURE (exact degrees)		
^oC	Celsius	1.8C+32	Fahrenheit	^oF
		ILLUMINATION		
lx	lux	0.0929	foot-candles	fc
cd/m^2	$candela/m^2$	0.2919	foot-Lamberts	fl
		FORCE and PRESSURE or STRESS		
N	newtons	0.225	poundforce	lbf
kPa	kilopascals	0.145	poundforce per square inch	lbf/in^2

*SI is the symbol for the International System of Units. Appropriate rounding should be made to comply with Section 4 of ASTM E380.
(Revised March 2003)

Table of Contents

List of Figures

List of Tables

Acknowledgments

The Alaska University Transportation Center (AUTC) and the State of Alaska Department of Transportation and Public Facilities (ADOT&PF) provided financial support for this research under AUTC projects #309010 and #410015.

Dr. Zhaohui (Joey) Yang, Associate Professor of Civil Engineering, University of Alaska Anchorage, was the Principal Investigator. Mr. Xiaoyu Zhang, former graduate student of University of Alaska Anchorage (UAA), was Research Assistant for both projects. Mr. Qiang Li, former graduate student of UAA, currently Ph.D. student at Purdue University, worked on Project #309010. Dr. Runlin Yang, Associate Professor of Civil Engineering, University of Science and Technology Beijing, China, contributed to this study by performing the shake table experiment. The authors are thankful to Dr. Jinchi Lu, Assistant Research Scientist at the University of California, San Diego, who provided technical advice on using OpenSees and OpenSeesPL, and Mr. Elmer E. Marx, Senior Bridge Design Engineer with ADOT&PF, who was actively involved in this study and offered thoughtful technical suggestions.

ABSTRACT

Two major earthquakes in Alaska, namely the 1964 Great Alaska Earthquake and the 2002 Denali earthquake, occurred in winter season when the ground crust was frozen. None of the then-existing foundation types was able to withstand the force from the frozen crust overlying liquefied soils. This project aims to study how a frozen ground crust affects the performance of bridge pile foundations and how to estimate the loads imposed by a laterally spreading frozen ground crust during earthquake-induced liquefaction. A shake table experiment was conducted to gain an in-depth understanding of the mechanism of frozen ground crust-pile foundation interaction, and to collect data to validate a solid-fluid coupled finite element (FE) model and a simplified analysis method, that is, the beam-on-nonlinear-Winkler-foundation (BNWF) or *p-y* approach. Loads imposed on pile foundations by a frozen crust were studied through solid-fluid coupled FE analyses of a typical bridge foundation in Alaska under two soil conditions—one with an unfrozen crust and the other with a frozen crust—and by comparison of results obtained from these two cases. The effectiveness of the *p-y* approach in predicting the response of piles subjected to frozen ground lateral spreading resting on liquefied soils was evaluated by comparing the results obtained from the p-y approach with results from FE model. Finally, guidelines are proposed for design practitioners for performance analysis of pile foundations embedded in liquefiable soils subjected to frozen ground crust lateral spreading with the *p-y* approach.

EXECUTIVE SUMMARY

This study investigates the effect of frozen ground crust on the seismic response of pile foundations in liquefiable soils. A shake table experiment was conducted to gain an in-depth understanding of the impact of frozen ground crust on a model pile. The results were used to validate two numerical approaches: solid-fluid coupled finite element (FE) modeling and the *p-y* approach. Loads imposed on pile foundations by the frozen crust were studied through solid-fluid coupled FE analyses of a typical Alaska bridge foundation. The effectiveness of the *p*-y approach in predicting the response of piles embedded in liquefiable soils subjected to laterally spreading frozen ground was evaluated. The main findings from this project are summarized below:

1. The shake table experiment shows that laterally spreading frozen ground crust forms two plastic hinges on the model pile: one near the frozen crust-loose sand interface and the other within the medium dense sand layer. The plastic hinge at the frozen crust-loose sand interface is formed because of the large distributed load (soil resistance) induced by the frozen ground crust; the plastic hinge in the medium dense sand layer is the direct result of lateral spreading of the ground crust.
2. Two approaches—the solid-fluid coupled FE modeling and the *p-y* approach—were confirmed as being quite effective in predicting the response of piles subjected to frozen ground crust lateral spreading, particularly the formation of plastic hinges.
3. Laterally spreading ground crust forms two plastic hinges on the pile for both frozen (with a frozen active layer) and unfrozen (with an unfrozen active layer) cases: one located near the frozen ground crust-loose sand interface (referred to as the upper plastic hinge) and the other within the medium dense sand layer (referred to as the lower plastic hinge).
4. The plastic deformation and hinge rotation demand are much higher in the frozen case than in the unfrozen case under similar seismic loading conditions.
5. The *p-y* approach is effective in predicting the location and plastic deformation demand at the upper plastic hinge, and the location of the lower plastic hinge. It underestimates the plastic deformation demand in the lower plastic hinge. However, with further study, this could be improved by using a different p-multipliers selection approach.

6. Guidelines are proposed for design practitioners to analyze the response of piles embedded in liquefiable soils subjected to frozen ground crust lateral spreading by the *p-y* approach. This includes how to obtain free-field displacement, select p-multipliers, model the frozen soil resistance, and account for the restraint offered by the superstructure.

CHAPTER 1 INTRODUCTION

1.1 Background

Liquefaction and associated ground failures have occurred during past major earthquakes across the world, including Alaska. A substantial portion of the ground failure and structural damage was a direct result of or related to liquefaction and lateral spreading of the ground crust. Lateral spreading is particularly damaging if a non-liquefiable crust rides on top of the liquefied soil. Moreover, when the ground crust is frozen, its physical properties including stiffness, shear strength, and permeability change by orders of magnitude (Akili 1971; Stevens 1973; Haynes and Karalius 1977; Vinson et al. 1983; Zhu and Carbee 1983; Zhang 2009). What would be the impact on a bridge foundation located in a frozen ground crust resting on a liquefied soil layer? How large are the generated loads when an earthquake occurs in winter and how should these loads be considered by the designer?

Lessons were learned from historical earthquakes in Alaska. In March 1964, Alaska experienced one of the largest earthquakes in recorded history: the Great Alaska Earthquake with a moment magnitude of 9.2. Numerous cases of bridge foundation damage associated with liquefaction-induced lateral spreading were reported in Southcentral Alaska after this earthquake. Ross et al. (1973) reported many observations indicating the liquefaction of cohesionless soils and landslides. The following are a few direct quotations from the authors' report: "'mud' oozing up in cracks"; "road embankment collapsing to the level of flood plain"; "embankment sliding to river centerline" (Figure 1.1); "downstream movement of the footing and upstream tilt of the pier shafts"; and "piers shifting or tilting longitudinally toward the channel centerline" (Figure 1.2). According to the statistical data, none of the then-existing foundation types was able to withstand the lateral forces, including cases where the superstructure had not yet been built (Figure 1.3).

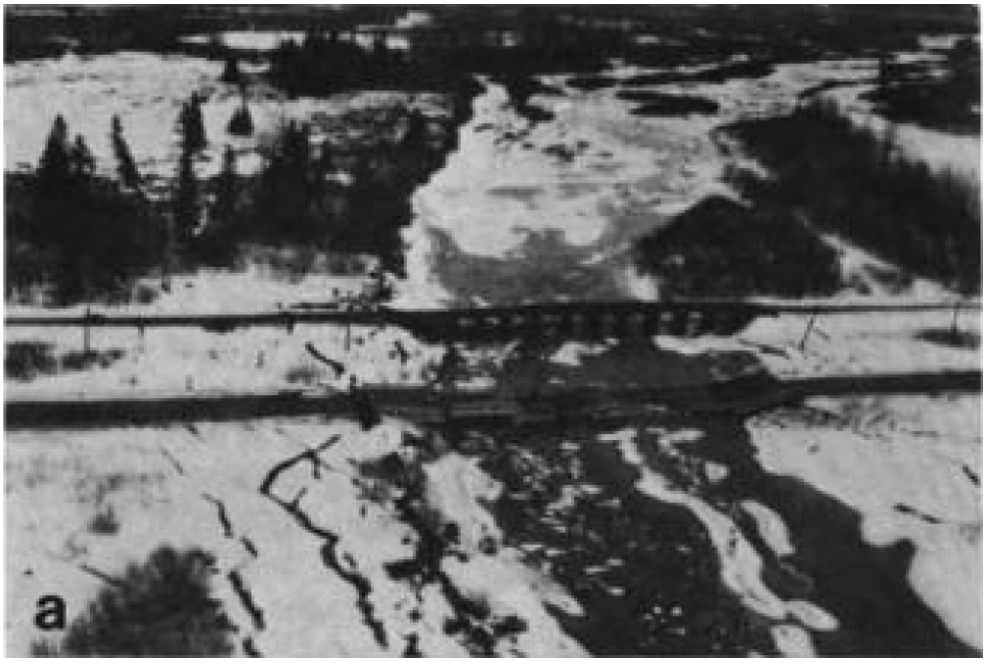

Figure 1.1. Displaced embankment and damaged bridges

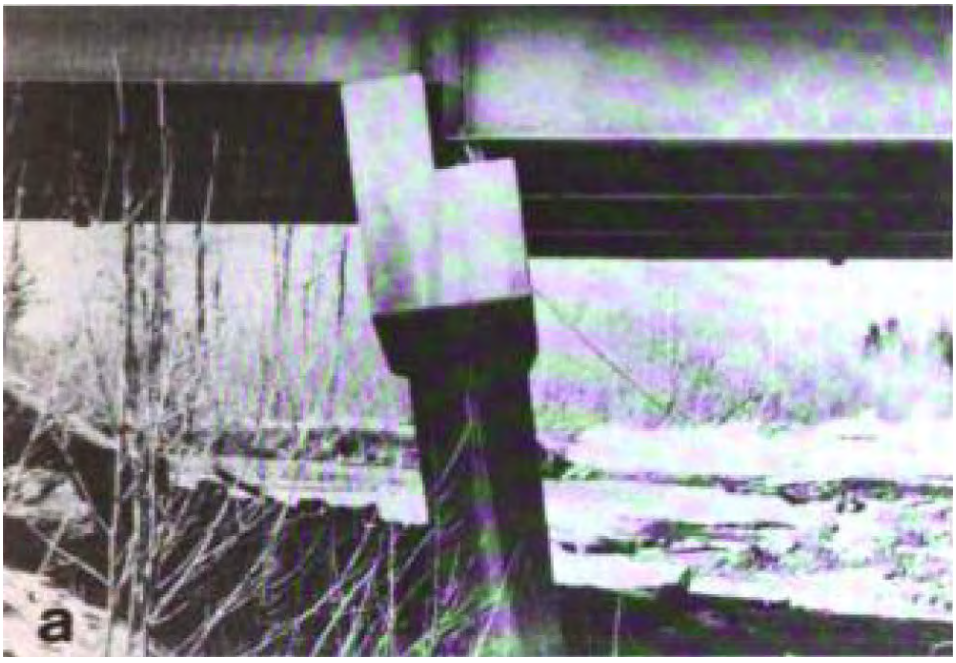

Figure 1.2. Tilted bridge pier due to laterally spreading frozen crust

Figure 1.3. Ground settlement and tilted bridge pier at a bridge construction site

The reason for such huge lateral loads was believed to be the frozen ground crust. A frozen crust overlying liquefiable soils is likely to generate significantly larger loads on foundations due to the distinct characteristics compared with the unfrozen soil. Coincidently, in November 2002, the Denali earthquake struck Interior Alaska, again in wintertime, resulting in extensive liquefaction and lateral spreading, as shown in Figure 1.4 (Shannon and Wilson Inc. 2002). With the past in mind, it is essential to better understand the influence of a frozen crust on soil-pile interaction in liquefiable soils for seismic design of bridge foundations in cold regions.

Figure 1.4. Lateral spreading observed in a bridge site after the 2002 Denali earthquake

1.2 Literature Review

Researchers around the world have studied soil-pile or soil-structure interaction and have used a number of methods in studying these interactions. The methods can be classified into three categories: (1) physical experiment (e.g., Shirato et al. 2008; Ashford et al. 2006; Cubrinovski et al. 2006; Rollins et al. 2005; Armstrong et al. 2008; Horazdovsky 2010); (2) solid-fluid coupled dynamic finite element (FE) modeling (e.g., Yang and Jeremic 2005; Abate et al. 2010; Elgamal et al. 2009; Lam et al. 2009; Cheng and Jeremic 2009; Lu et al. 2011); and (3) simplified analytic method (e.g. Boulanger et al. 1999; Takahashi et al. 2006; Zha 2005; Weaver et al. 2005; Naggar et al. 2005; McGann et al. 2011).

The category of physical experiment can be further classified into single-gravity shake table experiment (1-g test), centrifuge experiment (N-g test), and full-scale experiment. To perform a 1-g test, a scaled soil-foundation system is fixed to a platform and loaded with earthquake excitations. The N-g test overcomes the scaling problem by performing the scaled soil-foundation model test in a centrifuge. Due to the centrifugal force generated by spinning the model, the gravity in the soil-foundation model increases multiple times, and therefore stresses and strains are amplified. A full-scale experiment usually includes installing a full-size foundation and/or structure in the field and loading it by static force or dynamic force generated by blasting or other means.

The FE analysis can explicitly model the bridge superstructure and pile foundation system behavior, including the effects of bridge abutments and liquefaction of soils on the seismic response of the bridge system. In recent years, studies have shown that dynamic FE analysis is capable of better representing certain aspects of pile foundation behavior during earthquake loading and liquefaction-induced deformations (Elgamal et al. 2002; Finn and Fujita 2002; Yang et al. 2003). Dynamic FE analysis has been successfully used to simulate the failure modes of piles observed in past earthquakes (e.g. Fujii et al. 1998; Kagawa et al. 1997; Tao et al. 1998; Uzuoka et al. 2008; Cubrinovski et al. 2008).

Simplified analyses of piles in laterally spreading ground include the pseudo-static beam-on-nonlinear-Winkler-foundation (BNWF or *p-y*) approach and the limit equilibrium approach. In the limit equilibrium approach, pressure distribution along the resisting soils is assumed and is applied on a pile foundation to calculate the internal shear force and bending moment distributions (e.g., Dobry et al. 2003). Two alternatives to *p-y* approaches are depicted

by Boulanger et al. (2003). The first alternative requires free-field soil movement (y_{soil}) as an input; the second alternative applies limit pressures over the depth of laterally spreading soil (with the *p-y* springs removed in this interval). In either case, *p-y* springs are used to model the response of the underlying competent soil. In the second alternative, the applied lateral pressures are independent of the free-field soil displacements, since the soil movement is assumed large enough to cause the lateral pressures to reach their limiting values.

To conduct an analysis using the *p-y* approach, one of the key issues in modeling the soil-foundation interaction in liquefied ground is the subgrade reaction behavior. Findings from prior physical modeling studies (e.g., Wilson 1998; Dobry and Abdoun 2001; Tokimatsu et al. 2001; Ashford and Rollins 2002) show that the back-calculated *p-y* behavior of liquefied sand depends on soil relative density (Dr), prior displacement/strain history, and excess pore pressure (EPP) ratio in the far- and near-field, partial drainage and loading rate, and pile flexibility and head restraint, among others. These different studies reveal a wide range of subgrade reaction behaviors, which in return reflect the complexity of the phenomena.

Another key issue is the ultimate pressure of the ground crust layer. Using the *p-y* approach, Brandenberg et al. (2005) analyzed the data obtained from centrifuge modeling of single piles and pile groups embedded in a clay crust overlying a loose sand layer and a dense sand layer. They found that the peak lateral loads on piles due to laterally spreading clay crust can be well predicted by Matlock's "static" *p-y* curves, whereas his "cyclic loading" *p-y* curves were very conservative (Matlock 1970). The peak load produced by downslope spreading of the clay crust is more closely approximated by a static monotonic loading mechanism than by the displacement-controlled cyclic loading used in Matlock's studies. Brandenberg et al. (2005) also found that large relative displacements, that is, 40~100% of the pile cap height, were required to mobilize peak crust load when the soil beneath the crust liquefied, because a large length of the crust (uphill of the pile cap) was compressed before pressures were sufficient to cause passive failure of the soil crust. Another independent study of large-scale shake table tests on single piles by Cubrinovski et al. (2006) showed that the ultimate lateral pressure from a sand surface layer was about 4.5 times the resultant Rankine passive pressure, and a relative displacement of 10% of the crust layer thickness was required to mobilize the peak load. One of the remaining issues is how the relative stiffness between the crust layer and the underlying liquefied layer affects the load transfer behavior.

1.3 Study Objective

This project aims to advance the understanding of the impact of frozen ground crust on bridge foundations during liquefaction-induced lateral spreading and to investigate how to evaluate the lateral loads on bridge pile foundations induced by a laterally spreading frozen crust that overlies liquefiable soils during earthquakes. The objectives of this project are to:

1. Gain an in-depth understanding of the impact of frozen ground crust on a typical ADOT&PF-style bridge foundation (i.e., concrete-filled steel pipe pile) embedded in liquefiable soils overlying competent soils during earthquakes.
2. Validate numerical methods including the solid-fluid coupled FE model and *p-y* approach.
3. Propose guidelines for conducting simplified pseudo-static analysis to account for the loads on bridge foundations induced by a laterally spreading frozen crust during earthquakes.

1.4 Scope of Work

The scope of work, using a shake table experiment, solid-fluid coupled FE modeling, and the *p-y* approach, includes the following:

1. Conduct a shake table experiment to gain an in-depth understanding of the impact of frozen ground crust on a model pile foundation, and use the results to validate the FE model and the *p-y* approach.
2. Study the impact of the frozen crust on pile foundations through solid-fluid coupled FE analysis of a pipe pile foundation typically used in Alaska for bridge structures. Build two models to investigate the frozen ground crust effects: one with an unfrozen crust and the other with a frozen crust.
3. Evaluate the effectiveness of the *p-y* approach by comparing the results from the simplified approach with the results obtained from FE modeling.
4. Propose guidelines for design practices on how to perform simplified analysis of pile foundations subjected to liquefaction-induced lateral spreading of a frozen ground crust.

1.5 Organization of This Report

This report is divided into six chapters:

1. Chapter 1 introduces the background, literature review, study objectives, and scope of the work.
2. Chapter 2 presents a shake table experiment with experiment configuration, observation, results, and analyses.
3. Chapter 3 presents the validation process of two numerical approaches— FE modeling and the *p*-*y* approach—through comparison with results from the shake table experiment.
4. Chapter 4 analyzes a full-size soil-pile system by solid-fluid coupled FE modeling in both unfrozen and frozen conditions, and discusses the effect of frozen ground crust on the seismic performance of pile foundations in liquefiable soils.
5. Chapter 5 evaluates the capability of the *p*-*y* approach and proposes guidelines for analyzing pile performance by using this simplified method in design practices.
6. Chapter 6 summarizes the content of this report, presents the study's conclusions, and discusses suggestions for future study.

CHAPTER 2 SHAKE TABLE EXPERIMENT

2.1 Introduction

As indicated from the literature, lessons have been learned from Alaska's major earthquakes, such as that lateral spreading of a frozen crust overlying liquefiable soils can generate significant lateral force and induce extensive bridge foundation damage. Unfortunately, very limited studies have been carried out to investigate the impact of the frozen crust on built infrastructure during earthquake loading. Shake table experiments have been successfully applied in studying soil-pile interaction under liquefaction and liquefaction-induced lateral spreading conditions. Examples of shake table experiments on soil-pile interaction include Cubrinovski et al. (2006), Shirato et al. (2008), Ueng (2010), and Yao et al. (2004).

This chapter presents the results and analyses of a shake table experiment that investigated the mechanism and consequences of frozen crust-pile foundation interaction during earthquake-induced liquefaction and lateral spreading. This chapter describes the experiment model design, instrumentation plan, model preparation, frozen soil simulation, and recorded data including acceleration, pore pressure, and displacement time histories. Included in this chapter is an analysis of the bending moment induced on the pile by using recorded strain data, and a discussion of the mechanism of soil-pile interaction in the presence of frozen crust under a liquefaction condition. The shake table experiment was designed in detail by authors at the University of Alaska Anchorage, and later performed by Dr. Runlin Yang from Beijing University of Science and Technology, Beijing, China.

2.2 Shake Table Experiment

2.2.1 Shake Table Experiment Facility and Model Configuration

The shake table experiment was performed on a 3 × 3 m shake table. The payload capacity of the shake table is 10 tons, with a maximum acceleration ranging from 1.0 g (fully loaded) to 2.5 g (unloaded). Figure 2.1 shows the soil-pile system set up in a 3 × 3 × 1.3 m (L×W×H) steel container. The container has a wall thickness of 4 mm with a frame support system welded to the outside. A steel pipe pile with an outer diameter of 5 cm and wall thickness of 0.175 cm was used to model a bridge pile foundation, typically used in Alaska, at a scale of 1:15. The pile was fixed at the bottom of the soil container and has a lumped mass of 250 kg on its top to simulate the inertial effect of the bridge superstructure. The soil profile consists of a 30 cm frozen soil

crust overlying a 30 cm loose sand layer and a 60 cm medium dense sand layer. The crust has a 5° slope angle. A 25 cm wide opening between the left end of the frozen soil crust and the soil box was designed to mimic a river channel and allow the frozen crust to spread laterally during earthquake shaking. Water level was designed just above the interface between the loose sand and frozen soil to ensure that the sands were fully saturated. The sloping ground and river channel scenario resembles a typical topographical situation for a bridge site.

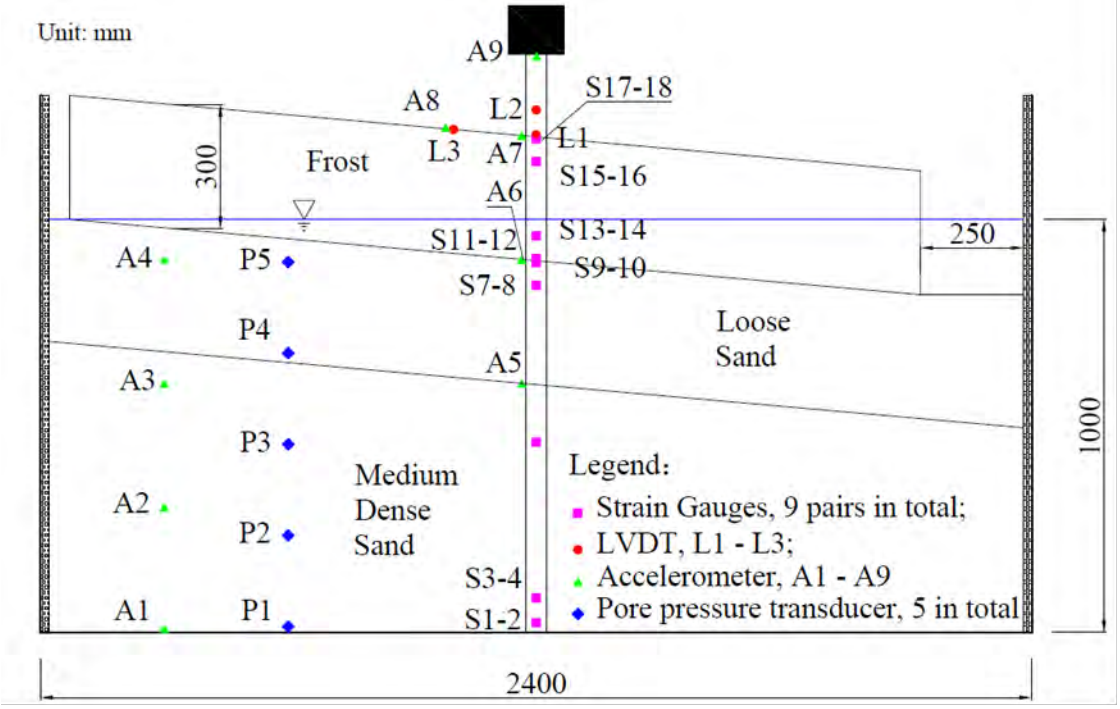

Figure 2.1. Layout of the shake table model

Figure 2.1 shows that four types of transducers were used in this experiment: pore pressure transducers (5, identified by “P”), accelerometers (9, identified by “A”), strain gauges (9, identified by “S”), and LVDTs (3, identified by “L”). Accelerometers and pore pressure sensors were placed at different locations in the soil profile to record acceleration and pore pressure. Strain gauges were installed on the pile to measure the strain values for quantifying the loads, which is also one of the foci of this study. Considering that concentrated strains and moments might be generated by the frozen crust, more strain gauges were installed at locations close to the loose sand-frozen soil interface and the top of the frozen soil. Note the reference point for all LVDTs is the soil container; therefore, the measure displacement is relative displacement to the soil container box. Among the LVDTs, L3 was assigned to measure the frozen crust lateral

displacement; L1 was assigned to measure pile deflection at the ground surface; and L2 was a backup sensor for L1 in case the expected strong interaction between the pile and the frozen crust damaged L1.Table 2.1 summarizes the instruments for this experiment.

Table 2.1. Summary of instruments for the shake table experiment

Instrument Name	Instrument Type	Location	Depth[a] (mm)	Distance[b] (mm)
A1	Accelerometer	Soil	-1280	890
A2	Accelerometer	Soil	-980	890
A3	Accelerometer	Soil	-680	890
A4	Accelerometer	Soil	-380	890
A5	Accelerometer	Pile	-610	0
A6	Accelerometer	Pile	-308	0
A7	Accelerometer	Pile	0	0
A8	Accelerometer	Soil	0	210
A9	Accelerometer	Pile	200	0
P1	Pore pressure transducer	Soil	-1240	600
P2	Pore pressure transducer	Soil	-1020	600
P3	Pore pressure transducer	Soil	-800	600
P4	Pore pressure transducer	Soil	-580	600
P5	Pore pressure transducer	Soil	-360	600
L1	LVDT	Pile	0	0
L2	LVDT	Pile	60	0
L3[c]	LVDT	Soil	0	200
S1	Strain gauge	Pile	-1180	25
S2	Strain gauge	Pile	-1180	-25
S3	Strain gauge	Pile	-1120	25
S4	Strain gauge	Pile	-1120	-25
S5	Strain gauge	Pile	-740	25
S6	Strain gauge	Pile	-740	-25

Table 2.1 Summary of instruments for the shake table experiment (continued)

Instrument Name	Instrument Type	Location	Depth[a] (mm)	Distance[b] (mm)
S7	Strain gauge	Pile	-370	25
S8	Strain gauge	Pile	-370	-25
S9	Strain gauge	Pile	-310	25
S10	Strain gauge	Pile	-310	-25
S11	Strain gauge	Pile	-290	25
S12	Strain gauge	Pile	-290	-25
S13	Strain gauge	Pile	-240	25

S14	Strain gauge	Pile	-240	-25
S15	Strain gauge	Pile	-60	25
S16	Strain gauge	Pile	-60	-25
S17	Strain gauge	Pile	0	25
S18	Strain gauge	Pile	0	-25

[a] Depth was measured vertically from the ground surface, and positive and negative values correspond with the above- and underground surfaces, respectively.

[b] Distance was measured horizontally from the pile centerline, and positive and negative values correspond with the upslope and downslope sides of the pile, respectively.

[c] L3 is placed 200 mm (4 times of pile diameter) away from pile, and thus it has been referred to as "far-field" in this report.

Figure 2.2 presents the moment-curvature response for the pipe pile section. This curve was obtained by a moment-curvature analysis based on the following mechanical properties: steel yield strength 235 MPa, Young's modulus 200 GPa, and strain-hardening ratio 0.005. Assuming a yield strain of 0.2% and a rupture strain of 5% for the steel pipe, the yield bending moment (M_y) of the pile was determined to be 0.8 kN.m and the bending moment capacity (M_c), to be 1.06 kN.m.

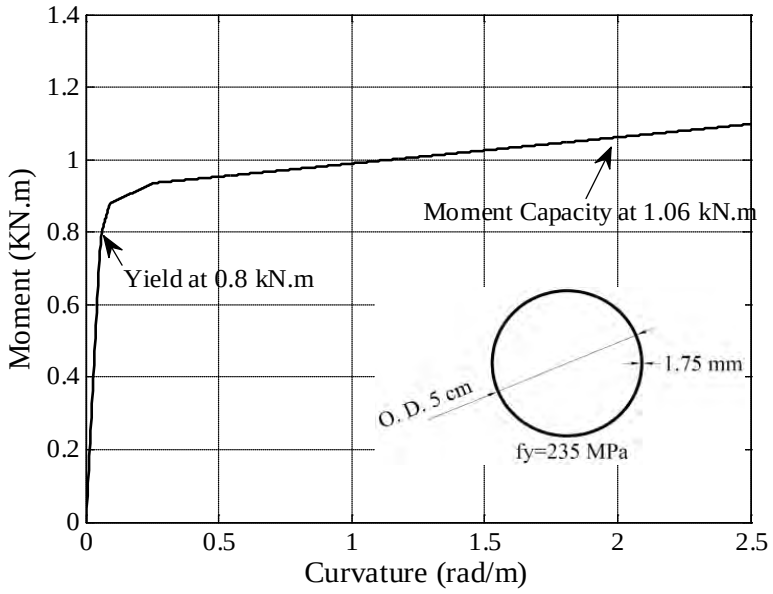

Figure 2.2. The pile cross section and its moment-curvature curve

2.2.2 Model Preparation

2.2.2.1 Soil Properties and Frozen Soil Simulation

Sieve analysis was carried out for the sands used in this experiment, and a particle-size distribution curve is shown in Figure 2.3. The sand is characterized by an average particle size

D_{50} of 0.33 mm. The loose sand layer has a saturated density of 1.7×10^3 kg/m^3 and relative density D_r of 40%, and the medium dense sand layer has a saturated density of 2.1×10^3 kg/m^3 and relative density D_r of 60%.

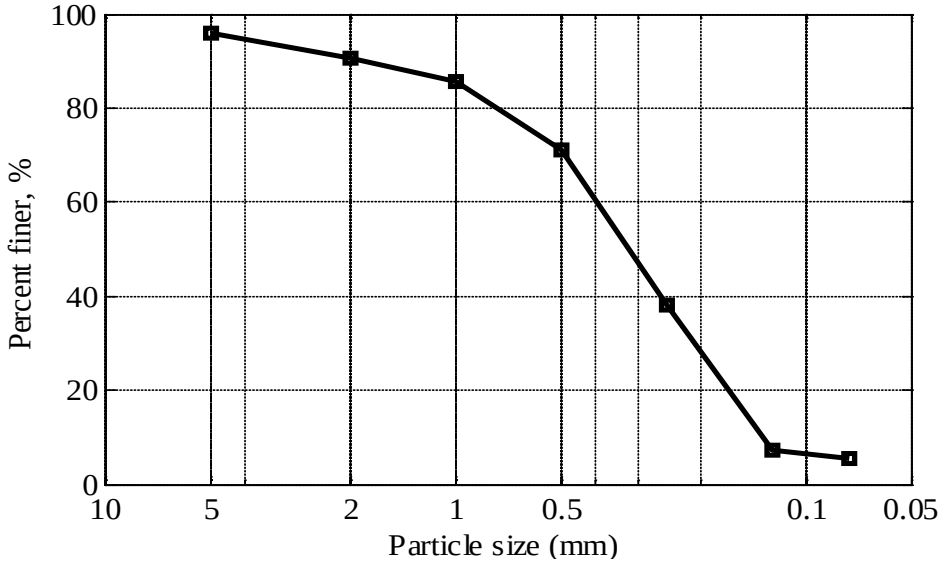

Figure 2.3. Sand particle-size distribution curve

Due to laboratory facility limitation, cemented sand was used to simulate frozen ground crust. The sand-cement-water mix ratio by weight was 9:1:1.8. Key mechanical parameters including density (ρ), compressive strength (q_u), strain at 50% ultimate strength (ε_{50}), and Young's modulus (E) need to be comparable to those of frozen soil. Based on a number of experiments, it has been determined that a sand-cement mixture at a certain ratio after a 72-hour wet curing has comparable mechanical properties. Specimens for obtaining mechanical properties were made at the same time that the ground crust in the model was poured (see Figure 2.4). Uniaxial compression tests (Figure 2.5) were conducted under variable strain rates ranging from 1×10^{-6} to 3×10^{-6} s^{-1}. Figure 2.6 shows the stress-strain curves obtained from four specimens. The mechanical properties of the four specimens are quite uniform, having the following average values: $\rho = 2.1\times10^3$ kg/m^3; $q_u = 0.51$ MPa; E = 310.1 MPa; $\varepsilon_{50} = 0.002$. Zhu and Carbee (1983) conducted laboratory tests of frozen Fairbanks silts at temperatures varying from -0.5 to -10°C, and reported q_u, E and ε_{50} values in the ranges of 0.4 ~17.3 MPa, 0.21 ~ 2.67 GPa, and 0.4×10^{-3} to 1.5×10^{-3}, respectively. By comparing the simulated frozen soil properties with those reported in Zhu and Carbee (1983), one can conclude that q_u and E of the simulated frozen soil specimens are within, but closer to, the lower bound of the range for frozen soils, and ε_{50} is within, but

closer to, the upper bound of frozen soils. In other words, the simulated frozen soil used in this study is similar to frozen soils at relatively high sub-zero temperature. Note that simulated frozen soil exhibits a brittle behavior that is similar to concrete, while frozen soil typically shows a more ductile behavior.

Figure 2.4. Cemented sand specimens

Figure 2.5. Snapshot of a uniaxial compression test of cemented sand specimen

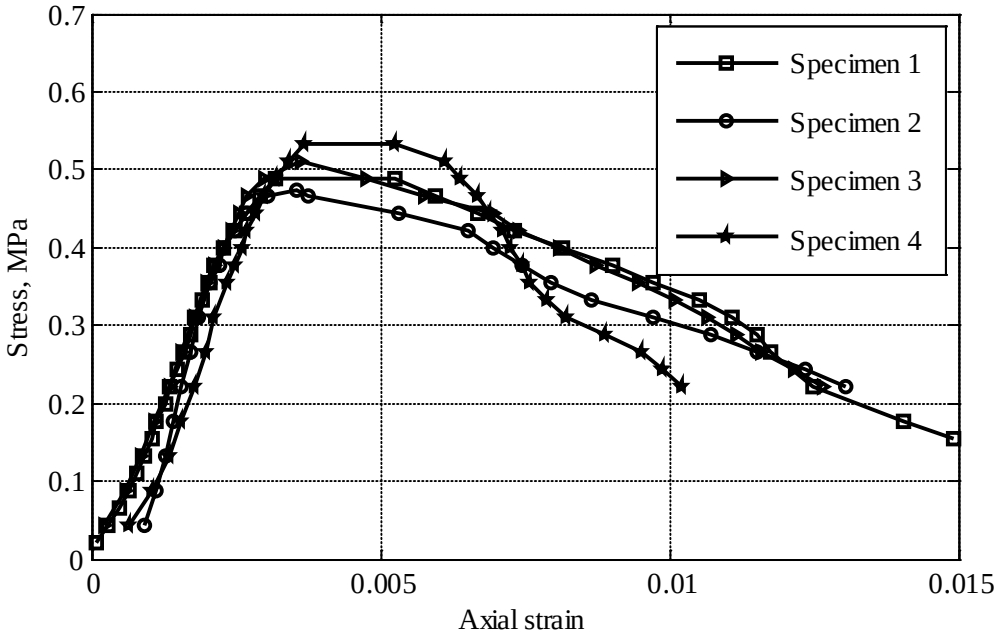

Figure 2.6. Stress-strain relations of cemented sands

2.2.2.2 Model Construction and Sensor Installation

Before preparing the soil-pile model in the container (Figure 2.7), energy absorption mats made of rubber material were glued to the inside surface of the soil container to reduce seismic wave reflection (Coe et al. 1985). Sands were placed carefully to form two layers, with the top layer being loose and the bottom layer being medium dense (see Figure 2.8). The sand-cement mixture was poured on top of the loose sand layer and a 5° slope was formed on the surface (see Figure 2.9). A portion of the river channel was visible on the right of Figure 2.9.

Figure 2.7. Soil box and pile with strain gauges installed and wired

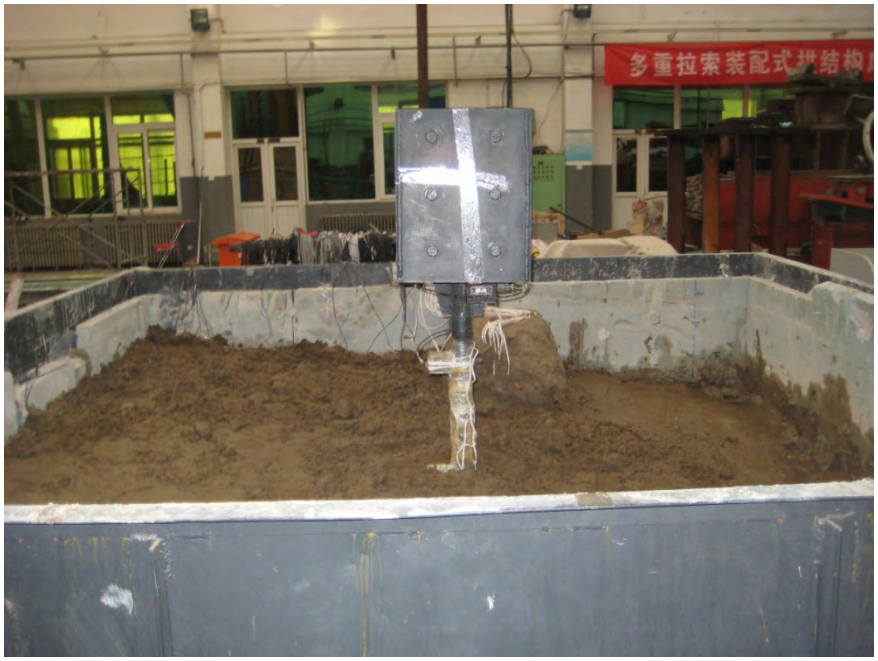

Figure 2.8. Smoothing the loose sand surface for placement of simulated frozen crust

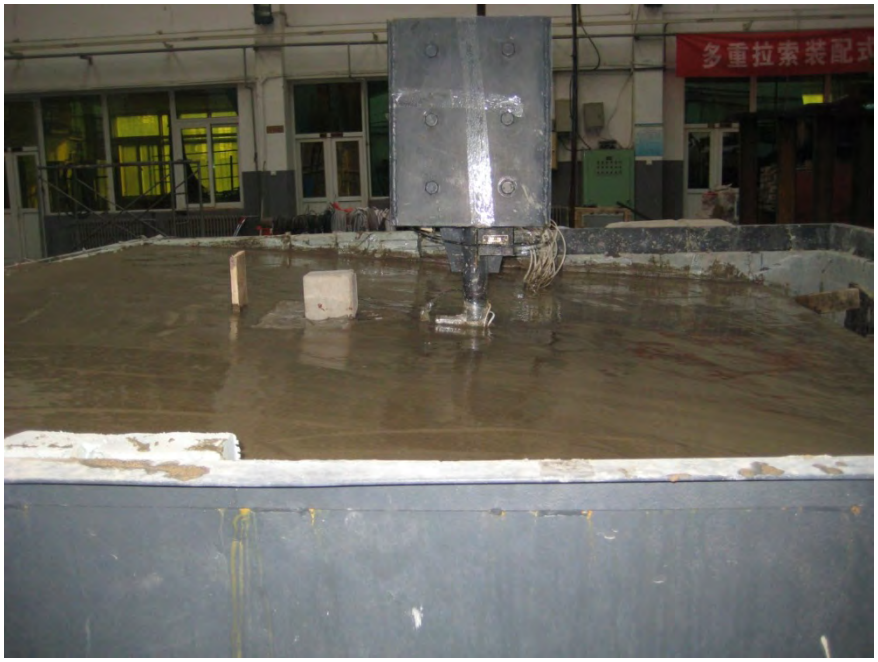

Figure 2.9. Cemented sands just placed for frozen crust simulation

Water was slowly added into the sand to about 60 cm above the bottom of the container before the placement of the sand-cement mixture, and added again after the placement of the sand-cement mixture to maintain the groundwater table at 18 cm above the bottom of the open channel. Strain gauges were sealed with epoxy, and accelerometers were housed in waterproof containers to protect them from damage due to submergence in water. All strain gauges and accelerometers were checked to ensure that these sensors were correctly wired. Figure 2.10 to Figure 2.12 show the details of the sensor and installation.

Figure 2.10. Pore pressure sensors

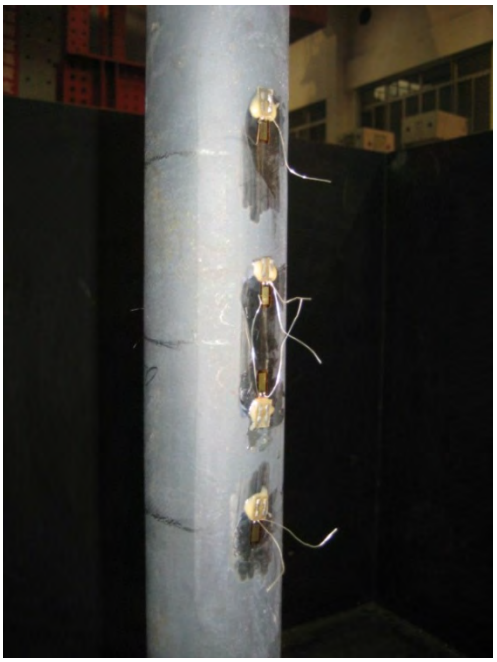

Figure 2.11. Strain gauges attached on the pile surface

Figure 2.12. An accelerometer in a waterproof enclosure as installed on the bottom of the soil container

2.3 Input Motion

The input motion experiment was performed by applying three stages of input motion, as shown in Table 2.2 and Figure 2.13. In the first stage, the model was loaded by a sinusoidal wave and scaled-down acceleration time histories recorded at Pump Station #10 along the Trans-Alaska Pipeline System during the 2002 Denali earthquake, named “Sine Wave” and “Scaled Denali Earthquake,” respectively. The sinusoidal wave had a peak acceleration of 0.05 g and the scaled-down Denali motion had a peak ground acceleration (PGA) of 0.15 g. The main purpose for these loadings was to check whether the model, instruments, and data acquisition system were functioning properly. Neither permanent deformation nor permanent bending moment was expected from these events.

Table 2.2. Input motion sequence

Test stage	Event name	PGA (g)	Duration (sec.)	Input Time (Local time)
#1	Sine Wave	0.03	20	8:20 a.m.
	Scaled Denali Earthquake	0.15	20	8:23 a.m.
#2	Japan Part 1	0.53	40	8:53 a.m.
	Japan Part 2	0.53	40	8:56 a.m.
#3	Scaled Japan Part 1	0.80	40	10:00 a.m.

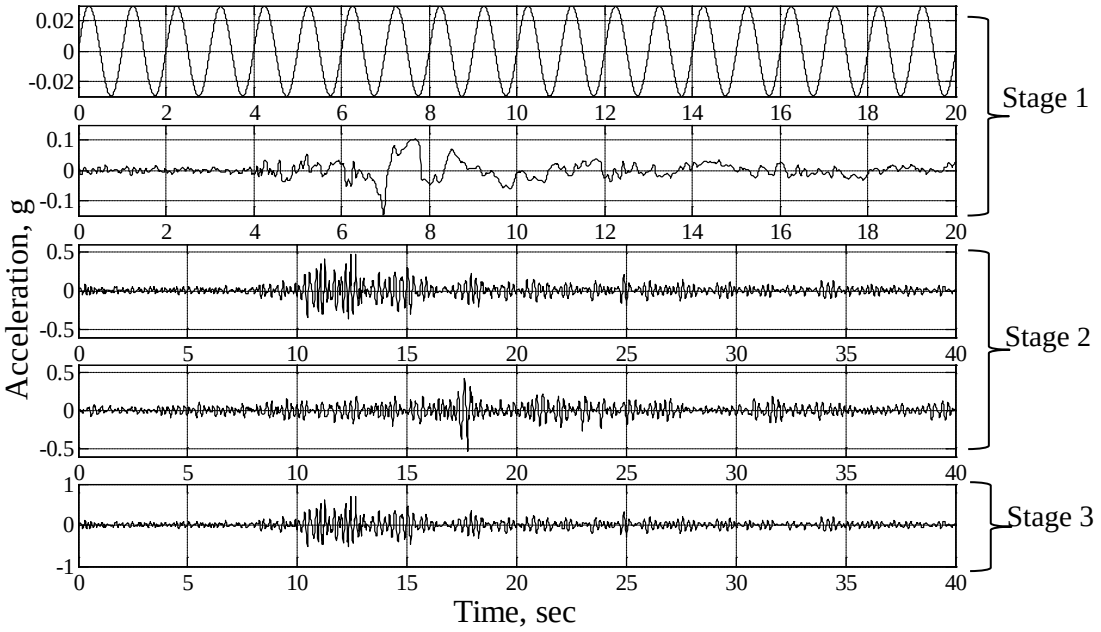

Figure 2.13**.** Acceleration time histories of input motions

In the second stage, after we ensured that the model, instruments, and data acquisition system were functioning properly, the model was loaded with acceleration time histories recorded at the AKTH04 station on the ground surface during the 2011 Tohoku Earthquake (M_w=9.0). This earthquake had a PGA of 0.53 g and duration of 80 sec. The source mechanism and magnitude of this earthquake are similar to those of the 1964 Great Alaska Earthquake. Due to the facility's limitations, however, the records for source mechanism and magnitude had to be split into two segments, named "Japan Part 1" and "Japan Part 2," respectively, and input to the shake table sequentially, A three-minute gap occurred in between to allow for this transition. Substantial permanent deformation and bending moment were expected from this stage of loading.

In the third stage, the first portion of the Japan record with its PGA scaled up to 0.80 g was used as the excitation. This motion was input about one hour after Test Stage 2 to allow time for the excess pore pressure to drop to hydrostatic pore pressure. We expected that residual displacement and bending moment from Test Stage 2 would exist. The purpose of this stage loading was to induce larger displacement and gather pile performance data.

2.4 Observation of Model Behavior

Figure 2.14 to Figure 2.18 show several representative snapshots during the experiment. Figure 2.14 shows the shake table model before the test. During Test Stage 1, no observable permanent deformation was noticed in either the ground crust or the pile.

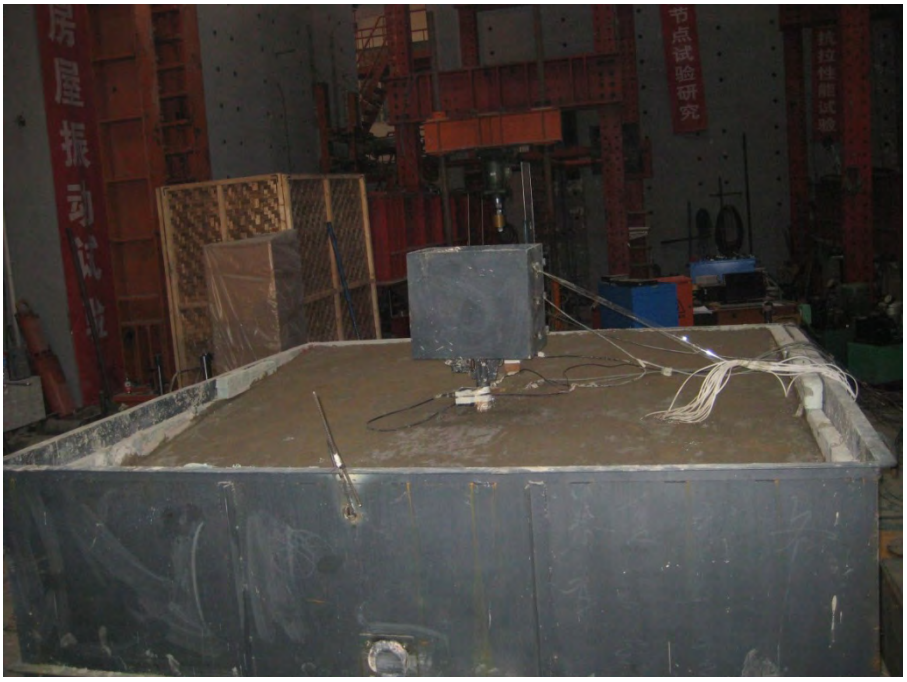

Figure 2.14. Model before loading

Figure 2.15. Cracks formed near the soil-pile interface

Figure 2.16. Gap formed between the soil and pile, and water spilled out

Figure 2.17. Tilted pile head

Figure 2.18. Lateral spreading of the simulated frozen crust

Starting at Test Stage 2, the following phenomena were observed: Cracks started to form on the frozen crust surface near the soil-pile interface after a few cycles of loading in Stage 2 (see Figure 2.15). As the input moved past the main shaking period, cracks gradually developed into a gap near the soil-pile interface, and water rose to the ground surface from the gap and spilled out (Figure 2.16). At the end of Test Stage 2, the pile head tilted about 15° toward the downslope direction (Figure 2.17), and the frozen crust laterally spread in the downslope direction for about 2 cm (Figure 2.18). During Test Stage 3, the frozen crust continued moving in the downslope direction for about 1 cm, and the pile head continued to tilt; water was seen spilling out of the gap long after the shaking ended.

These phenomena indicate that the input motions generated a considerable amount of excess pore pressure in the sand layer and induced full or partial liquefaction in Test Stages 2 and 3. Model excavation at the end of the experiment revealed that permanent deflection was found at 0.28–0.30 m and 0.7–0.8 m below the ground surface, respectively, indicating the formation of plastic hinges during the experiment.

2.5 Results and Analysis

2.5.1 Data Processing

The following sign conventions are defined to facilitate discussion: positive and negative depth values indicate the location above and below the ground surface, respectively; depth 0 m refers to the frozen ground surface. Displacement is defined as positive if it is along the downslope direction, and bending moment is defined as positive if it warps an element to the upslope direction in a "U" shape.

Recorded pore pressure data were first converted to excess pore pressure (EPP) by subtracting the hydrostatic pore pressure. Then the EPP ratio (r_u) was calculated by normalizing the EPP by the effective overburden pressure.

Assuming a linear distribution of strain along the pile cross section, measured strain data were converted to curvature by using Equations 2.1 and 2.2. Bending moment was evaluated by the moment-curvature relation of the model pile (see Figure 2.2).

$$\phi = \frac{\varepsilon}{h} \tag{2.1}$$

$$\varepsilon = \frac{1}{2}(\varepsilon_t - \varepsilon_c) \tag{2.2}$$

where ϕ is the curvature; ε is the strain; ε_t and ε_c represent tension and compression strains obtained from symmetrically installed strain gauge pairs on the pile; *h* is the distance from the strain measurement point to the neutral axis of the section and the outer-radius of the pile was used for *h* in this study.

2.5.2 Experiment Data from Test Stage 1

Figure 2.19 presents the time histories of r_u for several depths of the sine wave motion in Test Stage 1. Note that r_u for all depths is very small. This is expected since the input motion has a very low peak acceleration amplitude. Note the spikes at the depth of -1.25 m. Very similar spikes were also observed in the scaled Denali earthquake motion (see Figure 2.20). These spikes could be observed in all loading stages, as presented later, and the cause of these spikes is not clear, but we believe it might be due to this particular sensor's defect.

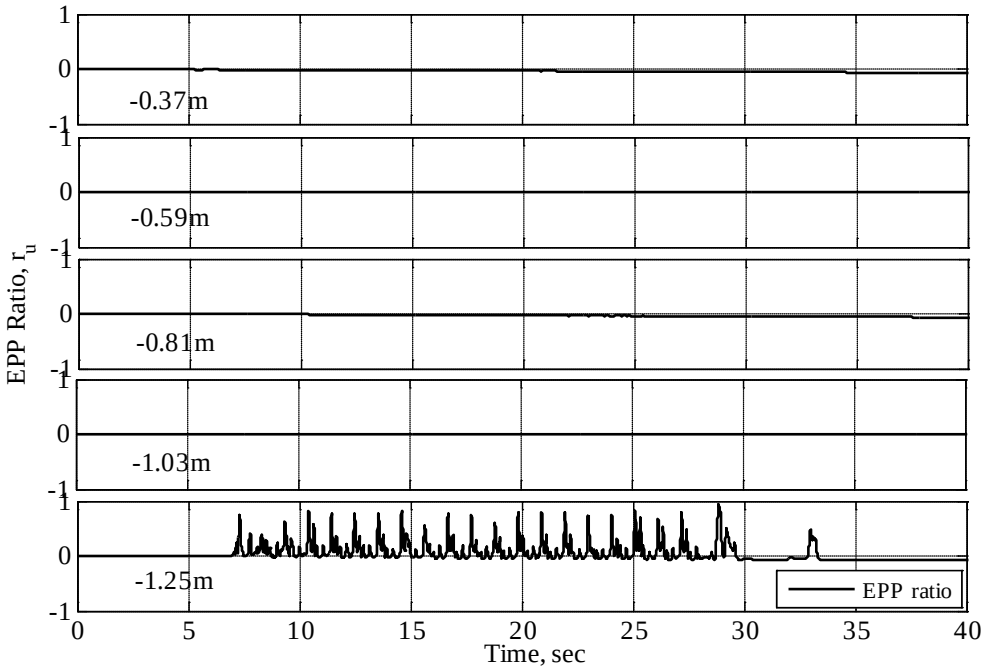

Figure 2.19. Excess pore pressure ratio for Test Stage 1 – Sine Wave

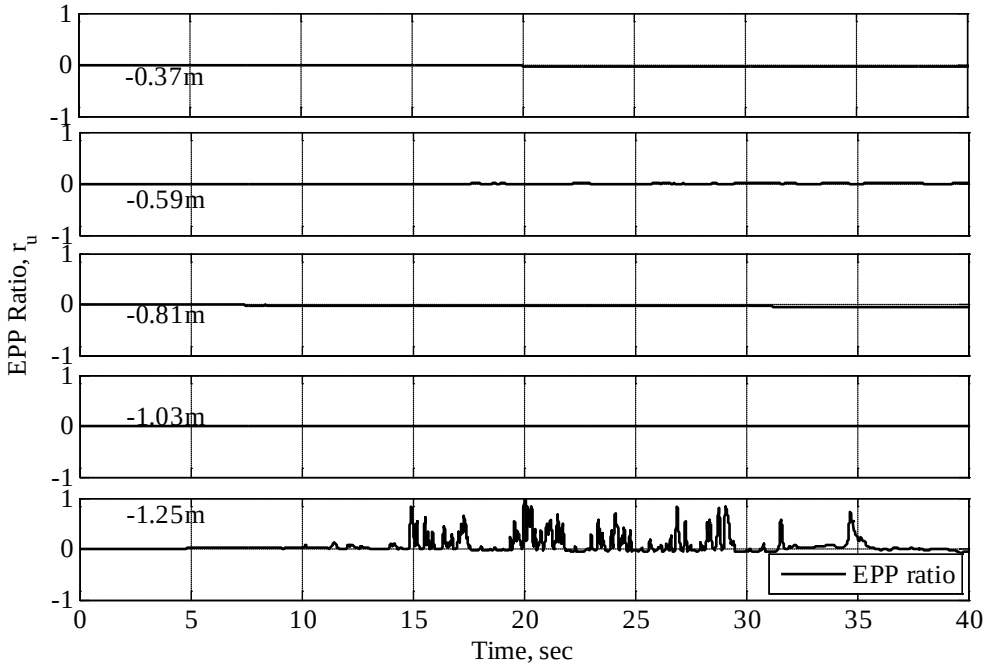

Figure 2.20. Excess pore pressure ratio for Test Stage 1 – Scaled Denali Earthquake

Figure 2.21 shows the recorded acceleration time histories at different depths in soil for the sine wave input. Except for a failed sensor, the other three accelerometers recorded signals that are very similar to the input in terms of both shape and magnitude. Figure 2.22 shows soil

acceleration for the scaled Denali earthquake input. It also displays a similar shape of the base input motion, but with some magnitude amplification.

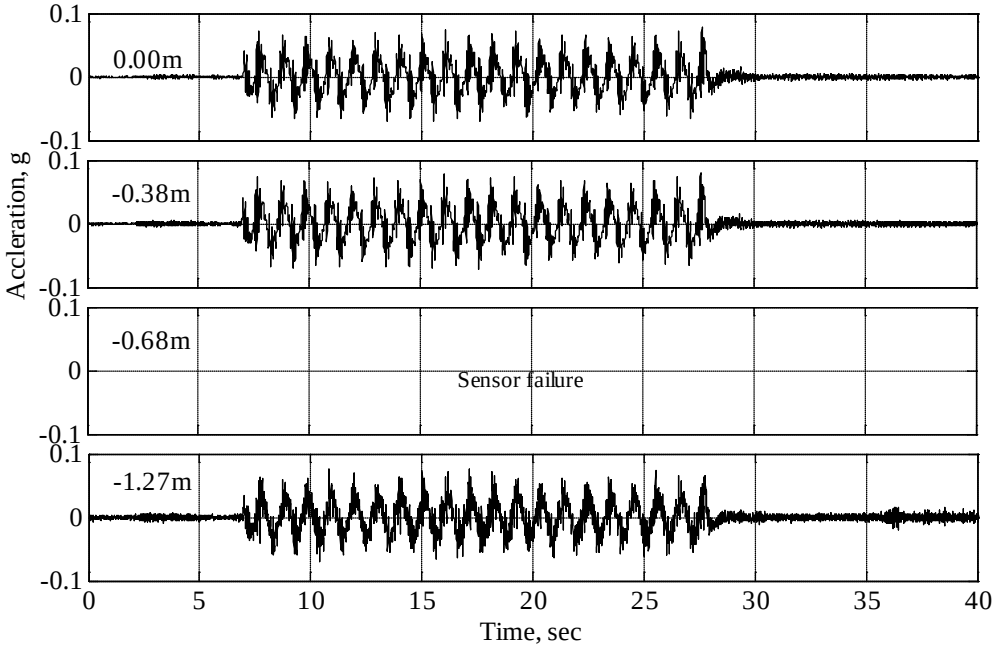

Figure 2.21. Acceleration time histories in soil for Test Stage 1 – Sine Wave

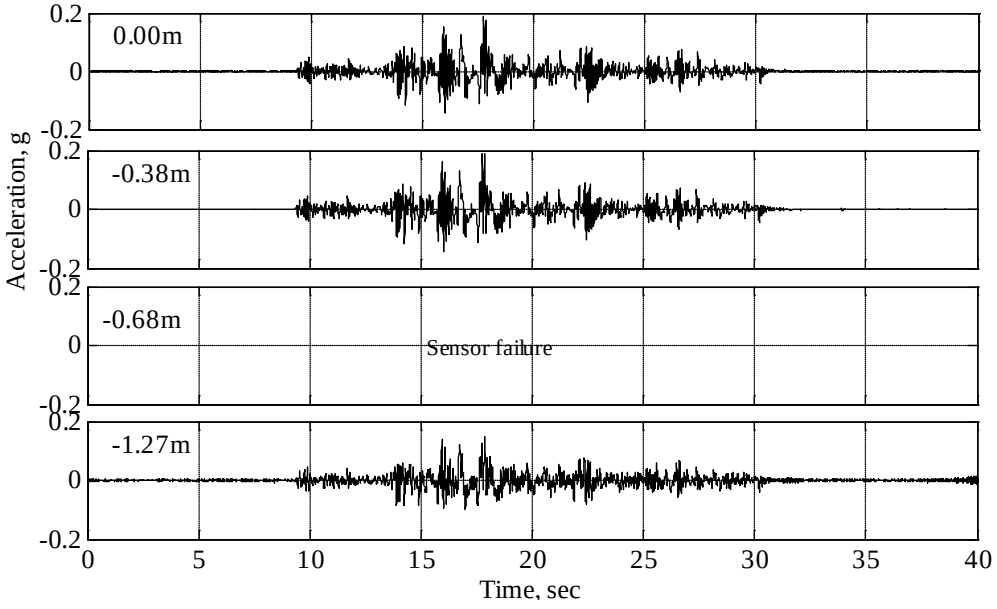

Figure 2.22. Acceleration time histories in soil for Test Stage 1 – Scaled Denali Earthquake

Figure 2.23 and Figure 2.24 show the displacement time histories from LVDTs for the sine wave and the scaled Denali earthquake motions, respectively. Displacement on the pile can be

seen fluctuating in a small range, but no permanent displacement is visible. No relative movement between the box and the simulated frozen crust is observed from the displacement time histories recorded by the "far-field" LVDT.

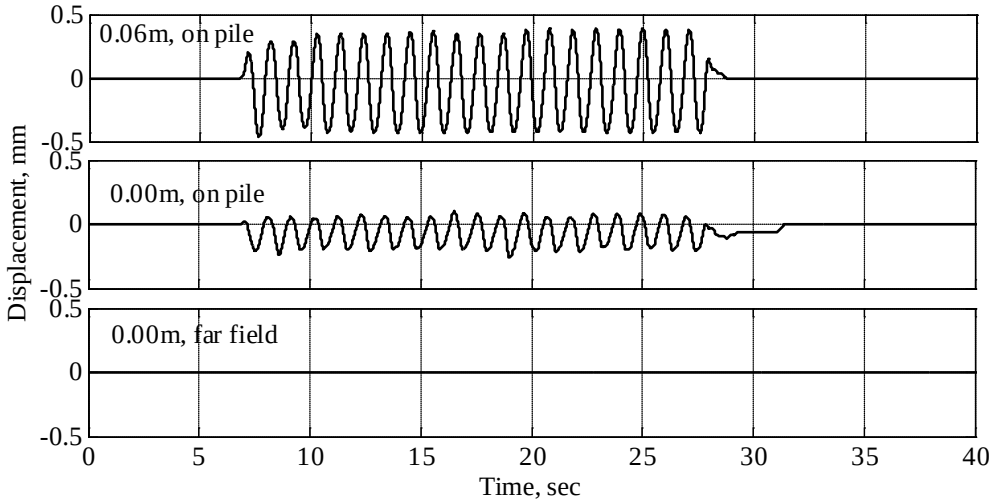

Figure 2.23. Displacement time histories for Test Stage 1 – Sine Wave

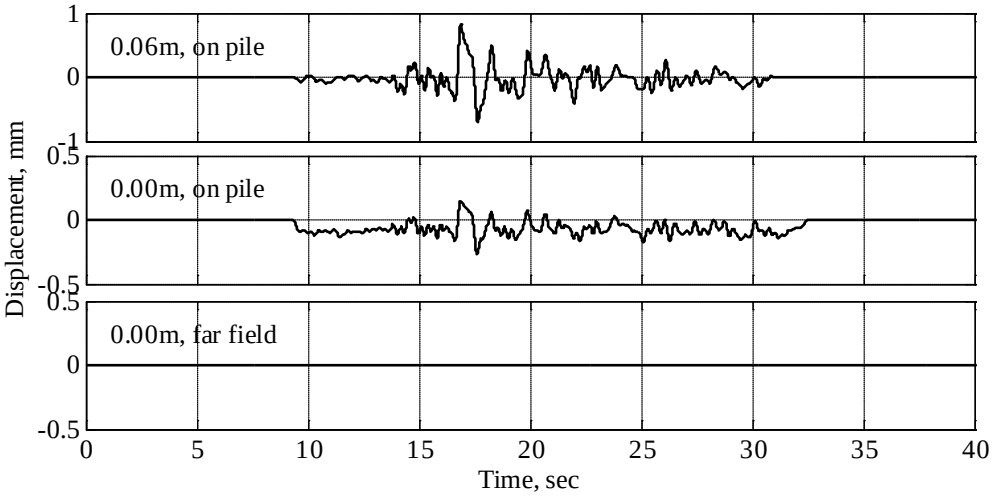

Figure 2.24. Displacement time histories for Test Stage 1 – Scaled Denali Earthquake

In summary, Test Stage 1 data show that the instruments and data acquisition system functioned properly and the model was ready for further high-intensity loading.

2.5.3 Experiment Data for Test Stage 2

Figure 2.25 shows the r_u time histories for Test Stage 2. At around 20 seconds, r_u began to build up quickly, when the first main shaking occurred. The corresponding maximum values of r_u for different depths are 31%, 39%, 41%, 33%, and 62% from the top to the bottom. The EPP

buildup indicates partial liquefaction in the loose and medium dense sand layers. As mentioned in Section 2.3, this earthquake record was input in two segments, with about 3 minutes of gap in between. A noticeable but not significant drop in the pore pressure time histories can be observed in Figure 2.25. Again, spikes are observed in the r_u time history at the depth of -1.25 m. Despite these spikes, a clear trend in the EPP buildup can still be observed.

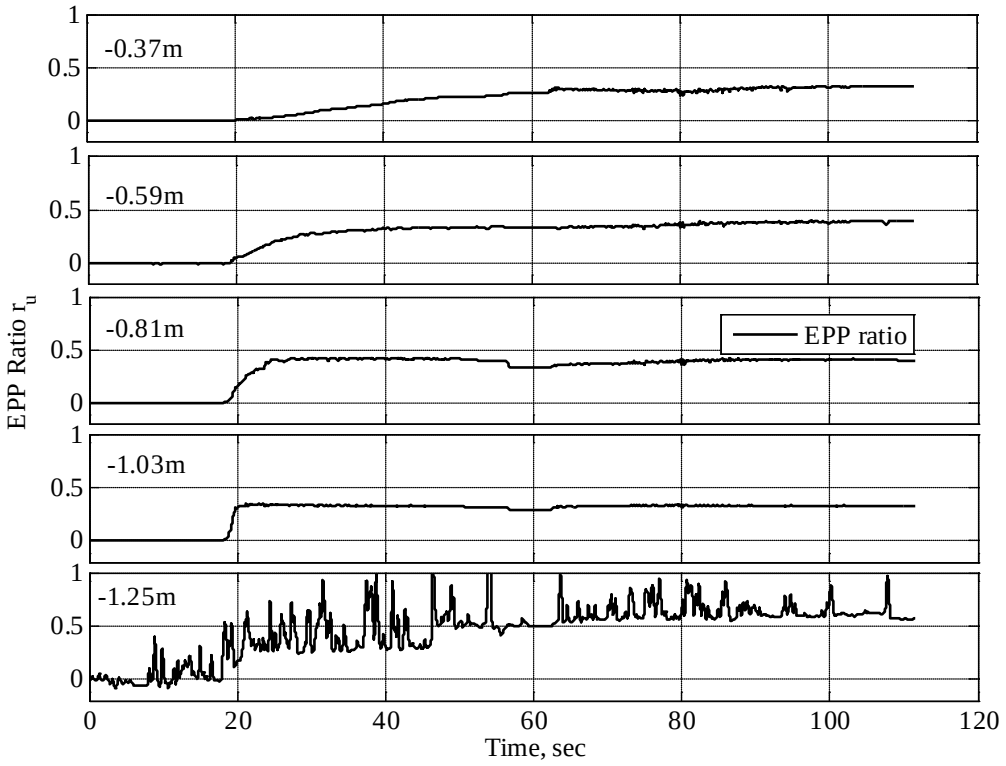

Figure 2.25. Excess pore pressure ratio time histories for Test Stage 2

Figure 2.26 presents acceleration time histories at different locations in the soil. No apparent features of liquefaction such as attenuation of ground acceleration amplitude and disappearance of high-frequency signal (Kostadinov and Yamazaki 2001) can be observed. Since the sand layer only went through partial liquefaction, considerable effective contact and shear modulus existed in the soil, and a relatively high-frequency wave still propagated to the ground surface. Another possible reason for the high-frequency components is the relative simple design of the soil container, which did not completely prevent the seismic wave from reflecting at the boundary. As mentioned previously, the motion used in this loading stage was characterized by double acceleration peaks, which correspond to about 19 sec. and 80 sec., respectively. These two time instants will be referred to frequently later in this section of the report.

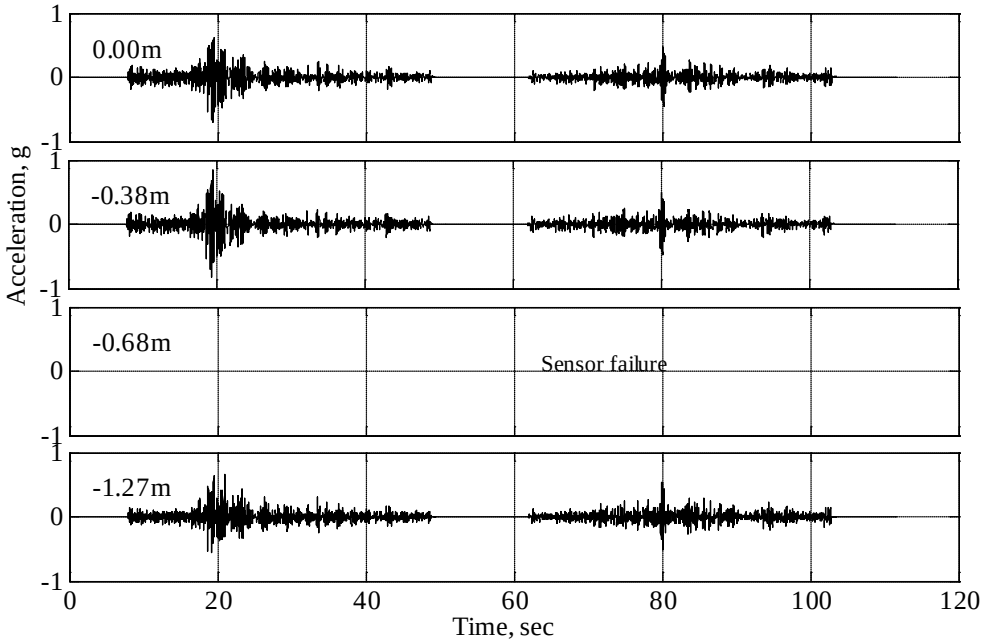

Figure 2.26. Acceleration time histories recorded in soil for Test Stage 2

Figure 2.27 shows the displacement time histories measured at two locations on the pile and at a “far-field” location on the frozen ground crust. Observe in Figure 2.27 that the displacement for all locations was very small, up to 19 sec. into the shaking. After that time, displacement started to increase quickly at around 20 sec., which corresponds to the occurrence of the first peak of input motion. The displacement remained almost flat to the end of the first segment of shaking. It is clear that displacement of the pile continued at the end of Part 1 excitation, as indicated by the abrupt change in displacement during the 3-minute gap between the two segments of loading. This displacement is likely due to tilting of the pile and the creep of the sand-cement mixture that was not fully cured. Such abrupt change is not present in the displacement time history recorded on the frozen crust. The displacement remained almost constant from the beginning of Part 2 shaking to 75 sec., and gradually increased until 80 sec. At 80 sec., a sharp increase is apparent in the displacement time history recorded on the frozen crust and in the time history recorded on the pile. Displacement kept increasing, although quite slowly, until the end of Part 2 shaking.

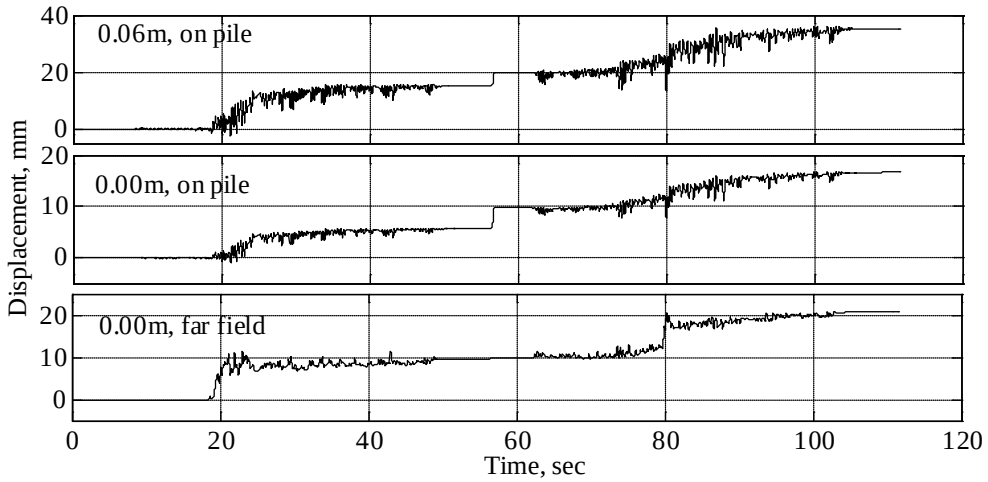

Figure 2.27. Displacement time histories for Test Stage 2

The maximum lateral spreading of the frozen ground crust reached 2.1 cm, or 40% of the pile diameter. By comparing the displacement of the frozen crust with that of the pile at the ground surface, one notes that the frozen crust moved ahead of the pile, which implies that the pile deflection was driven primarily by lateral spreading of the frozen crust. Figure 2.28 shows the difference between the frozen crust lateral spreading and the pile deflection at the ground surface. The maximum difference is about 10 mm, which is roughly the maximum gap formed between the frozen crust and the pile. Note that the deflection of the pile at 0.06 m above the ground surface is far greater than that at the ground surface, indicating that the pile tilted by a fairly large angle, which agrees well with the observations presented in Section 2.4.

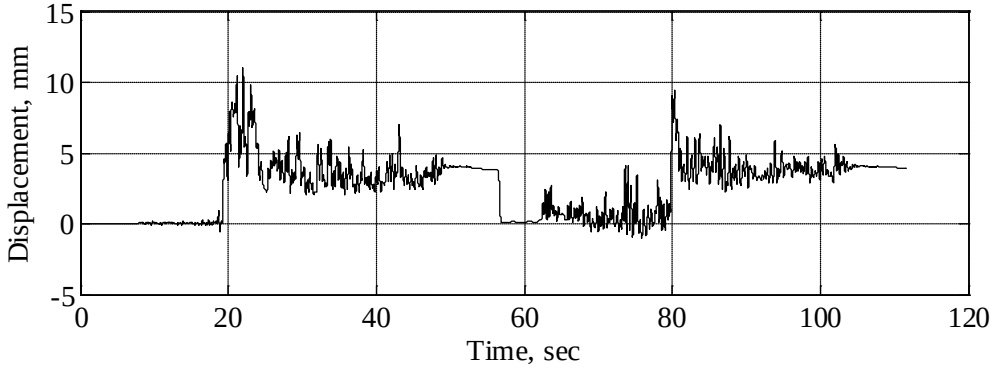

Figure 2.28. Relative displacement of the far-field soil and pile at the ground surface

Figure 2.29 shows the time histories of bending moment recorded at different locations on the pile. The strain gauges located at the ground surface were damaged due to strong frozen crust-pile interaction. From Figure 2.29, it is apparent that, overall, the bending moments at the

depths of -0.29 m and -0.74 m are much larger than other locations. Note that the bending moment concentrations at these locations have different signs, indicating that the pile bent in opposite directions. Careful examination of the bending moment time histories at these locations reveals different trends. At depth -0.29 m, the bending moment reached the yield bending moment when the first peak of input motion occurred, and started to drop slightly, even though the frozen crust lateral spreading increased gradually before the second peak of the input motion occurred. At depth -0.74 m, however, the bending moment increased quite gradually, reaching the yield bending moment when the second peak of input motion occurred at 80 sec., and remained high until the end of shaking.

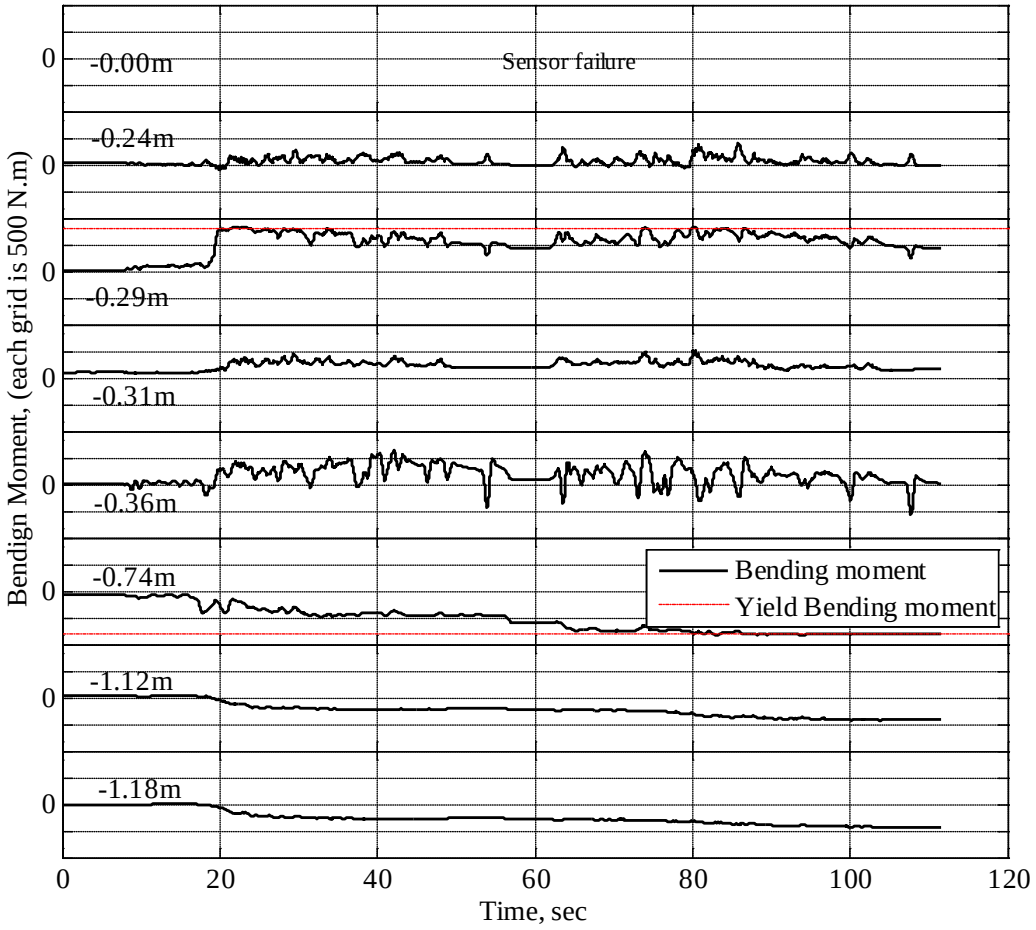

Figure 2.29. Bending moment time histories

The bending moment envelope along the pile depth is shown in Figure 2.30 to illustrate the location of possible plastic hinges. It is easy to see from Figure 2.29 that the shaking formed two bending moment concentrations: one at the frozen ground crust-loose sand interface, and the

other in the middle of the partially liquefied medium dense sand layer. The bending moments at both locations reached the pile's yield bending moment, indicating the formation of plastic hinges. The yielding of the pile at different times for these locations reveals the different mechanisms that are responsible for the formation of plastic hinges. The plastic hinge at the frozen crust-loose sand interface (at -0.29 m) started to form at the occurrence of the first peak of input motion (around 20 sec.), when the frozen crust lateral spreading was about 0.9 cm. It is very likely that this plastic hinge formed because of the large distributed load (soil resistance) applied on the pile by the laterally spreading frozen crust. Later, as lateral spreading of the frozen crust increased gradually, the bending moment actually dropped slightly, possibly due to yielding and creep of the cemented sand. A similar trend was observed in the bending moment time histories at the same depth after the occurrence of the second peak for like reasons. For the plastic hinge in the middle of the partially liquefied medium dense sand layer (-0.74 m), the bending moment started to form at the time of the second peak of input motion (around 80 sec.), when lateral displacement of the frozen crust reached it maximum value 2.1 cm. The bending moment remained high, while lateral spreading remained around 2.1 cm until the end of shaking. Apparently, this plastic hinge formation was due to lateral spreading of the ground crust.

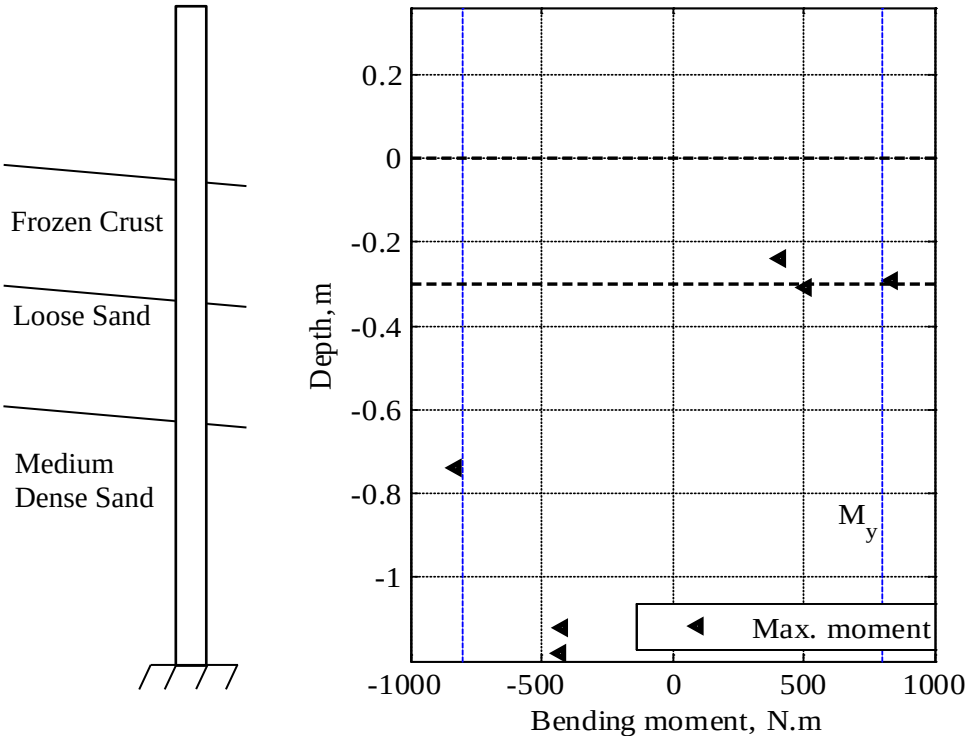

Figure 2.30. Bending moment envelope along the pile depth

2.5.4 Experiment Data for Test Stage 3

Test Stage 3 was performed to induce more lateral spreading and gather additional data of pile performance under larger lateral spreading. The time histories of acceleration, displacement, bending moment, and EPP ratio are presented in this section. Since the previous loading stage already pushed the pile into inelastic behavior, one would expect significant permanent displacement and bending moment of the pile. Generally, the trends of these time histories are similar to those from Test Stage 2.

Figure 2.31 presents the r_u time histories at different depths. Maximum r_u reached 19% in average at different depths. Compared with r_u time histories of Test Stage 2 (see Figure 2.25), r_u is lower, although the input motion had larger amplitude. The main cause of this difference is that, after the previous shaking in Test Stage 2, the loose sand layer became denser during the pore water dissipation process at the one-hour interval between Test Stages 2 and 3. In fact, the frozen crust settled about 3 cm after Test Stage 2, which is a direct indication of densification of the sand layers, particularly the loose sand layer. In addition, the water table dropped about 1 cm after Test Stage 2. Note that these factors were not considered in the calculation of r_u for Test Stage 3.

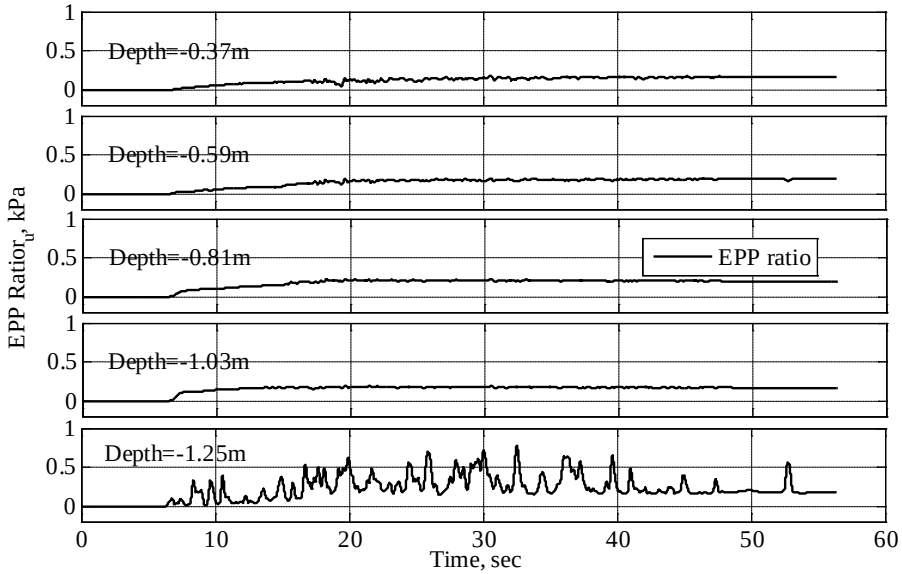

Figure 2.31. EPP ratio time histories for Test Stage 3

Figure 2.32 shows that the frozen crust continued to move to the downslope side for about 1.1 cm, and the pile at the ground surface deflected an additional 9 mm. Due to sensor failure, no data were available from the LVDT, located 0.06 cm above the ground surface.

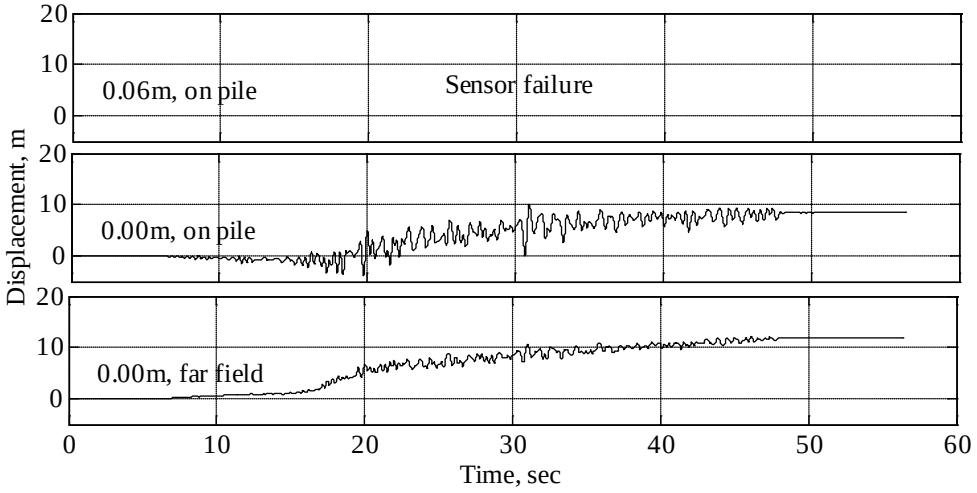

Figure 2.32. Displacement time histories for Test Stage 3

Figure 2.33 shows the bending moment time histories. Note the large residual bending moments from Test Stage 2. The bending moment in locations at or below -0.74 m remained almost constant in this stage due to formation of plastic hinges or unchanged pile deflection. At depth -0.24 m, one can observe a sudden increase to the pile yield bending moment at around 20 sec. The possible reason is that the large inertial force from the pile head formed more cracks and gap at the frozen crust-pile interface, and the pile continued to tilt. In return, the inertial force and the p-Δ effect due to pile tilting induced a large bending moment that yielded the pile to a depth of -0.24 m. The yielding of the pile also affected the plastic hinge already formed at -0.29 m in Test Stage 2 and reversed the bending direction.

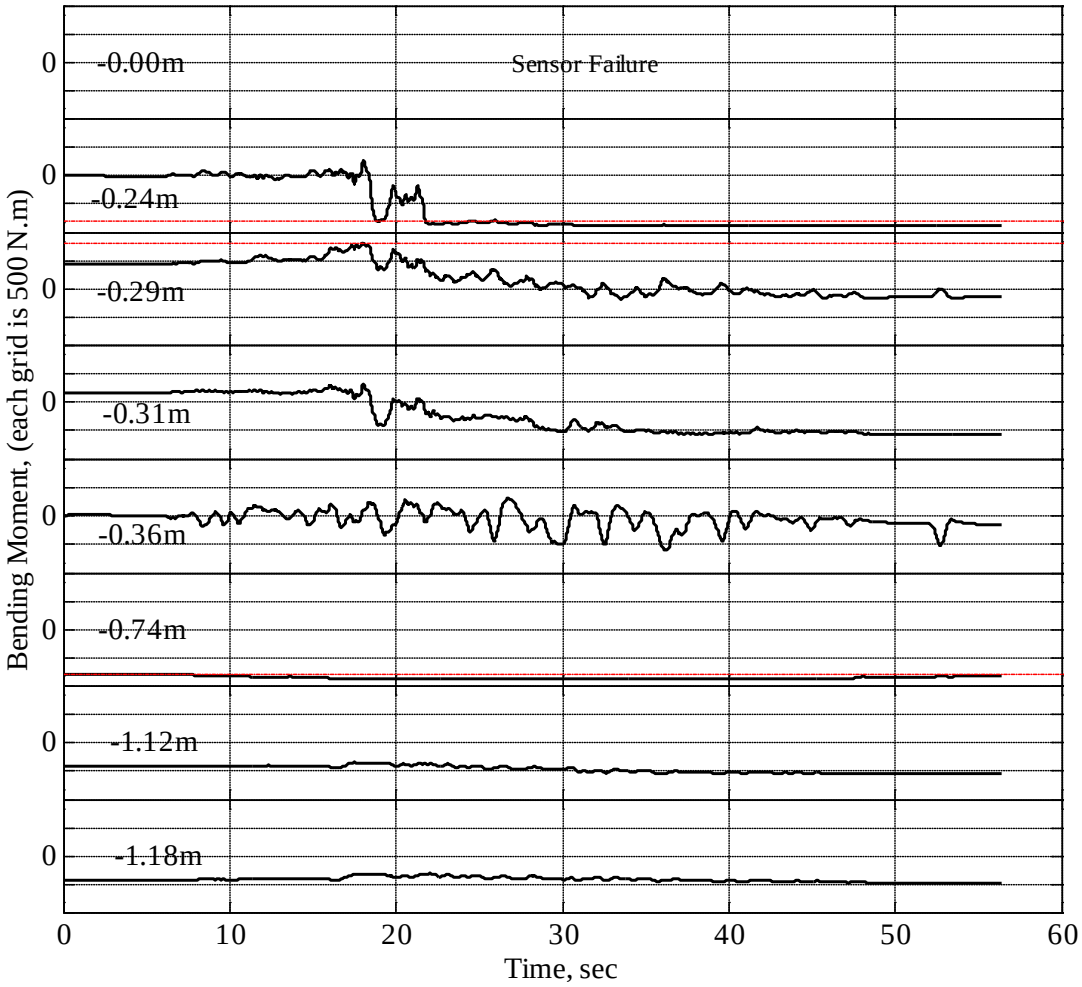

Figure 2.33. Bending moment time histories for Test Stage 3

2.5.5 Pile Deflection

Although limited pile deflection data are available from the experiment, the overall shape of the deflected pile at the end of Test Stage 2 can be derived qualitatively, as shown in Figure 2.34. Four triangles indicate the recorded or measured pile deflection data. The deflection shape from the pile top to the ground surface was defined by the known deflection data. No measured deflection data are available below the ground surface except at the bottom of the pile, which is fixed to the soil container. However, two locations can be identified to sketch the deflection shape. These locations are the interface of the frozen crust and loose sand, and -0.74 m (within the medium dense sand layer). As previously shown in Figure 2.30, bending moment data reveal a positive bending plastic hinge at the frozen crust-loose sand interface and a negative bending moment concentration at -0.74 m within the medium dense sand layer. Recalling the sign

conventions defined previously in this section, the pile deflection with two plastic hinges bending in opposite directions can be sketched, as shown in Figure 2.34.

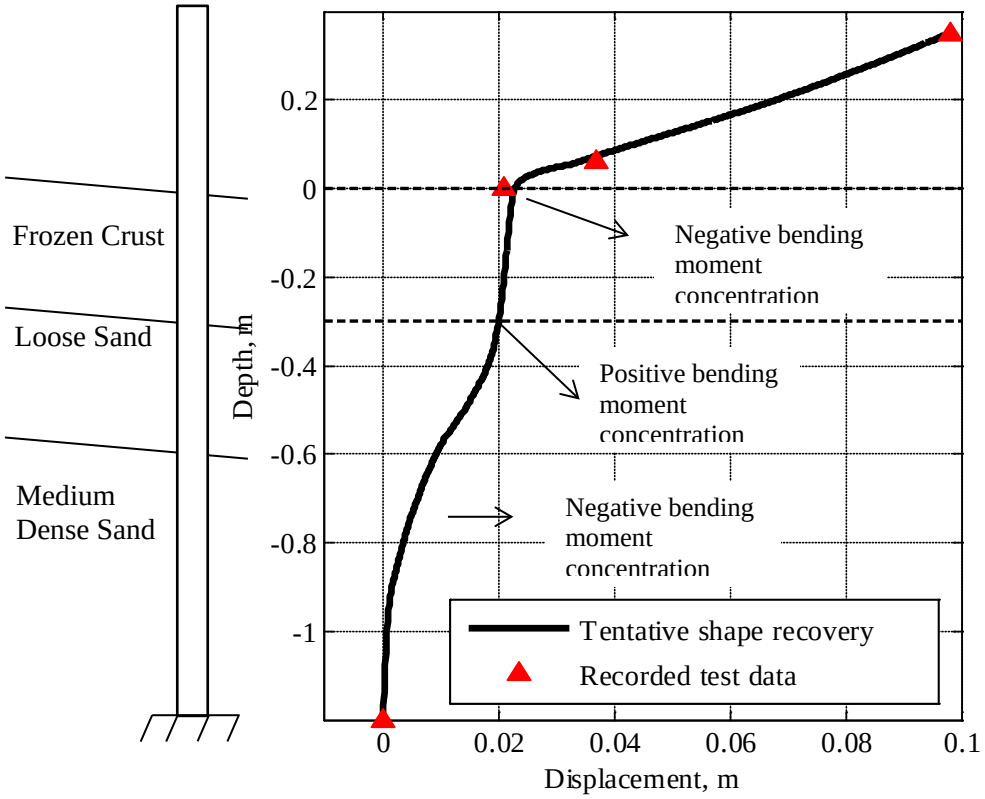

Figure 2.34. Deformed shape estimated by observation and measurement

2.6 Summary and Discussion

2.6.1 Summary

A model pile embedded in loose to medium dense sands underlying a frozen ground crust simulated by cemented sands was constructed and tested on a shake table to investigate the frozen ground crust-pile interaction during liquefaction-induced lateral spreading. Partial liquefaction was induced in the sands, and lateral spreading of 2.1 cm was induced in the frozen ground crust for loading Stage 2. The following conclusions are based on recorded data and observations made during the experiment:

1. Cemented sands can be used to simulate the frozen ground crust. After wet curing for about 72 hours, the properties of cemented sand specimen demonstrate mechanical properties similar to those of frozen soils reported in literature.

2. Partial liquefaction was induced during the experiment with excess pore pressure ratio in the range of 30% to 60%. Water was observed spilling out from the gap formed between the frozen crust and pile. Considerable ground crust lateral spreading, that is, 2.1 cm or 40% of the pile diameter, was induced in Test Stage 2.
3. Test data show that the shaking formed two plastic hinges in the model pile. One plastic hinge, located at the frozen ground crust-loose sand interface, started to form at the occurrence of the first PGA. The other, located in the partially liquefied medium dense sand layer, started to form at the occurrence of the second PGA, when the lateral spreading of the frozen ground crust reached its maximum value.
4. The plastic hinge at the frozen ground crust-loose sand interface formed because of the large distributed load (soil resistance) induced by the frozen ground crust; the plastic hinge in the partially liquefied medium dense sand layer formed by lateral spreading of the ground crust.

2.6.2 Discussion

There were certain limitations in this experiment due to budget constraints and the shake table test facility that was used. However, the findings are valid despite these limitations. They include:

1. A welded steel box, instead of a laminate box, was used as the soil container. The steel box may cause seismic wave reflection at its boundaries. The approach used to minimize the reflection was to glue seismic wave absorption material such as rubber mat on the inside surface of the box. Coe et al. (1985) found that rubber mats have the desirable damping characteristics to help attenuate seismic waves.
2. Both the soil domain and the pile are in small scale, and the force and displacement obtained from the experiment cannot be scaled to a full-size model. However, the mechanism of the frozen ground crust-pile interaction under liquefaction-induced lateral spreading condition is valid, and the results obtained from this experiment can be used to validate numerical approaches, as presented in Chapter 3.
3. A bridge superstructure constraint was not modeled in the experiment. Only the inertial interaction with a bridge deck was simulated by a lumped mass. Thus, any constraint provided by bridge superstructure that would reduce the lateral deformation is not considered in the model.

CHAPTER 3 VALIDATION OF NUMERICAL MODELS

3.1 Introduction

The confidence of nonlinear finite element (FE) analyses hinges on the calibration or validation of the computer model. Physical data from either case histories or physical model tests can be very useful in this process. Solid-fluid coupled three-dimensional FE modeling is a complex dynamic analysis based on constitutive soil models. This chapter presents validation of the capability of solid-fluid coupled FE modeling in capturing the essence of the frozen ground crust-pile interaction under liquefaction and lateral spreading. The beam-on-Winkler-foundation (BNWF or *p-y*) method is widely used in practice as a simplified approach. By applying a newly developed frozen soil *p-y* model (Li 2011), we attempt to model the frozen ground crust-pile interaction under liquefaction and lateral spreading with the *p-y* method and evaluate the effectiveness of the simplified approach in modeling this complex problem based on experiment data.

3.2 Finite Element Modeling of the Shake Table Experiment

3.2.1 Model Description

3.2.1.1 Finite Element Platform

Solid-fluid coupled FE modeling has been applied to study soil-pile interaction during earthquake shaking. The Open System for Earthquake Engineering Simulation (OpenSees), which has emerged as an effective research tool for studying dynamic soil-pile interaction (Mazzoni et al. 2006), has been applied to study the performance of the soil-pile system subjected to earthquake loading. A graphic user interface, OpenSeesPL (http://cyclic.ucsd.edu/openseespl), developed for conducting soil-pile interaction analysis based on OpenSees, was used for pre- and post-processing of the soil-pile FE model.

3.2.1.2 Finite Element Model

Due to symmetry, only half of the soil-pile system was modeled. The final mesh is shown in Figure 3.1. Soils including the pore fluid were modeled by the eight-node brick u-p element; the steel-pipe pile was modeled by the nonlinear beam-column element and fiber section. The elastic beam column element was used to model rigid links to couple the soil and pile elements and take into account the pile size effects. A shear-beam boundary was used to model the boundary condition of the soil container.

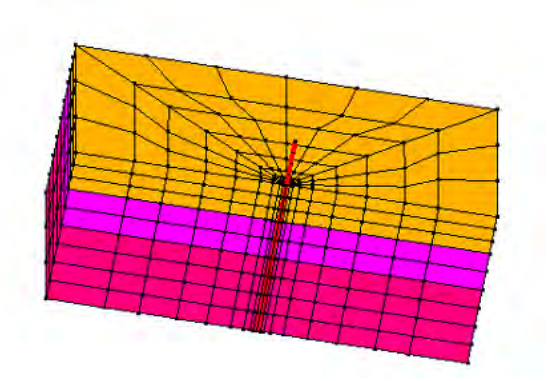

Figure 3.1. Half FE mesh of the soil-pile system

3.2.1.3 Constitutive Model for Soil Liquefaction

Saturated soil consists of solid particles and pore fluid. During earthquake shaking-induced shear loading, the soil skeleton goes through complex contraction and dilation processes and generates excess pore pressure (EPP), which leads to soil liquefaction when the EPP exceeds the hydrostatic pore pressure before the earthquake loading. Given a slope angle on the ground surface, even if very mild, the shear force along the slope due to gravity drives the non-liquefied ground crust downslope and causes lateral spreading. Soil constitutive models can model the complex interaction between the soil particles and the pore fluid including dilation and contraction effects. In this study, soil was modeled as solid-fluid coupled material based on Biot's theory of porous medium (Mazzoni et al. 2006). Each node of a soil element has four degrees of freedom: three for solid displacement (u_x, u_y, and u_z) and one for fluid pressure (p).

The constitutive model for cohesionless soil (Parra 1996; Yang and Elgamal 2002; Elgamal et al. 2003) implemented in OpenSees was used to model unfrozen sands. This model was developed based on the multi-yield-surface plasticity theory (Prevost 1985), and its yield surfaces are depicted in Figure 3.2. In this model, emphasis was on controlling the magnitude of cycle-by-cycle permanent shear strain accumulation in clean medium dense sands (Yang and Elgamal 2002; Yang et al. 2003; Lu et al. 2006). Special attention was given to the deviatoric-volumetric strain coupling (dilatancy) under cyclic loading (see Figure 3.3), which causes increased shear stiffness and strength at large cyclic shear strain excursions (i.e., cyclic mobility). In OpenSees, this model is identified as "PressureDependMultiYield." The parameters used in the soil constitutive model in this study are generic data for clean sand, available in OpenSeesPL.

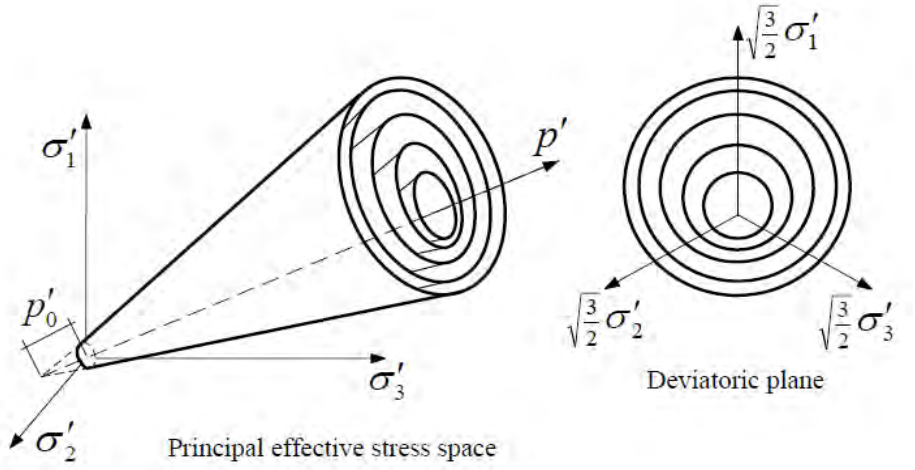

Figure 3.2. Multi-yield surfaces in principal stress space and deviatoric plane

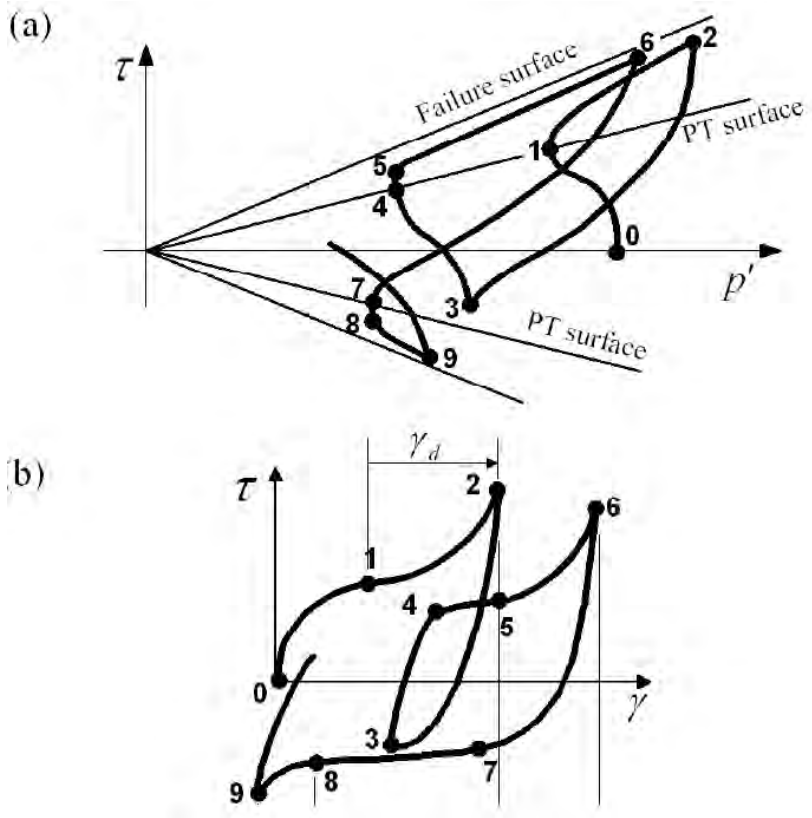

Figure 3.3. Shear-effective confinement and shear stress-strain response

No material model is readily available in OpenSees for modeling frozen soils. Note that low confining pressure has little effect on the compressive strength or axial strain at failure (Baker et al. 1982; Vinson et al. 1983), and seasonally frozen ground crust typically occurs at the top few feet. Thus, frozen soil may be satisfactorily modeled by pressure-independent models such as

those for cohesive soils (e.g., clay) with appropriate parameters (Yang et al. 2012). This study used the "PressureIndependentMultiYield" material in OpenSees to model frozen crust. PressureIndependentMultiYield is a nonlinear hysteretic kinematic plasticity material model (Parra 1996; Yang 2000; Yang et al. 2003) with a von Mises multi-surface (Iwan 1967; Mroz 1967). This constitutive model was used to simulate monotonic or cyclic response of materials whose shear behavior is insensitive to the confinement change. Figure 3.4a and b illustrate pressure-independent yield surfaces and shear stress-strain response, respectively.

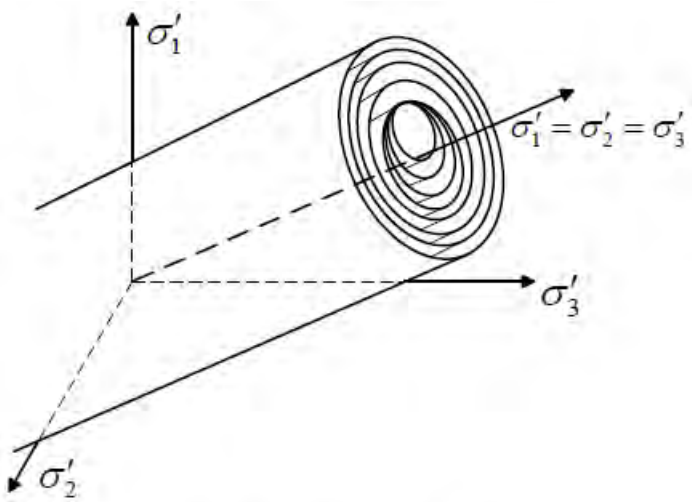

(a) Von Mises multi-surface.

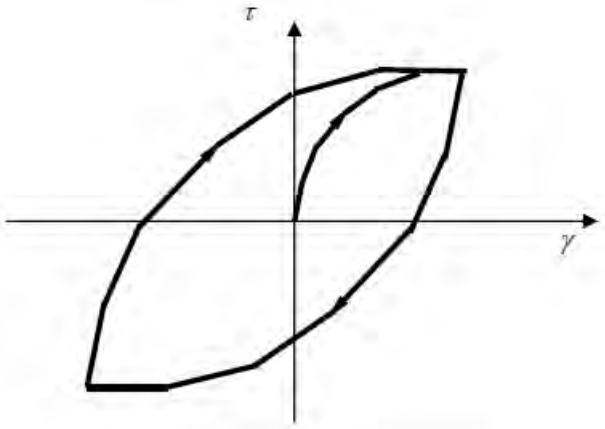

(b) Hysteretic shear response.

Figure 3.4. The von Mises multi-surface kinematic plasticity model

3.2.1.4 Steel Model

Steel material was modeled by the uniaxial bilinear steel material model with kinematic hardening and optional isotropic hardening described by a nonlinear evolution equation (Mazzoni et al. 2006); this material is named “Steel01” in OpenSees. Figure 3.5 shows the stress-strain relationship. The steel used in this experiment has the following mechanical properties: Young’s modulus of 200 GPa, yield strength of 235 MPa, and a strain-hardening ratio of 0.005.

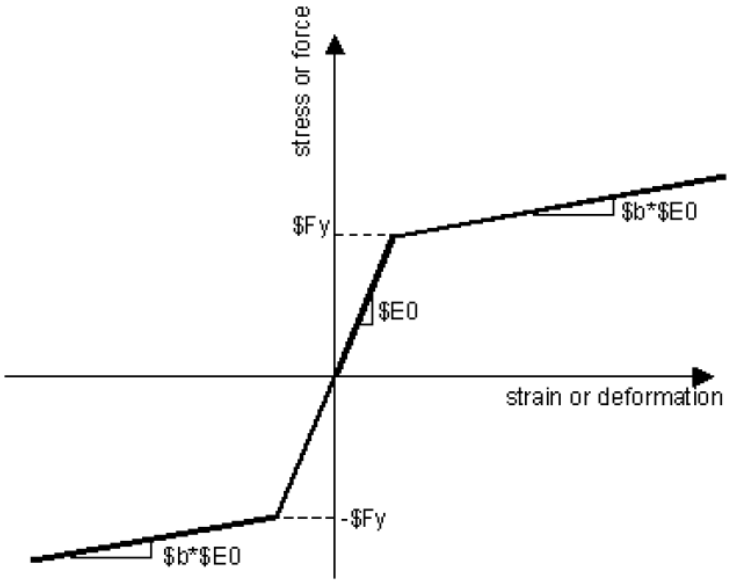

Figure 3.5. Stress-strain relationship of the Steel01 material

3.2.1.5 Base Input Motion

As presented in Chapter 2, the experiment was loaded in three stages. Stage 1, which consisted of short-duration and low-PGA excitations, checked the data acquisition system; Stage 2 used the 2011 Tohoku Earthquake as the base input motion; Stage 3 used the amplified “Japan Part 1” as the input motion. Considering Stage 1, loading induced little soil and pile deformation. Stage 3 loading had considerable residual pile deflection and bending moment carried over from the previous loading stage. This study chose to model the Stage 2 experiment.

Stage 2 loading was a horizontal motion recorded by the Japan nation-wide strong-motion seismograph network (K-NET) at the Hachimori station during the 2011 Tohoku Earthquake (see Figure 3.6). Note that two peak ground accelerations occurred during the earthquake. The only difference in base motion between the FE modeling and the shake table experiment is that this

motion was input in two halves in the experiment, with a three-minute gap between the two segments, and it was input into the FE model as a single record with a gap. As mentioned in Chapter 2, the three-minute gap only caused a slight drop in excess pore pressure and an increase in pile deflection.

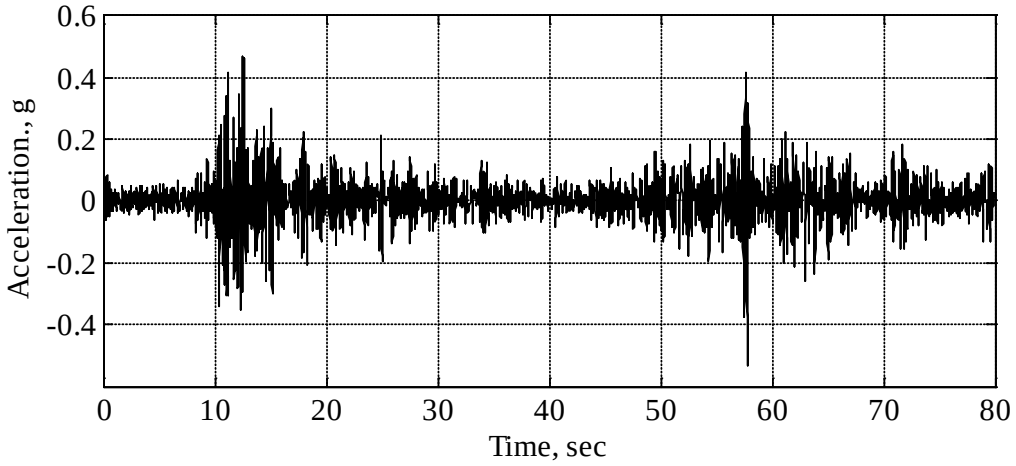

Figure 3.6. Base input motion from the 2011 Japan earthquake

3.2.2 Finite Element Modeling Results

3.2.2.1 Lateral Spreading of the Frozen Crust

Figure 3.7 shows the time history of lateral displacement of the frozen crust obtained from FE modeling. Although the timing of the sudden increase in lateral displacement is quite different from that observed in the experiment, the trends are similar to each other. The frozen crust was found to move about 2.4 cm (about 50% of pile diameter) in the downslope direction, which is slightly larger than the maximum lateral spreading observed in the experiment, that is, 2.1 cm.

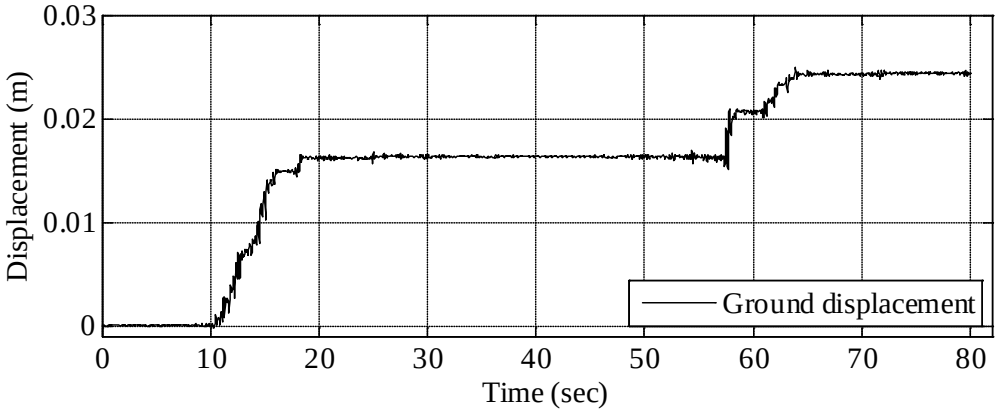

Figure 3.7. Ground surface displacement time history from FE modeling

3.2.2.2 Pile Response

Figure 3.8 presents a pile deflection snapshot at the end of shaking. Note that the pile underwent large deflection at the ground surface and bottom of the frozen crust due to the high stiffness and large strength of the frozen ground crust. The observed pile deflection data are also plotted in Figure 3.8 for comparison. Based on this snapshot, the tilting angle of the pile portion above the ground surface is about 10°, which is comparable to the tilt angle of 15° measured in the experiment.

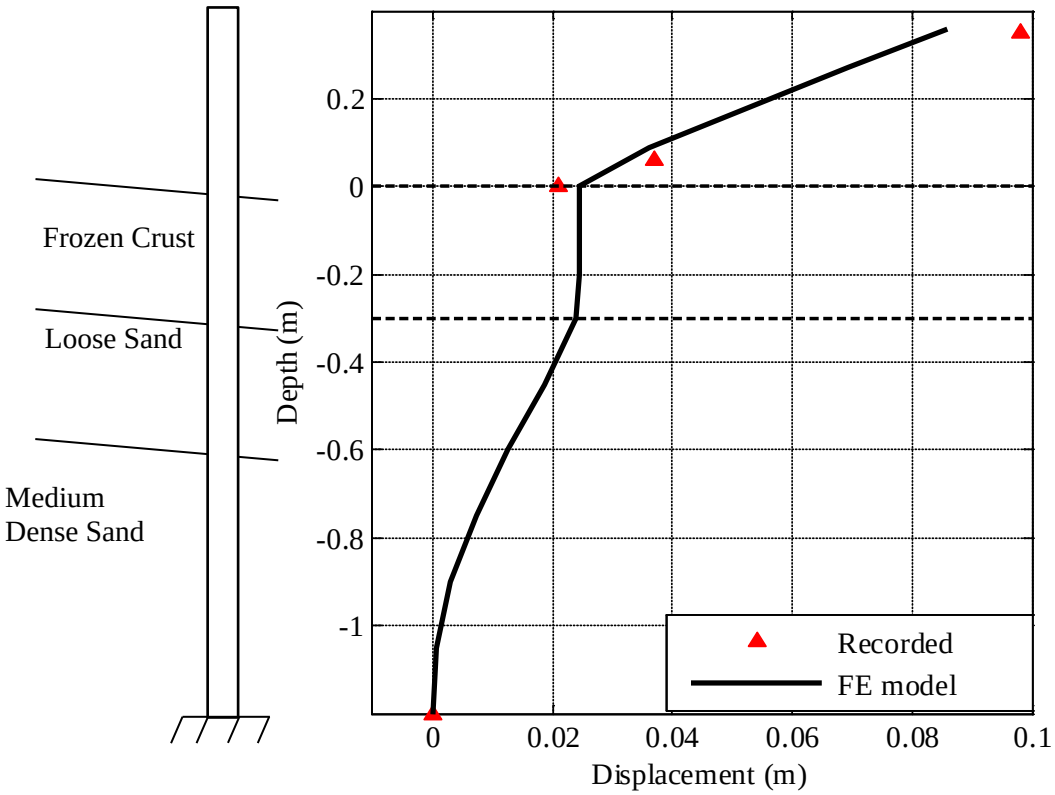

Figure 3.8. Snapshot of the pile deflection at the end of shaking from FE modeling

Figure 3.9 presents the bending moment envelope along the pile elevation and data from the experiment. This plot shows that solid-fluid coupled FE modeling can well predict the bending moment concentration at around -0.3 m in terms of both location and magnitude. For the plastic hinge at -0.75 m, the FE model correctly predicted the location, but slightly underpredicted the bending moment value.

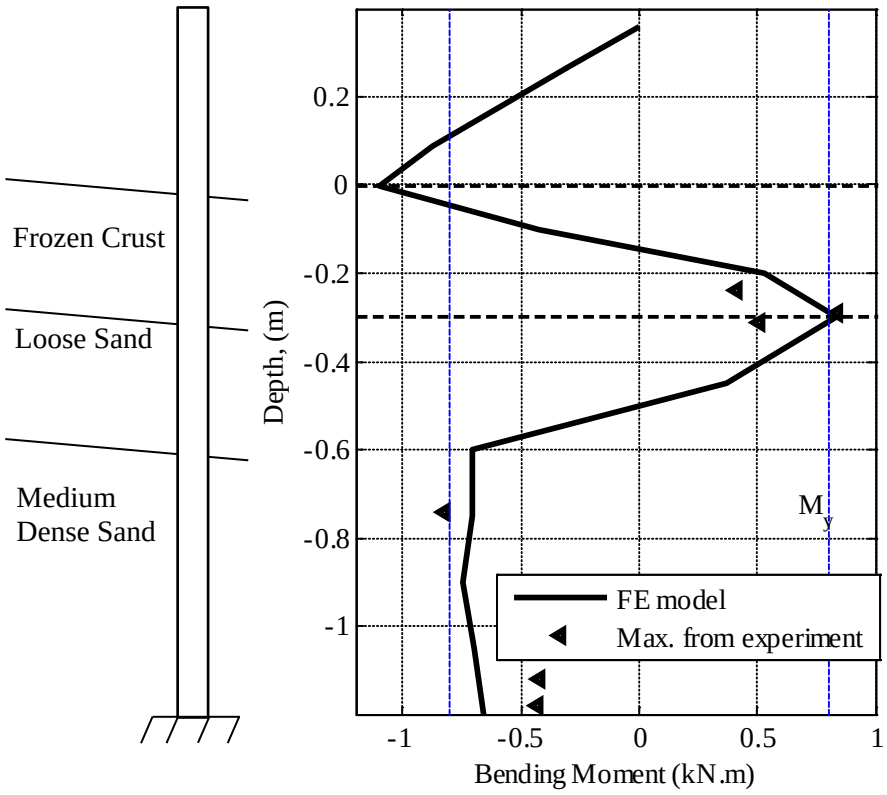

Figure 3.9. The maximum bending moment along the pile depth from FE modeling

For the plastic hinge predicted at ground surface, no experiment data are available for comparison. This plastic hinge is the combined result of inertial force, p-Δ effect and confinement of frozen crust. Based on field experiments and analyses, Li (2011) reported that this plastic hinge could occur at very shallow depth (less than 0.75 pile diameter). In the experiment, because of extensive cracking and damaging of the cemented sand, this plastic hinge moved from the ground surface to lower depth. The soil model adopted for frozen soil is incapable of modeling the crack and damage; hence, the FE model is unable to predict the location of this plastic hinge. However, we believe that this weakness is insignificant, since in reality much less cracking and gapping are expected due to higher strength and ductile, rather than brittle, behavior of frozen soils in the field. Further, the response of the pile at and above the ground surface is also relatively easy to analyze by structural-analysis methods.

In summary, the solid-fluid coupled FE model proved reasonably effective in predicting the two plastic hinges formed at -0.3 m and -0.75 m.

3.3 Modeling the Shake Table Experiment by the p-y Approach

3.3.1 Model Details

3.3.1.1 Model Configuration

As mentioned in Chapter 1, the static *p-y* approach has been successfully applied in modeling pile foundations subjected to laterally spreading ground crust induced by earthquakes. In addition, a simplified method such as the *p-y* approach is more attractive to practicing engineers. LPILE (http://www.ensoftinc.com) was used to perform this analysis. LPILE is a commercial program that analyzes laterally loaded piles using the *p-y* method. The soil lateral behavior was modeled as nonlinear springs with prescribed nonlinear lateral load-transfer (*p-y*) curves. Various soil *p-y* models and pile types are available in the software. LPILE also allows user-defined *p-y* curves and nonlinear pile sections. A flexible definition of pile head boundary conditions and loading is also allowed. By using LPILE, the pile was discretized into 80 nonlinear beam elements. The moment-curvature curve of the pile presented in Section 2.2.1 was input to LPILE. The *p-y* relations for regular sands are based on American Petroleum Institute (API) (1987).

3.3.1.2 Frozen Soil *p-y* Curve

Crowther (1990) carried out a study to analyze laterally loaded piles embedded in layered frozen soil and constructed frozen soil *p-y* based on frozen soil shear strength and strain criteria, but unfortunately, the *p-y* curves proposed had significant creep effect that made it inappropriate for analysis during earthquake loading. Li (2011) proposed a *p-y* curve based on back-calculated *p-y* values and existing *p-y* curves for weak rock (Reese 1997) and clay (Matlock 1970). This frozen soil *p-y* curve was used in the present analysis.

Figure 3.10 shows the *p-y* curve, which consists of a parabolic section and a constant section, as described by Equations 3.1 and 3.2.

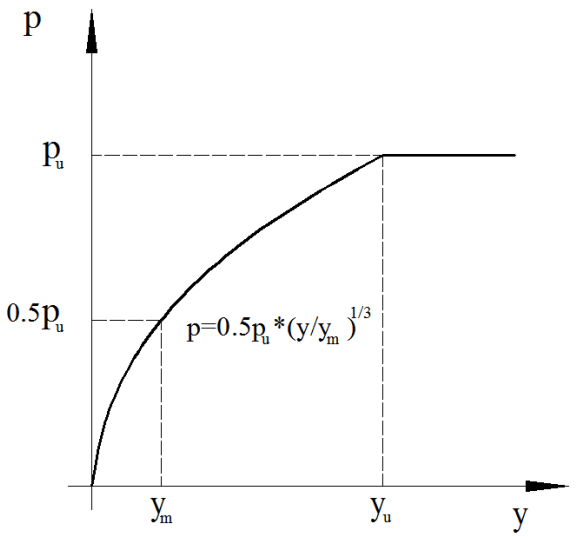

Figure 3.10. Sketch of the p-y curve for frozen soil

$$p = \frac{p_u}{2}\left(\frac{y}{y_m}\right)^{1/3} \quad \text{for} \quad y \leq y_u \qquad 3.1$$

$$p = P_u \quad \text{for} \quad y > y_u \qquad 3.2$$

where p_u is the ultimate resistance of frozen silt and can be derived through Equations 3.3 and 3.4; y_m is the pile deflection corresponding to half of the soil's resistance; p represents soil lateral resistance per pile unit length (kN/m); and y is the lateral deflection corresponding to each p.

$$p_u = q_u b\left(1.5 + 0.25\frac{x_{fs}}{b}\right) \quad \text{for} \quad 0 \leq x_{fs} \leq 12b \qquad 3.3$$

$$p_u = 4.5 q_u b \quad \text{for} \quad x_{fs} > 12b \qquad 3.4$$

where q_u is the compressive strength of the frozen silt, b is the diameter of the pile, and x_{fs} is the frozen soil depth below the ground surface.

$$y_m = k_m b \qquad 3.5$$

where k_m is a constant and equal to the strain at which 50% of the ultimate strength is developed. The value of y_u can be determined by solving for the intersection of Equations 3.1 and 3.2, and is shown in Equation 3.6.

$$y_u = 8y_m \tag{3.6}$$

Based on a series of compressive strength experiments by Haynes and Karalius (1977), the q_u was found to be related to frozen soil temperature (T) by Equation 3.7.

$$q_u = (0.145\frac{ksi}{MPa})\times(2.15 - 0.33T + 0.01T^2\ MPa) \tag{3.7}$$

For the shake table experiment in this case, since q_u is a constant for the frozen crust, the frozen soil *p-y* can be directly calculated based on Equations 3.1 and 3.2

3.3.1.3 Approximating Soil Strength Reduction in Liquefaction

As previously discussed, sand layers underwent partial liquefaction during the shake table experiment. The p-multiplier approach has been successfully applied to the drained *p-y* resistance of sand for approximating the effects of liquefaction on soil resistance reduction for design purposes (Wilson et al. 1998; Boulanger et al. 1997; JRA 2002). Based on centrifuge and shake table experiments of single piles and pile groups, Boulanger et al. (2003) provided recommendations on how to represent the equivalent *p-y* behavior of liquefied soils. For instance, the suggested value of p-multiplier varies from 0.1 to 0.5 depending on the standard penetration test (SPT) counts for inertial loading analysis. The authors concluded that peak lateral loads imposed on piles by laterally spreading nonliquefied soils could be reasonably predicted using existing *p-y* curves. For partially liquefied soil, Dobry et al. (1995) summarized a correlation of p-multiplier (also called degradation parameter C_u) and excess pore pressure ratio based on quasi-static cyclic displacement loading of a pile after liquefaction. Figure 3.11 shows this correlation.

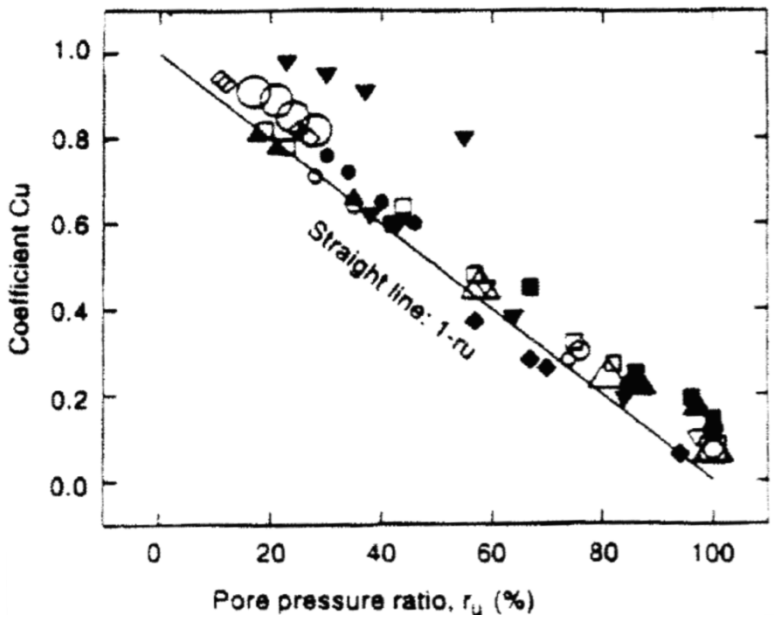

Figure 3.11. Degradation parameter C_u versus pore pressure ratio r_u from centrifuge tests

Recall the excess pore pressure ratio obtained from the experiment as presented in Figure 2.25. For this study, p-multipliers were evaluated using the excess pore pressure ratio according to Figure 3.11; its variation along the pile depth is shown in Figure 3.12.

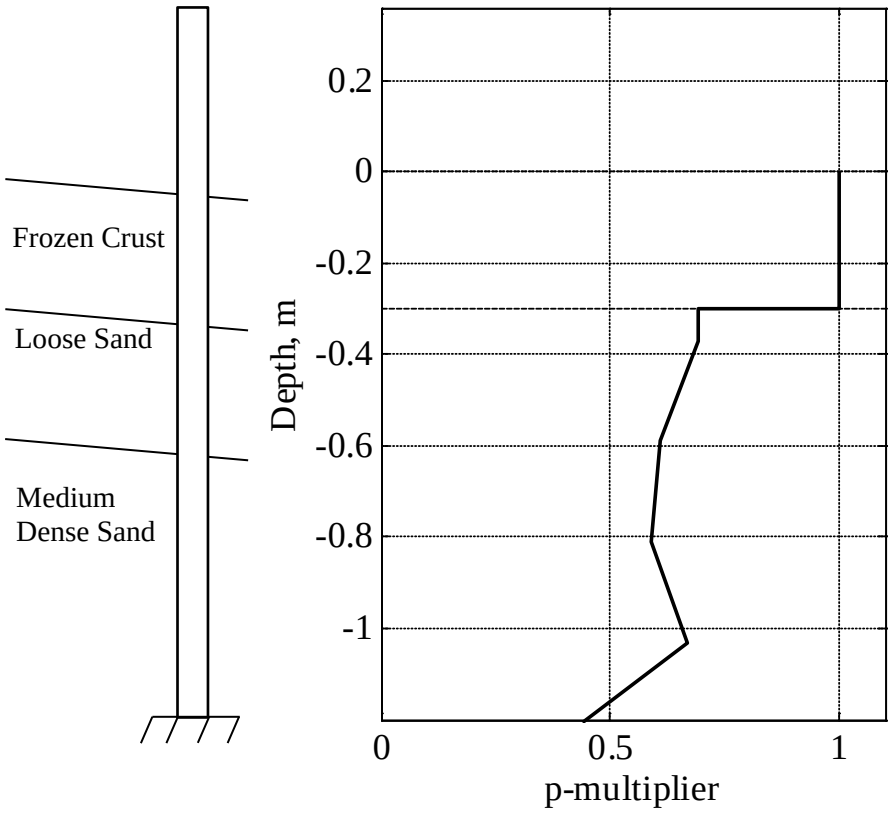

Figure 3.12. P-multiplier (C_u) variation along the pile depth

3.3.1.4 Loading

As discussed in Chapter 1, two methods are available for modeling lateral spreading loads: one, by applying a limit pressure directly on the pile nodes, and the other, by imposing free-field soil displacements. Brandenberg and Boulanger (2007) recommended the second alternative, that is, displacement-based BNWF pushover analysis.

The loading pattern was assumed constant in the nonliquefied crust and linearly decreasing in the liquefied sands. A sketch of the loading is shown in Figure 3.13. The lateral displacement recorded on the ground surface in Stage 2 of the shake table experiment, 2.1 cm, is used to determine the final displacement of the frozen crust. Inertial force was considered by applying half of the PGA-induced inertial force on the pile top.

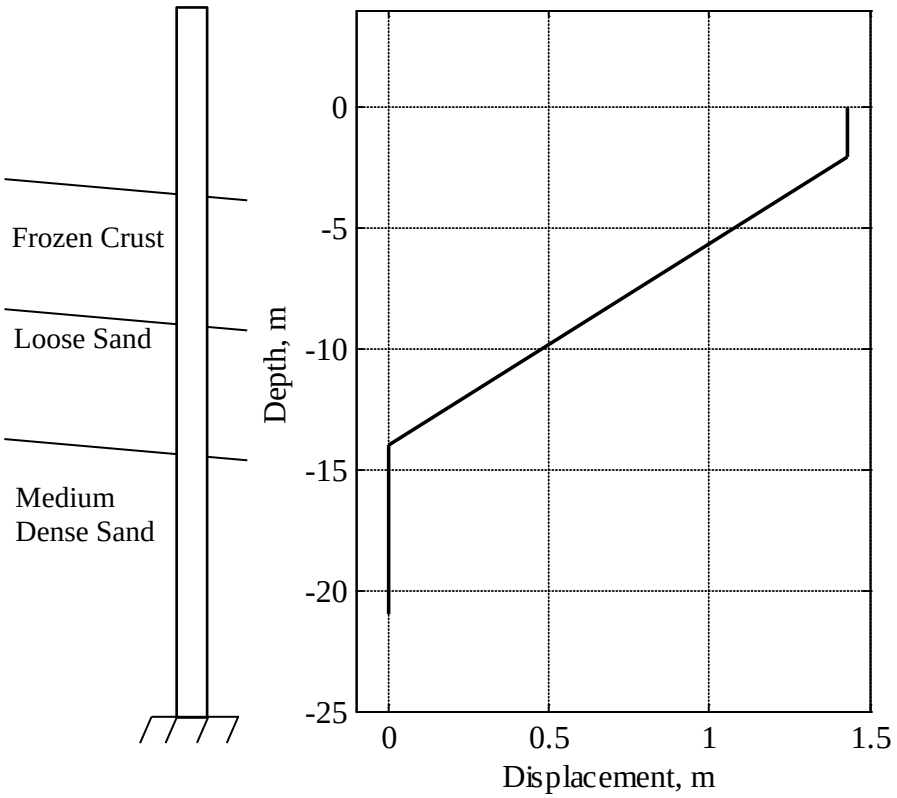

Figure 3.13. Lateral spreading load of the *p-y* approach for the shake table experiment modeling

3.3.2 Analysis Results

Figure 3.14 presents the *p-y* curves for several selected locations, including the bottom of the frozen crust (depth = -0.3 m), the interface of the loose sand and medium dense sand layer (depth = -0.6 m), and the bottom of the medium dense sand layer (depth = -1.2 m). Note in Figure 3.14 that the ultimate frozen soil resistance at a depth of -0.3 m is ten times that at a depth of -0.6 m and is 2.5 times that at a depth of -1.2 m, and the deflection required to attain ultimate resistance for the frozen soil is much smaller than that for unfrozen soil.

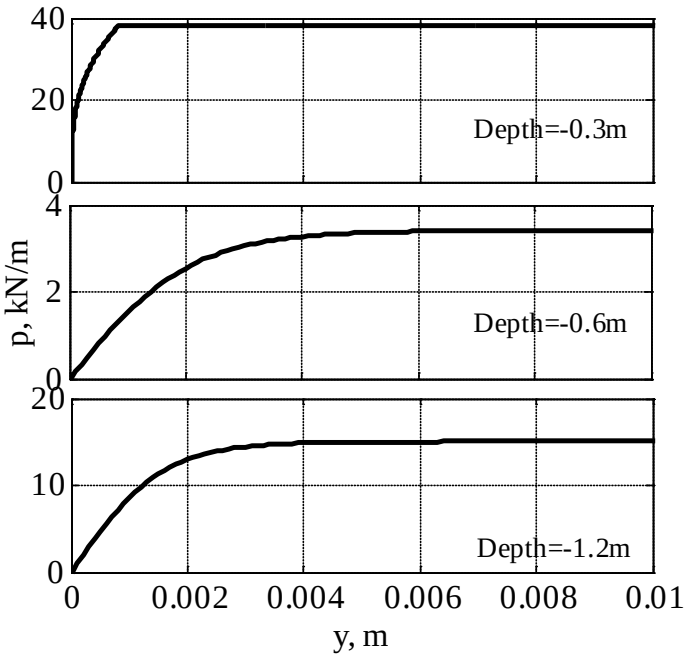

Figure 3.14. *P-y* curves for selected depths

Figure 3.15 presents the pile deflection predicted by the *p-y* approach. When compared with the experiment data, the *p-y* model predicted a similar deflection shape below the ground surface. However, the *p-y* model significantly underpredicted pile deflection above the ground surface. The reason for this difference in prediction is lack of inertial loading on the pile top. Further, a pseudo-static *p-y* analysis is incapable of modeling the effects of inertial force during kinematic loading. In the shake table experiment, it was observed that inertial force yielded the pile and induced permanent deformation.

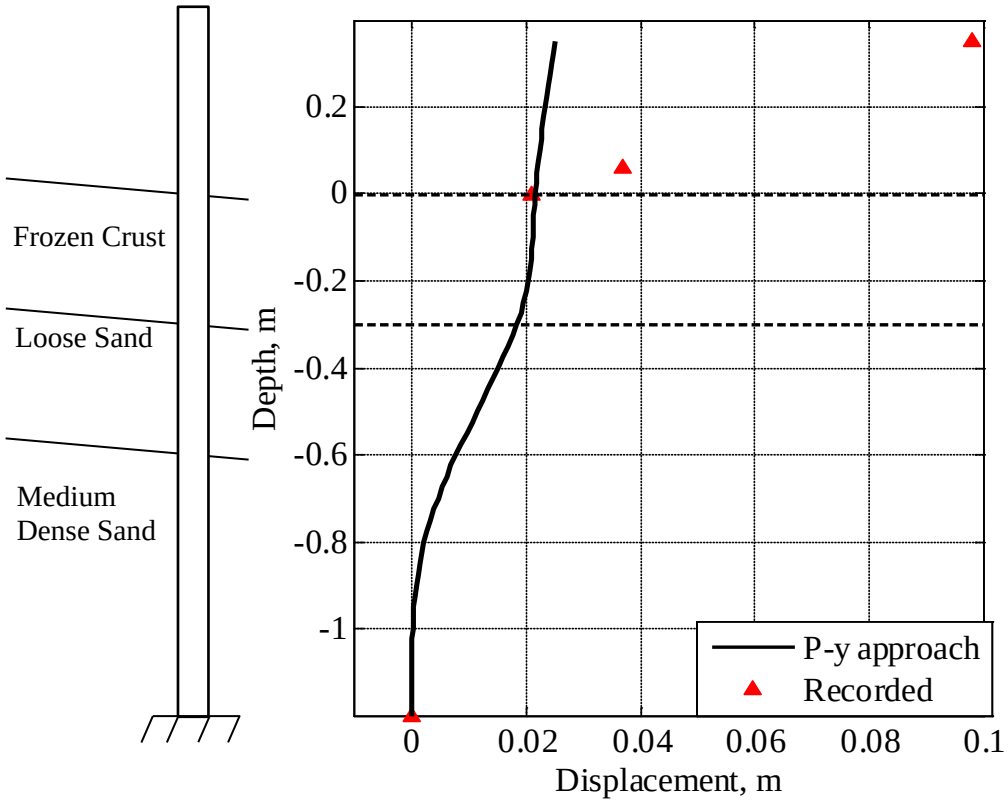

Figure 3.15. Pile deflection predicted by the *p-y* approach

Figure 3.16 presents the predicted bending moment profile by the *p-y* approach. The results obtained from the experiment and from FE modeling are also shown for comparison. Note in Figure 3.16 that the magnitude of the plastic hinge at the frozen soil-loose sand interface as observed from experiment data is well predicted by the *p-y* approach, with the location being slightly off. Similar to the FE model, the *p-y* approach was able to predict the location of the bending moment concentration within the medium dense sand layer, but underpredicted the magnitude of the maximum bending moment. The *p-y* approach was not able to predict the plastic hinge at the ground surface. However, this weakness is insignificant due to similar reasons given in Section 3.2.2.

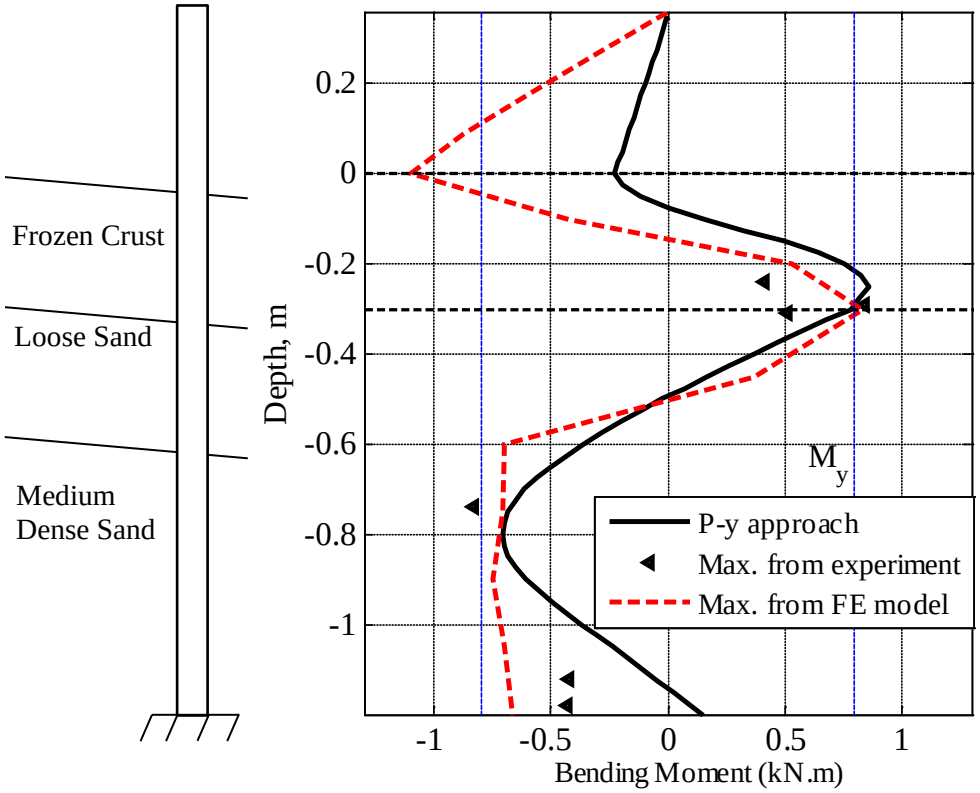

Figure 3.16. Pile bending moment predicted by the *p-y* approach

In summary, the *p-y* approach was able to predict the formation of plastic hinges at the frozen ground crust-loose sand interface and within the medium dense sand layer with good accuracy. This method also has the potential for use in predicting the response of full-size piles in liquefiable soils with a frozen crust.

3.4 Summary

Two approaches—solid-fluid coupled FE modeling and the *p-y* approach—were used to model the shake table experiment. By comparing the results from the two numerical approaches with those from the experiment, both models were confirmed as effective in predicting the pile response under lateral spreading of a frozen ground crust, particularly the formation of plastic hinges at the frozen crust-loose sand interface and within the medium dense sand layer.

CHAPTER 4 ANALYSIS OF SINGLE PILE PERFORMANCE USING SOLID-FLUID COUPLED FINITE ELEMENT MODELING

4.1 Introduction

The shake table experiment provided valuable data for the validation of two computer models for analyzing the pile performance of pile foundations embedded in a frozen crust under liquefaction and lateral spreading. This chapter applies the computer models to a selected bridge foundation and studies the impact of the frozen ground crust on the pile performance under similar conditions.

Based on a typical bridge from the ADOT&PF bridge inventory, supported on commonly used pile foundations that penetrate a liquefiable sand layer, two cases of the same soil-foundation system were created: one named “frozen case” (with a frozen ground crust) representing the typical winter conditions in Alaska, and the other named “unfrozen case” (with an unfrozen ground crust) representing the summer conditions in Alaska. Both models have liquefiable soils underlying the ground crust, and the ground crust has a small slope angle that is common in a bridge site.

Soil reactions and pile response are analyzed by solid-fluid coupled finite element (FE) modeling, and are presented for both the frozen and unfrozen conditions to illustrate the key characteristics of pile performance in liquefiable soils underlying a frozen crust.

4.2 Site Condition and Pile Configuration

4.2.1 Soil Profile

In this study, an idealized soil profile was created based on the general soil conditions in Alaska. The soil profile has a 2 m thick ground crust layer consisting of clayey silt that freezes in winter and thaws in summer (also referred to as the active layer). The active layer was subdivided into four sub-layers to accommodate the substantial variation of compressive strength and other mechanical properties due to temperature variation when it is frozen. The active layer overlies a 6 m thick loose sand layer that rests on a 6 m thick medium dense sand layer and a 7 m thick dense sand layer. A 3° sloping ground surface is assumed. All the soil layers except for the active layer are assumed saturated. Figure 4.1 presents such a typical soil profile.

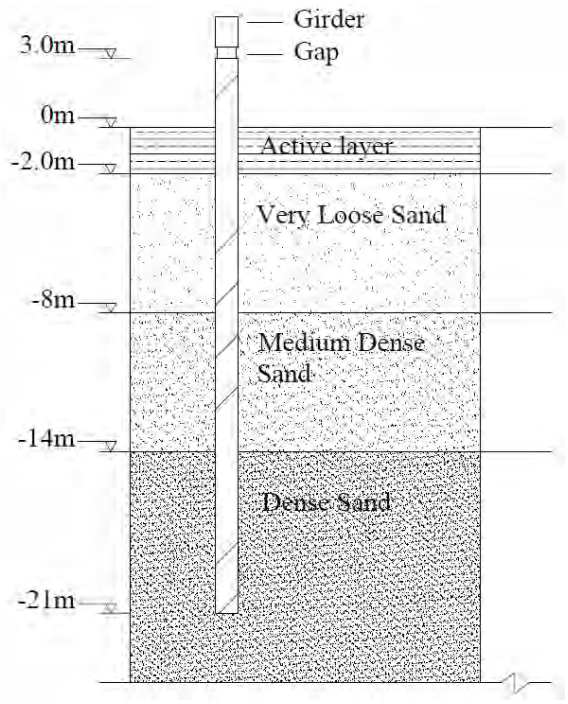

Figure 4.1. The soil-pile system of a typical bridge foundation system used in Alaska

Table 4.1 lists the parameters for the frozen and unfrozen status of the active layer. For the frozen case, mechanical parameters were selected from a series of unconfined uniaxial tests of naturally frozen soils obtained from a bridge site in Anchorage, Alaska (Yang et al. 2012). Frozen soil uniaxial compressive strength is very sensitive to soil temperature (Haynes and Karalius 1977). A temperature profile increasing linearly from -12° to 0°C was assumed for the frozen active layer. However, a constant average temperature was defined for each frozen soil sublayer. Table 4.2 lists the properties of the soil layers underlying the active layer used in this analysis.

Table 4.1. Summary of the soil properties for the active layer

Depth (m)	Status	Permeability (m/s)	Mass density (kg/m^3)	Shear modulus (kPa)	Bulk modulus (kPa)	Cohesion (kPa)	Friction angle (°)	Peak shear strain
0-0.5	-10.5°C	1.0×10^{-8}	1.8×10^3	2.5×10^6	5.4×10^6	2600	25	0.01
	Unfrozen	1.0×10^{-7}		7.5×10^4	2×10^5	50	30	0.1
0.5-1.0	-7.5°C	1.0×10^{-9}	1.8×10^3	2.1×10^6	4.6×10^6	2200	25	0.01
	Unfrozen	1.0×10^{-7}		7.5×10^4	2×10^5	50	30	0.1
1.0-1.5	-4.5°C	1.0×10^{-8}	1.8×10^3	1.7×10^6	3.8×10^6	1700	25	0.01
	Unfrozen	1.0×10^{-7}		7.5×10^4	2×10^5	50	30	0.1
1.5-2.0	-1.5°C	1.0×10^{-8}	1.8×10^3	1.3×10^6	2.9×10^6	1200	25	0.01
	Unfrozen	1.0×10^{-7}		7.5×10^4	2×10^5	50	30	0.1

Table 4.2. Summary of the soil properties for unfrozen layers

Depth (m)	Soil Type	Status	Permeability (m/s)	Mass density (kg/m^3)	Shear modulus (kPa)	Bulk modulus (kPa)	Friction angle (°)	Peak shear strain
2.0-8.0	Loose Sand	Unfrozen	6.6×10^{-5}	1.9×10^3	5.5×10^4	1.5×10^5	30	0.1
8.0-14.0	Medium Dense Sand	Unfrozen	6.6×10^{-5}	1.9×10^3	7.5×10^4	2.0×10^5	33	0.1
14.0-24.0	Dense Sand	Unfrozen	6.6×10^{-5}	2.1×10^3	1.3×10^5	3.9×105	40	0.1

4.2.2 Pile Configuration

Concrete-filled steel pipe (CSP) piles are widely used for constructing highway bridge foundations in Alaska. For this study, the pile dimensions and parameters were selected based on the North Fork Campbell Creek Bridge constructed in 2007 in Anchorage, Alaska. The total length of the piles is 24 m, with 3 m above the ground surface. The CSP pile has an outer diameter of 0.9 m and a wall thickness of 0.019 m. Ten steel reinforcing bars (#11) are evenly placed at 0.4 m away from the pile center, which represents a reinforcing ratio of 1.52%. Note that the CSP pile connects to the cap beam with a 5 cm gap by which only the reinforced-concrete part of the CSP pile is extended to the cap beam. Figure 4.2 shows both the CSP and the “gap” sections of the foundation. This gap section of the pile has a much smaller plastic hinging moment than the CSP section. The intention of the gap design is to prevent hinging in the pile cap beam. A moment-curvature analysis was conducted based on parameters

listed in Table 4.3 and Table 4.4, and the results are shown in Figure 4.3 and Figure 4.4. The first yield bending moment (M_y) and moment capacity (M_c) of sections were determined by the yield and rupture strains of the outmost steel fibers, respectively. In summary, the CSP section has a M_y of 6200 kN.m and M_c of 10,400 kN.m, and the gap section has a M_y of 1100 kN.m and M_c of 1900 kN.m.

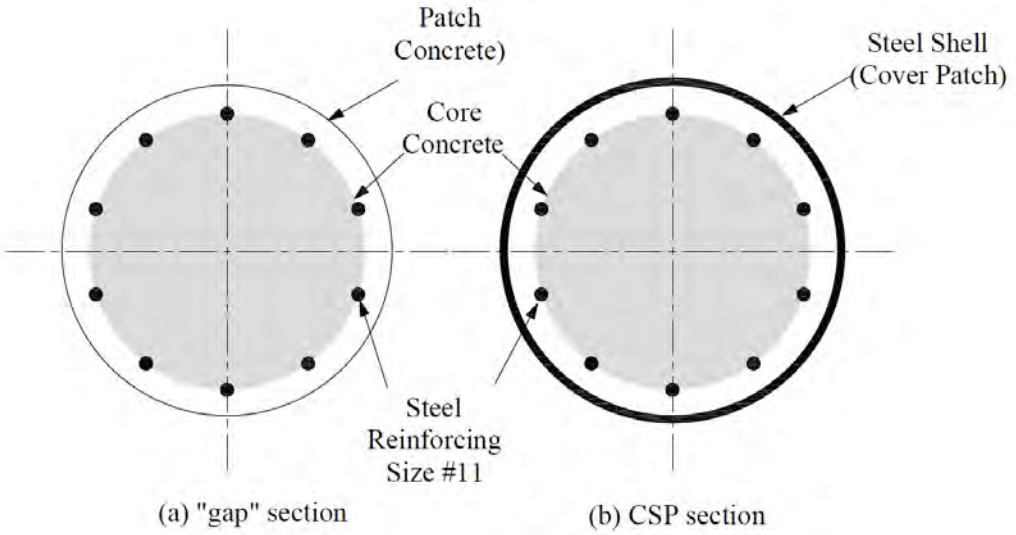

Figure 4.2. Configuration of the CSP and the “gap” sections

Table 4.3. Properties of the concrete material

Properties	Concrete type	Value
Unconfined compressive strength (MPa)	Patch / cover	45.5
	Core	93.5
Strain at maximum strength	Patch / cover	0.0025
	Core	0.0125
Crushing strength	Patch / cover	43.0
	Core	90.0
Strain at crushing strength	Patch / cover	0.004
	Core	0.02

Table 4.4. Properties of the steel material

Rebar	Yield strength (MPa)	470
	Yield strain	0.002
	Initial elastic tangent (GPa)	200
	Strain-hardening ratio	0.01
	Rupture strain	0.05
Steel Pipe	Yield strength (MPa)	335
	Yield strain	0.002
	Initial elastic tangent (GPa)	200
	Strain-hardening ratio	0.01
	Rupture strain	0.05

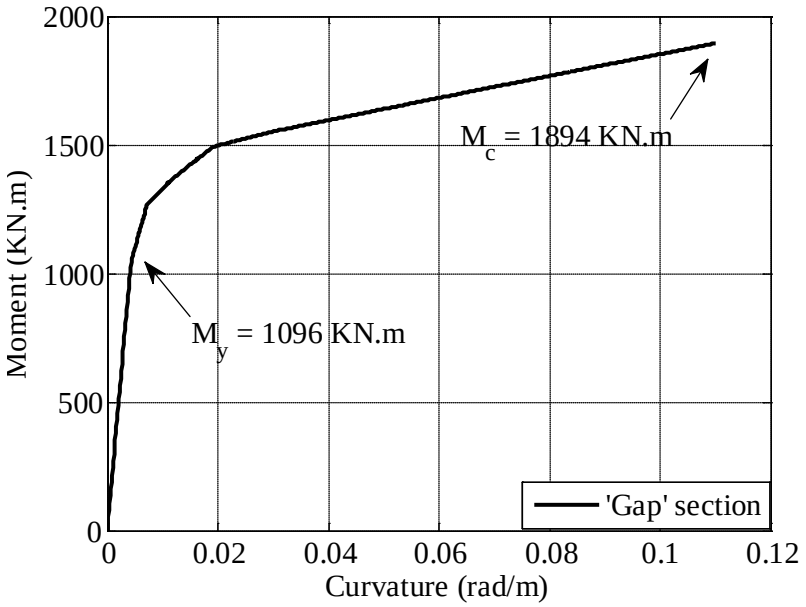

Figure 4.3. Moment-curvature curve for the “gap” section

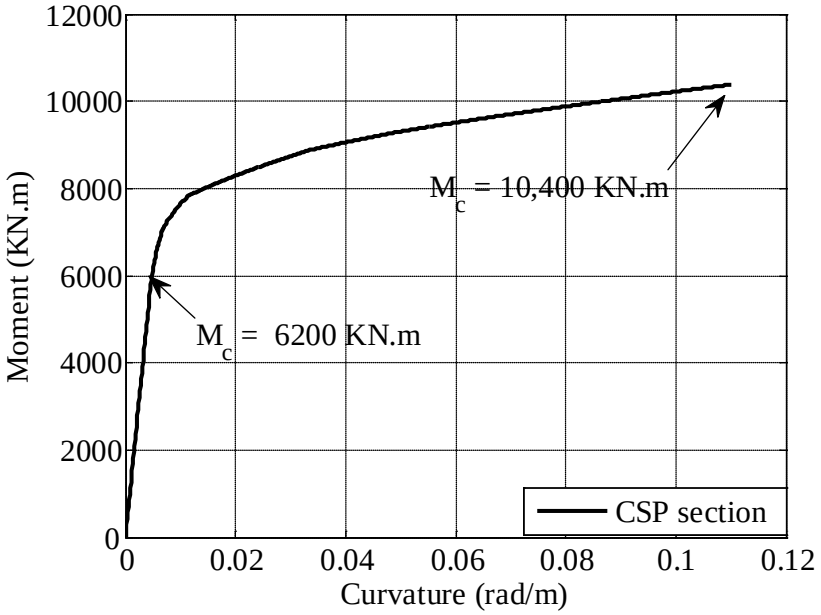

Figure 4.4. Moment-curvature curve for the CSP section

4.2.3 Base Input Motion

A horizontal motion recorded at Pump Station #10 along the Trans-Alaska Pipeline System during the 2002 Denali earthquake was used as the base input (Figure 4.5). Deep stiff soil underlies this site. The record has a duration of 82 seconds and a PGA of 0.3 g.

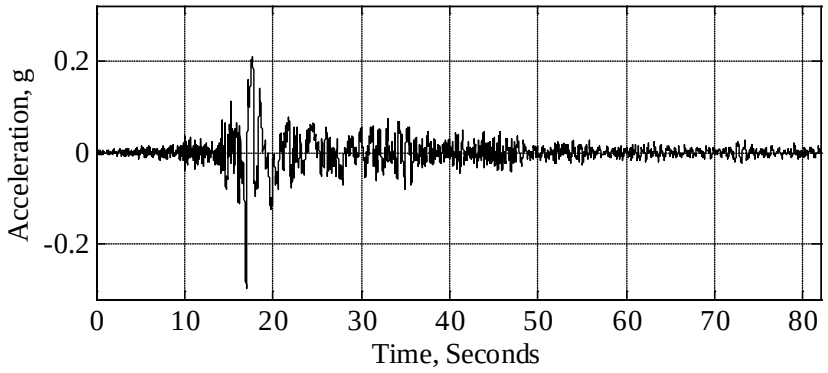

Figure 4.5. Base input motion from the 2002 Denali earthquake.

4.3 Finite Element Modeling of the Soil-Pile System

4.3.1 Model Configuration

The Open System for Earthquake Engineering Simulation (OpenSees) (Mazzoni et al. 2006) and the graphic user interface OpenSeesPL (http://cyclic.ucsd.edu/openseespl) were again used to perform the analysis. Due to symmetry, only half of the soil-pile system was modeled (see

Figure 4.6). The dimensions of the FE model are 50 m (longitudinal or X) × 25 m (transverse or Y) × 25.05 m (vertical or Z). The bottom of the soil domain is 3 m below the pile tip, and the input motion was applied in the X-direction at the base of the model. The soils were modeled by 1550 eight-node brick elements, and the pile was modeled by three-dimensional nonlinear beam-column elements with fiber sections. The pile elements were connected with the surrounding soil nodes with rigid links (i.e., elastic beam-column elements). The soil-pile interface was modeled as cohesionless material to mimic the gapping behavior. The following boundary conditions were defined: (1) the bottom of the soil domain was fixed in the X-, Y-, and Z-direction; (2) these front and back side nodes were fixed in the Y-direction and were free in the X- and Y-direction. The nodes on the left, right, and back sides were given equal degrees of freedom in all depths in the X- and the Z-direction to simulate vertically propagating shear waves; nodes above the groundwater table were fixed in pore water pressure (set to zero).

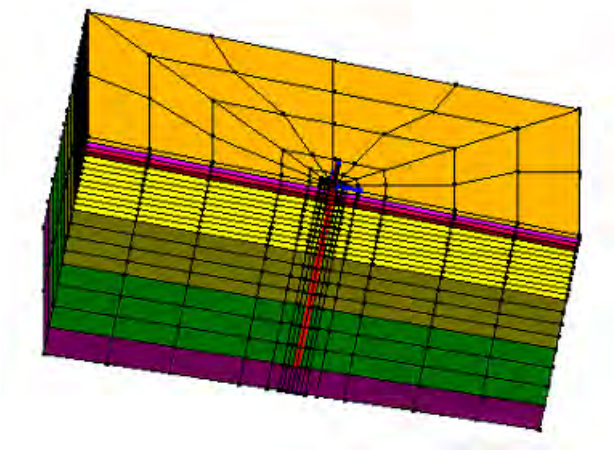

Figure 4.6. The FE mesh of the soil-pile system

4.3.2 Constitutive Models

The concrete was modeled by the uniaxial Kent-Scott-Park concrete material model with degraded linear unloading/reloading stiffness and no tensile strength according to the work of Karsan-Jirsa (1969). Constitutive models for steel, sandy soil, and frozen soil described in Section 3.2.1 were used in this analysis as well.

4.3.3 Consideration of Superstructure Constraint

The constraints of the bridge superstructure affect the frozen ground crust-pile interaction, and they are quite different from each other in the longitudinal and transverse directions. For a

typical design of highway bridges in Alaska, such as the one used on the North Fork Campbell Creek site, girders are discontinuous, and they are laid on top of the cap beam with shallow shear keys to prevent them from moving transversely. In the longitudinal direction, the horizontal constraint to the pile top would be the friction between the girder and the cap beam, which is very small. Due to lack of constraint in the rotation of the pile top and the cap beam, the pile top is free to rotate.

In the transverse direction, however, the constraint is quite different. Since the cap beam is almost rigid and supported by multiple piles, the cap beam as well as the pile top is not allowed to rotate in this direction. It seems that the deck would have some, but quite small, constraint to the pile top and cap beam in this direction as well, because the girders are discontinuous and there are gaps between the deck and the abutments. This horizontal constraint was considered by applying a linear-elastic spring. Assuming the bridge abutments are totally fixed and the bridge deck is in linear-elastic range, the total lateral stiffness of the deck was estimated to be 1×10^5 kN/m. Only 1% of the total stiffness, that is, 1,000 kM/m, was used for a single pile in the modeling, for reasons discussed above. The inertial interaction was not modeled due to the relative small impact of the superstructure mass in this case.

The ground crust typically laterally spreads toward the river channel because of the slope and the existence of an open surface. If a bridge intercepts with a river channel at right angles, the lateral spreading typically occurs in the longitudinal direction of the bridge. A bridge, however, does not always intercept with the river channel perpendicularly, such as in the case of a skewed bridge. Therefore, it is possible that lateral spreading could also occur in the transverse direction. In this research, the frozen ground crust was assumed to laterally spread in the transverse direction of the bridge, which represents a more dangerous case for the bridge substructure due to constraint of the bridge substructure and superstructure.

4.4 Results and Discussion

4.4.1 Unfrozen and Frozen Cases

Two three-dimensional FE models were constructed, with one model simulating winter conditions, when the active layer becomes frozen, and the other model simulating summer conditions, when the active layer becomes unfrozen. These models share identical dimensions, parameters (except for the active layer), and base input motion. Yang et al. (2012) indicate that

low temperature in winter can increase the strength of both concrete and steel, but this was not considered in the frozen case model.

4.4.2 Soil Response

4.4.2.1 Acceleration

Figure 4.7a and b present acceleration time histories along the longitudinal direction in the soil column at depths of 0 m, 4.67 m, 11 m, and 21 m for both unfrozen and frozen cases, respectively. One can observe from Figure 4.7a and b that at the dense sand layer, the acceleration time histories for both cases are very similar to base input motion, as presented in Figure 4.5. One can observe considerable changes as the motions propagate from the dense sand layer to the ground surface: more long-period components are present within the loose sand layer and in the ground surface, and the amplitude of acceleration decreases. The alteration of acceleration time histories including frequency and amplitude indicate liquefaction in the loose sand layer (Kostadinov and Yamazaki 2001).

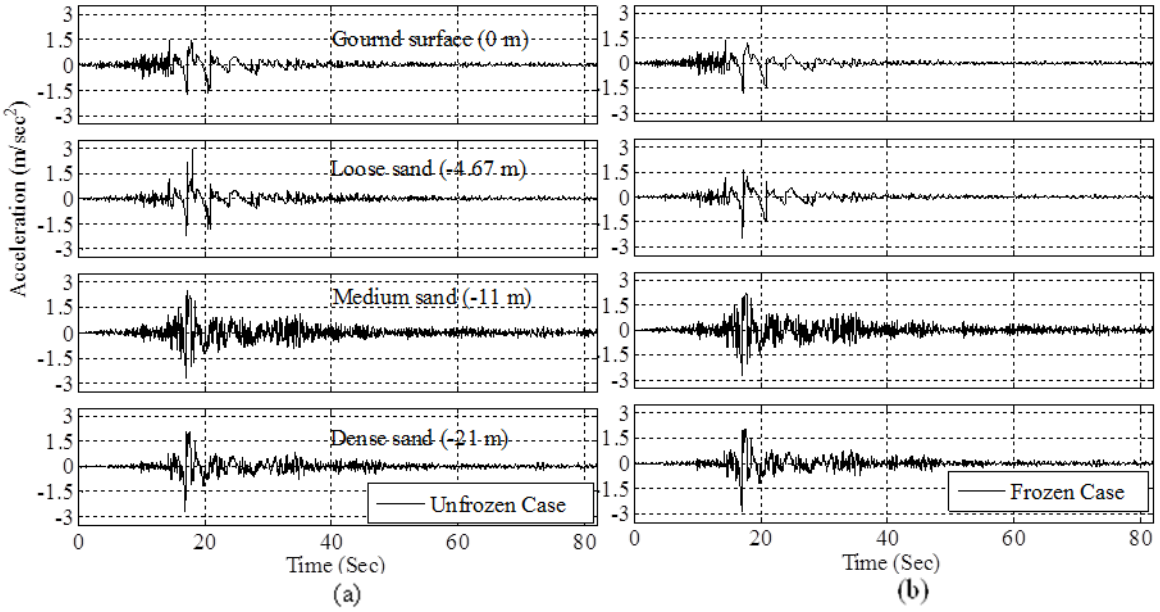

Figure 4.7. Acceleration time histories in the soil column for (a) unfrozen case and (b) frozen case

4.4.2.2 Excess Pore Pressure

Excess pore pressure (EPP) ratio (r_u) time histories for selected depths—4 m and 6 m (within the loose sand layer), 9.5 m and 12.5 m (within the medium dense sand layer), and 18.7 m and 21 m (within the dense sand layer)—are plotted in Figure 4.8 for both unfrozen (a) and

frozen (b) cases. Note that the r_u time histories and peak values are quite similar for both cases. Also, note that r_u ranges from 70% to 100% in the loose sand and medium dense sand layers, and ranges from 40% to 50% in the dense sand layer for both cases. This suggests that shaking-induced liquefaction is similar for both cases; the loose and medium dense sand layers were mostly liquefied, while the dense sand layer only underwent partial liquefaction. This finding echoes the conclusion that was drawn about liquefaction based on the observation of frequency and amplitude changes in acceleration time histories.

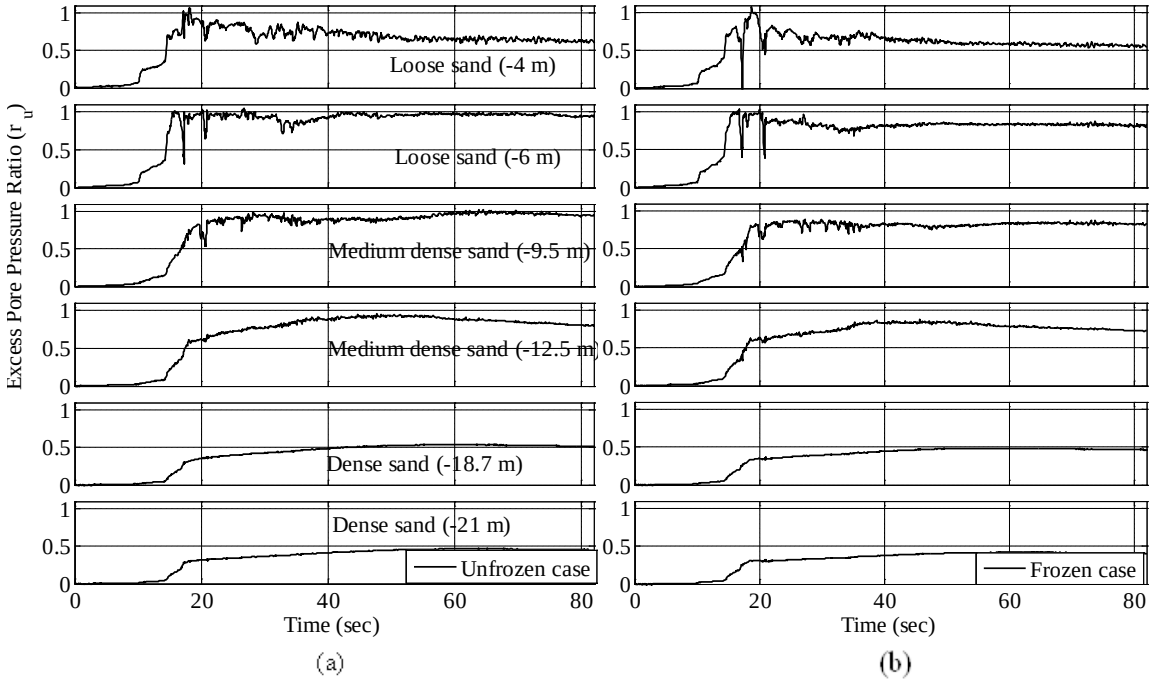

Figure 4.8. Excess pore pressure ratio in sand layers for (a) unfrozen case and (b) frozen case

4.4.2.3 Frozen Soil Shear Strain Time Histories

Frozen soil behavior is of key interest in this study. Figure 4.9 presents the strain rate time histories produced from two selected frozen soil elements: one located at 0.9 m (referred to as near-field) and the other at 18.7 m (referred to as far-field) away from the pile center at the depth of 0.89 m. The strain rate values from the near-field are much larger than the strain rate values from the far-field, obviously due to the frozen soil-pile interaction. Generally, the peak strain rate values in the near-field frozen soil elements are in the range of -3×10^{-3} to -7×10^{-3} per sec.

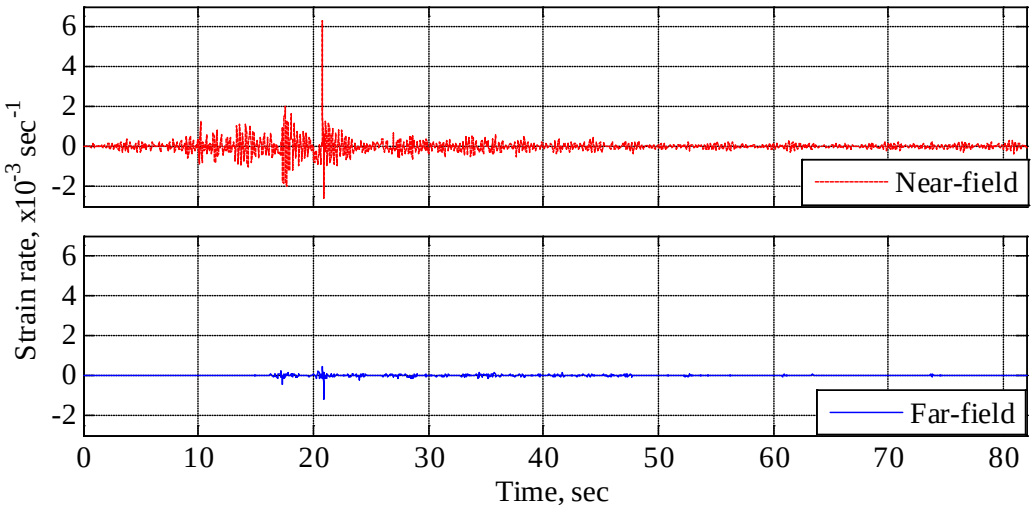

Figure 4.9. Strain rate time histories in the frozen soil

4.4.2.4 Ground Displacement

During the base excitation, the lateral resistance of the loose and medium dense sand layers was significantly reduced due to liquefaction. Because of the mild ground inclination (3°), a downslope driving shear stress component was imposed to the soil-pile system under gravity, which causes downslope lateral spreading during the earthquake. Figure 4.10a and b present the respective ground surface lateral spreading time histories for both cases. These time histories were displacements in the longitudinal direction recorded at a soil node that is 12.5 m away from the pile center to exclude pile-induced local strain/deformation on the frozen crust. The trends of lateral spreading for both cases are quite similar. At the end of base excitation, the final displacement was 1.53 m for the unfrozen case (see Figure 4.10a) and 1.43 m for the frozen case (see Figure 4.10b). The difference in ground crust lateral spreading between the frozen and unfrozen cases was 7%. The decrease in lateral spreading in the frozen case was likely caused by a slightly stronger pinning effect due to higher ground crust stiffness and strength than the unfrozen case. However, the difference is quite small, which will facilitate the comparison of the pile performance between these cases.

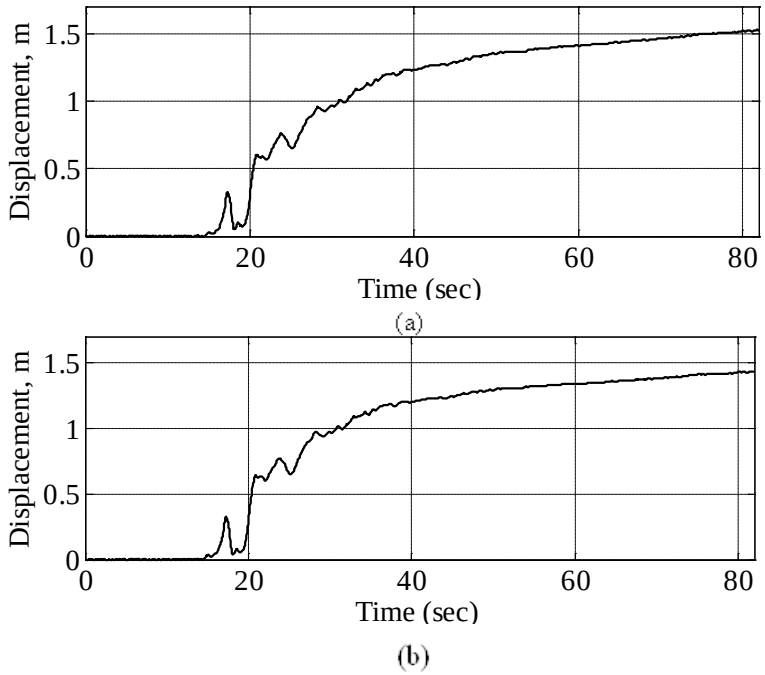

Figure 4.10. Lateral spreading time histories of the ground crust for (a) unfrozen case and (b) frozen case

Figure 4.11 shows the relative displacement between the ground crust and pile at the ground surface. Note in Figure 4.11 that the maximum relative displacement of the unfrozen case (see Figure 4.11a) is about 2 cm and that of the frozen case is about 0.1 cm (see Figure 4.11b). These values indicate the possible widths of the gap in both cases. Recall that the observed gap between the model pile and the simulated frozen ground crust in the shake table experiment was 10 mm (see Figure 2.28).

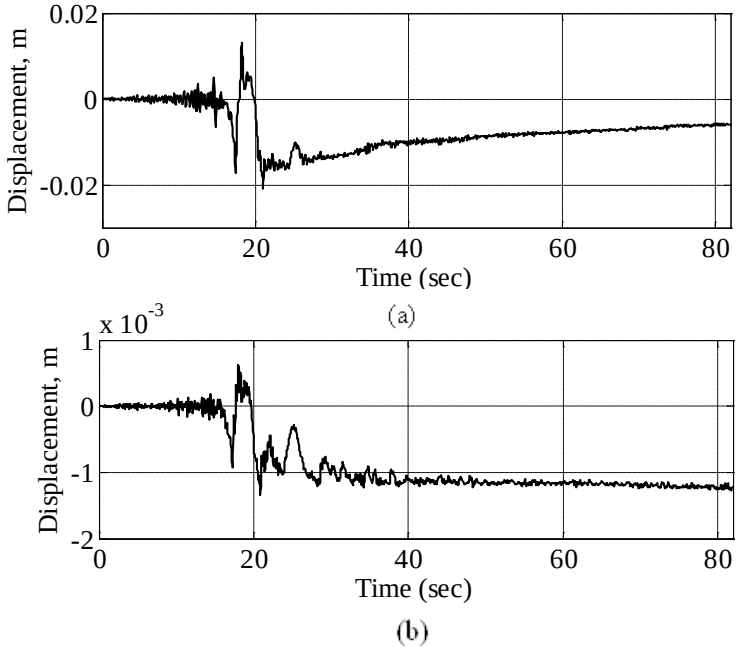

Figure 4.11. Relative displacement between the ground crust and pile on the ground surface for (a) unfrozen case and (b) frozen case

4.4.3 Pile Response

Figure 4.12 presents maximum pile deflection, rotation, bending moment, and shear force along the pile depth. One can see in Figure 4.12a that the deflection profiles for both cases are quite similar for the pile portion below the ground crust-loose sand layer interface. However, deflection profiles (see Figure 4.12b) for the pile above this interface are very different. The pile in the frozen case remained almost vertical due to the strong confinement of the frozen crust, while the same portion in the unfrozen case was able to rotate moderately. These different behaviors, which are reflected by the difference in pile rotation at this pile segment, further translate into the difference in bending moment profile. Due to the strong confinement of the frozen ground crust, a sharp increase in the pile rotation can be easily observed just below the frozen ground crust-loose sand interface, which translates into a large curvature and hence a bending moment concentration for the frozen case (see Figure 4.12c). The peak bending moment reaches 11,060 kN.m, exceeding the bending moment capacity (i.e., M_c = 10,400 kN.m) and indicating failure of the large CSP pile. For the unfrozen case, there is also an abrupt increase in rotation at the interface, but not as sharp as that observed in the frozen case. Corresponding to this abrupt increase in rotation, one can find a bending moment concentration at the interface. The peak bending moment in the unfrozen case is 9,390 kN.m, well exceeding the first yield

bending moment (i.e., M_y = 6,200 kN.m) but significantly less than the bending moment capacity. The bending moment differences between the frozen and unfrozen case are due to a greater plastic deformation demand and hinge rotation in the frozen condition (also refer to Figure 4.14). Not only are the demands greater, but also the moment gradient is much steeper, indicating a smaller plastic hinge zone.

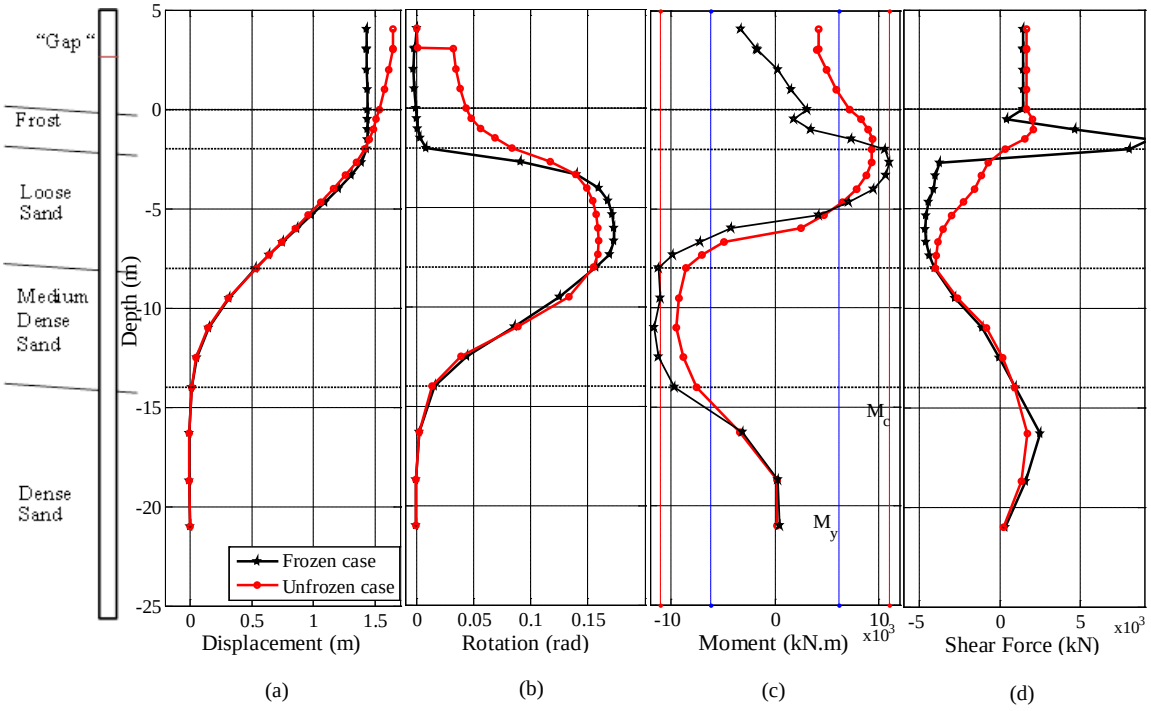

Figure 4.12. Maximum deflection, rotation, bending moment, and shear force for unfrozen and frozen cases

For both cases, one can observe a sharp change in pile rotation approximately in the middle of the medium dense sand layer, which translates into another bending moment concentration (referred to as lower plastic hinge). The maximum bending moment in the frozen case is 11,620 kN.m, exceeding the bending moment capacity and indicating failure of the large size CSP pile; that in the unfrozen case is 9,530 kN.m, which is below the bending moment capacity. Note that the center of the upper and lower plastic hinges is located at -2.7 m and -11.0, respectively. The bending moment time histories at -2.7 m and -11.0 m are shown in Figure 4.13a and b, which helps reveal the mechanism responsible for the formation of both the upper and lower plastic hinges. For the unfrozen case, the bending moment at both locations increases gradually with

ground crust lateral spreading (see Figure 4.10), and reaches its maximum value at around 50 sec. The time histories are almost identical, except that the sign is opposite. For the frozen case, a distinctly different trend can be observed in the bending moment for both locations. For the lower plastic hinge, the bending moment increases gradually in a similar trend as the unfrozen case. For the upper plastic hinge, the bending moment, however, oscillates rapidly around 19 sec. and reaches its maximum value around 20 sec., when the PGA of input motion occurs. This peak value is likely due to the large distributed load (soil resistance) of the laterally spreading frozen ground crust, as mentioned earlier. One can conclude that the lower plastic hinge was a direct result of the ground crust lateral spreading, and the upper plastic hinge was due to the large distributed load or soil resistance induced by the frozen ground crust. This conclusion is consistent with the conclusion drawn in Chapter 2 based on the analysis of the shake table experimental data.

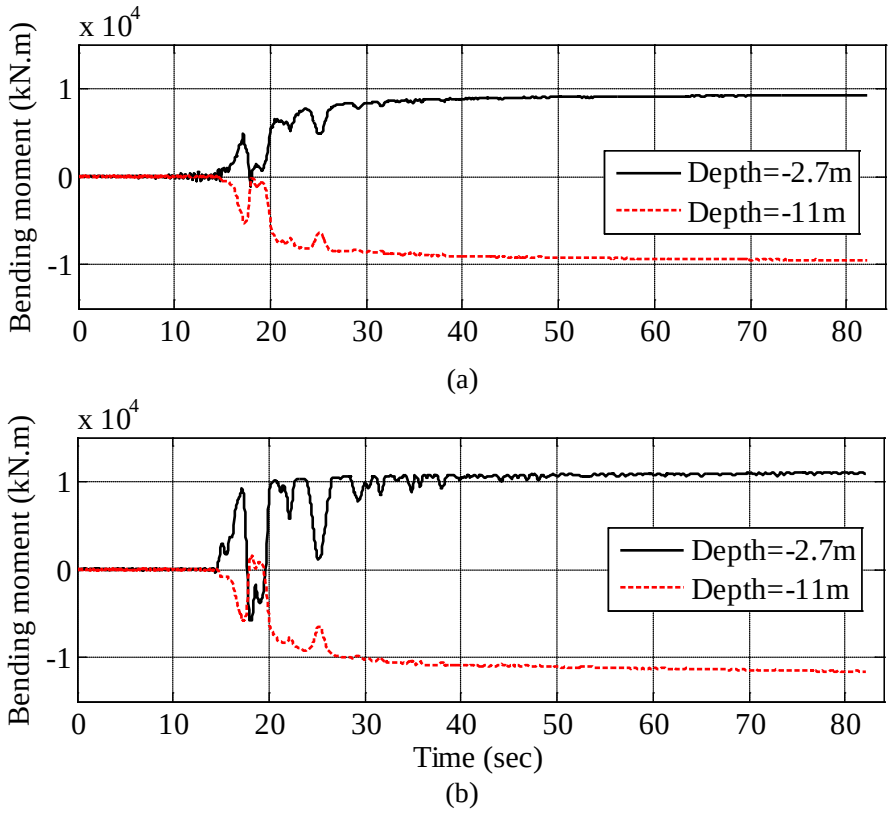

Figure 4.13. Bending moment time histories for the upper and lower plastic hinges for (a) unfrozen case and (b) frozen case

Since the pile underwent significant plastic deformation, pile bending moment values may not be very effective to indicate the significant difference in pile performance between frozen and unfrozen cases. Figure 4.14 presents the maximum curvatures induced along pile depth for both frozen and unfrozen cases. One can see from Figure 4.14 that the respective peak curvatures induced at the upper plastic hinge are 0.05 and 0.15 for the frozen and unfrozen cases; that for the lower plastic hinge are -0.06 and -0.19 for the unfrozen and frozen cases. It indicates that the curvature at either the upper plastic hinge or lower plastic hinge increases by 200% from unfrozen case to frozen case at the same lateral spreading. This shows that the pile is subjected to much greater hinge rotation/plastic deformation demand in the frozen case than in the unfrozen case.

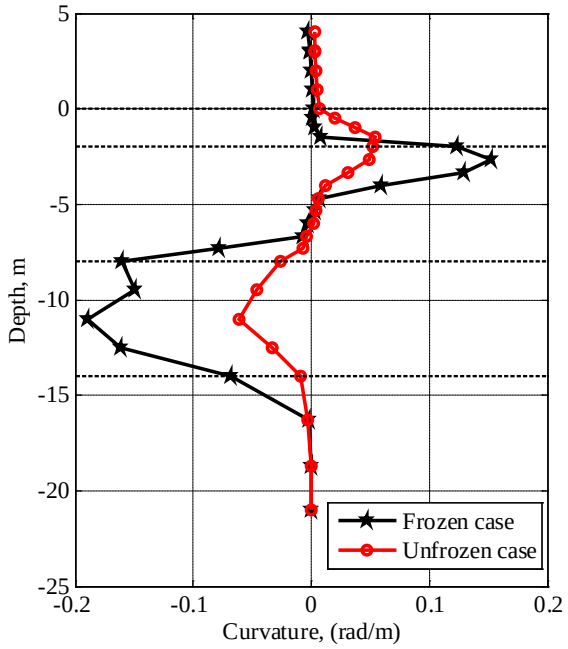

Figure 4.14. Maximum curvatures induced along pile depth for both frozen and unfrozen cases

4.4.4 Gap Response

In Figure 4.12a, note that at the “gap” section, the deflection curve shows a clear “kink” in the unfrozen case, while such a feature cannot be observed in the frozen case. Figure 4.12b clearly reveals that an abrupt change in rotation occurs at the “gap” location, but does not occur in the frozen case. The abrupt change in rotation translates into a bending moment concentration, which is apparent in Figure 4.12c. The maximum bending moment in the unfrozen case reaches

about 4,210 kN.m, well exceeding the bending moment capacity (1,896 kN.m) and indicating that the failure of the "gap" section occurs early in lateral spread-induced loading on the foundation system. That for the frozen case reaches 1,700 kN.m, exceeding the yield bending moment (1,096 kN.m) but well below the bending moment capacity. The reason for the different behaviors of the "gap" section is still the strong confinement of the frozen ground crust, which does not allow the embedded pile section to rotate, therefore inducing less rotation on the "gap" section. Considering that two plastic hinges are formed in the foundation in both cases, the performance of the "gap" section is of less significance.

The bending moment above ground surface level was the result of the constraint of the superstructure and the pile head deflection. Since the constraint was quite soft, the bending moment was relatively small. However, it is sufficient to fail the "gap" section in the unfrozen case and yield the same section in the frozen case. Figure 4.15 shows the bending moment time histories of the "gap" section for both frozen and unfrozen cases. This figure helps reveal when the "gap" section fails. With M_y and M_c marked in the figure, it is clear that the bending moment for the unfrozen case exceeds M_y at about 18 sec., indicating the "gap" failure. For the frozen case, the bending moment increases very slowly and does not exceed M_c.

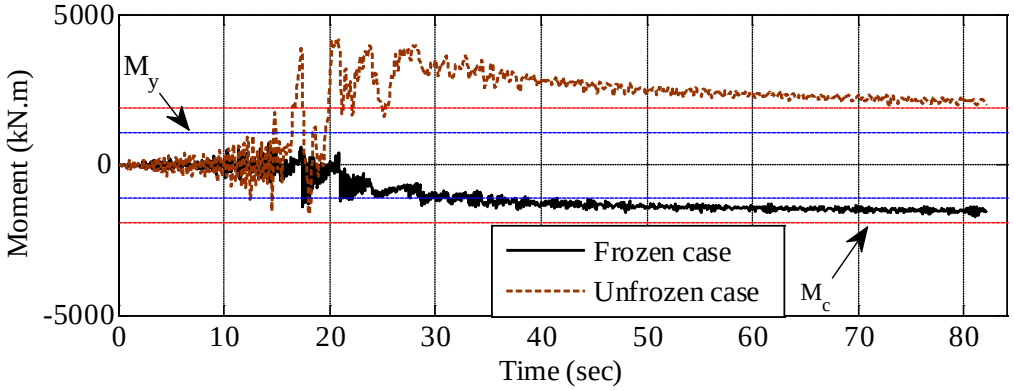

Figure 4.15. Bending moment time histories at "gap" for both cases

4.5 Pile Pinning Effect

As shown in Section 4.4.2.4, the lateral spreading of a frozen crust can cause significant load on pile foundations. In return, the restraining force from piles can reduce the lateral displacement of the ground crust, which is referred to as pile pinning effect.

The pile pinning effect was investigated by studying four frozen cases with different sizes of pile, using solid-fluid coupled FE modeling. These four cases include one case without pile and

the other three cases with a 12 in., 24 in., or 36 in. pile. The pile head is free of inertial force and rotational and lateral constraints. In other words, the superstructure constraint is not considered. The soil domain is 50 m (longitudinal or X) × 25 m (transverse or Y) × 50 m (vertical or Z) with a 3° sloping ground surface and is the same for the four cases. Table 4.5 lists the configuration of these pile sections.

Table 4.5. Pile section configurations

Pile outer diameter (in.)	Pipe thickness (in.)	Internal radius (in.)	Bar size	Number of rebars	Reinforcement ratio (%)
12	0.25	5.842	#4	6	1.06
24	0.5	11.684	#7	7	0.93
36	0.75	17.526	#11	10	1.53

Figure 4.16 presents ground surface lateral spreading time histories in the longitudinal direction for all cases. The soil node located at 12.5 m away from pile center was used to retrieve far-field displacement data, which excludes the pile-induced local strain/deformation on the frozen crust.

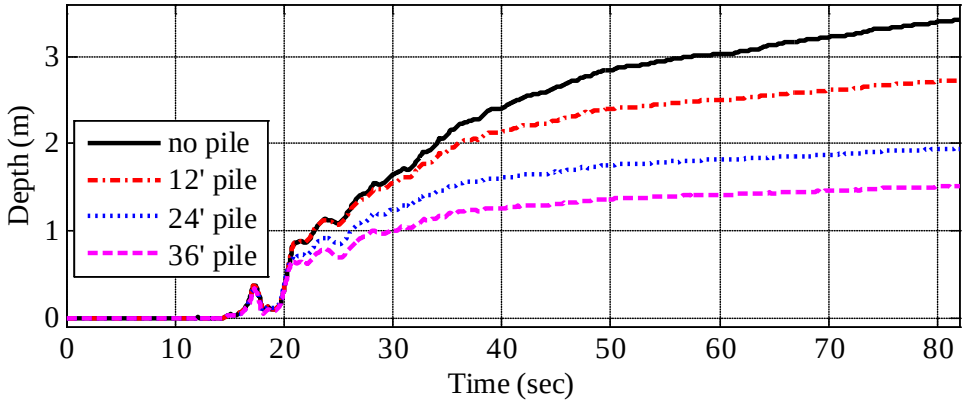

Figure 4.16. Far-field ground surface lateral displacement time histories

As can be seen in Figure 4.16, the displacement time history curves in four cases exhibit a very similar trend. The maximum lateral displacements, however, are very different (see Table 4.6). Note that with a pile installed in the soil domain, the lateral movement of the ground crust of a specific size can be reduced by 20% to 56%, with a larger pile reducing a larger amount of lateral spreading.

Table 4.6. Summary of the ultimate ground lateral displacements

Case Name	Final Disp. (m)	Change
no pile	3.42	0%
12" pile	2.73	20%
24" pile	1.95	43%
36" pile	1.51	56%

Also, note that the 36 in. pile case produces a maximum lateral displacement of 1.51 m, which is 0.08 m larger than that of the “frozen case” presented in Figure 4.10b. This difference is due to the pile head constraints and inertial force. The difference also indicates that in this case the bridge superstructure only has insignificant influence on the pile pinning effect.

It would be very useful if one could factor the pile pinning effect in assessing ground lateral spreading for design purposes. In fact, the magnitude of lateral spreading is very sensitive to the soil profile, particle-size distribution, and fines content of the liquefiable layers, topographical data including surface slope angle, and size of the laterally spreading ground crust (potential cracking of the ground crust due to ground shaking), among others. For such a complex problem, accounting for the pile pinning effect via design charts generated by a computer model, however, is very difficult, if not impossible, to achieve.

4.6 Summary

In this chapter, solid-fluid coupled FE modeling was used to study the effect of the frozen ground crust on the performance of pile foundations subjected to liquefaction-induced lateral spreading. Two cases—unfrozen and frozen—were analyzed with selected ground motion excitation. By comparing soil and pile responses from both cases, the following observations were made:

1. Two plastic hinges were observed in both frozen and unfrozen cases: the upper plastic hinge near the ground crust-loose sand interface and the lower plastic hinge within the medium dense sand layer.
2. The hinge rotation/plastic deformation demand were much higher in the frozen case than in the unfrozen case under similar seismic loading conditions. Results show that the large-size CSP pile would not be able to survive the lateral spreading in the frozen case, but would otherwise survive in the unfrozen case.

3. The upper plastic hinge formed because of the large distributed load or soil resistance induced by the frozen ground crust; the lower plastic hinge was the direct result of ground crust lateral spreading.

The modeling results from these cases are intended for use in examining the impact of frozen ground crust on pile performance in reference to unfrozen ground crust. The lateral spreading predicted by the solid-fluid coupled FE model does not necessarily represent what would occur in the field, since the computer model results, particularly the lateral spreading of the ground crust, are very sensitive to the soil constitutive model, the slope angle and size of the ground crust, and other factors. The subject of lateral spreading is revisited in Chapter 5.

CHAPTER 5 A SIMPLIFIED APPROACH

5.1 Introduction

This chapter focuses on the analysis of pile performance with a simplified method. The *p-y* approach, or beam-on-nonlinear-Winkler-foundation (BNWF) approach, was validated in Chapter 2 by the shake table experiment data. The capability of the *p-y* approach, or BNWF approach, to predict the pile response of full-size pile foundations is further confirmed by analyzing the "frozen case" and comparing its prediction results with those from coupled fluid-solid finite element (FE) analysis, as presented in the previous chapter. A set of guidelines is proposed for designers who analyze the response of pile foundations under lateral spreading using the *p-y* approach.

5.2 Model Description

5.2.1 Model Details

The commercial program LPILE was used to perform the analysis of the "frozen case," which was described in the previous chapter. The 25.05 m long pile was discretized to 500 elements, with soil *p-y* springs connected to each pile node below the ground surface. Two user-defined nonlinear sections—the CSP section and the "gap" section—were defined based on the moment-curvature response presented in Figure 4.3 and Figure 4.4. A sketch of the model is shown in Figure 5.1.

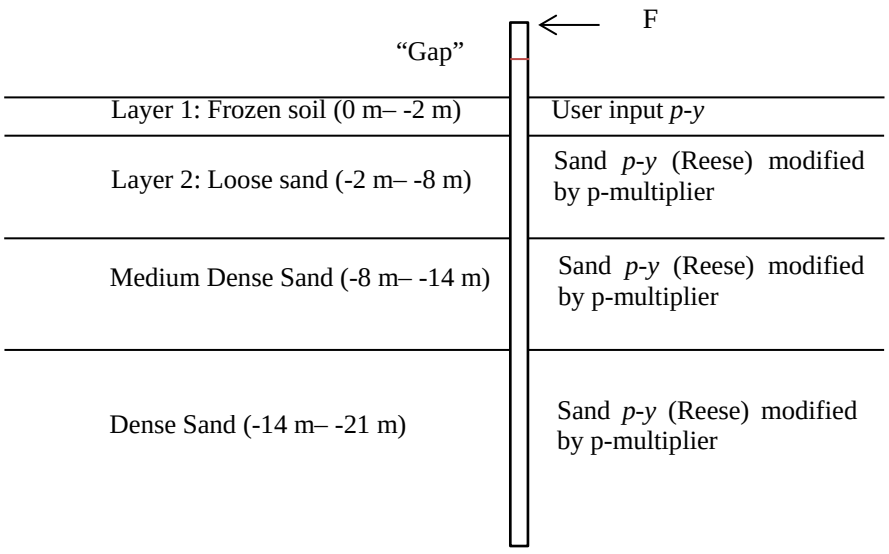

Figure 5.1. LPILE model

5.2.2 Soil *p-y* Model

The sand *p-y* model developed by Reese et al. (1974) was used for sandy soils in this analysis. The *p-y* curve proposed by Li (2011) was used to model frozen soil. Table 5.1 summarizes the soil parameters used in this analysis. Details of the *p-y* curve were summarized in Section 3.3.1.2.

Table 5.1. Soil parameters for defining *p-y* curves

Soil type	Depth (m)	Status	γ'[a] (kN/m^3)	ω[b] ($^\circ$)	k[c] (kPa/m)	ε_{50}[d]	q_u[e] (MPa)
Frozen soil	0	-12°C	18	-	-	0.001	5.8
Frozen soil	-2	-1°C	18	-	-	0.001	2.0
Loose sand	-2 ~ -8	Unfrozen	7	29	5430	-	-
Medium dense sand	-8 ~ -14	Unfrozen	10	35	16000	-	-
Dense sand	-14 ~ -21	Unfrozen	11	40	33900	-	-

[a] Effective unit weight
[b] Friction angle
[c] Soil modulus parameter
[d] Axial strain corresponding to 50% of ultimate compressive strength
[e] Unconfined compressive strength

The user-input *p-y* curves were specified in LPILE for the top (0.0 m) and bottom layer (2.0 m) of the frozen crust. These curves are shown in Figure 5.2. For unspecified frozen soil layers, LPILE uses linear interpolation to generate the *p-y* curve. As can be seen in the figure, the *p-y* curve at the ground surface is much stiffer than that at the bottom of the frozen crust, due to the temperature increase with depth.

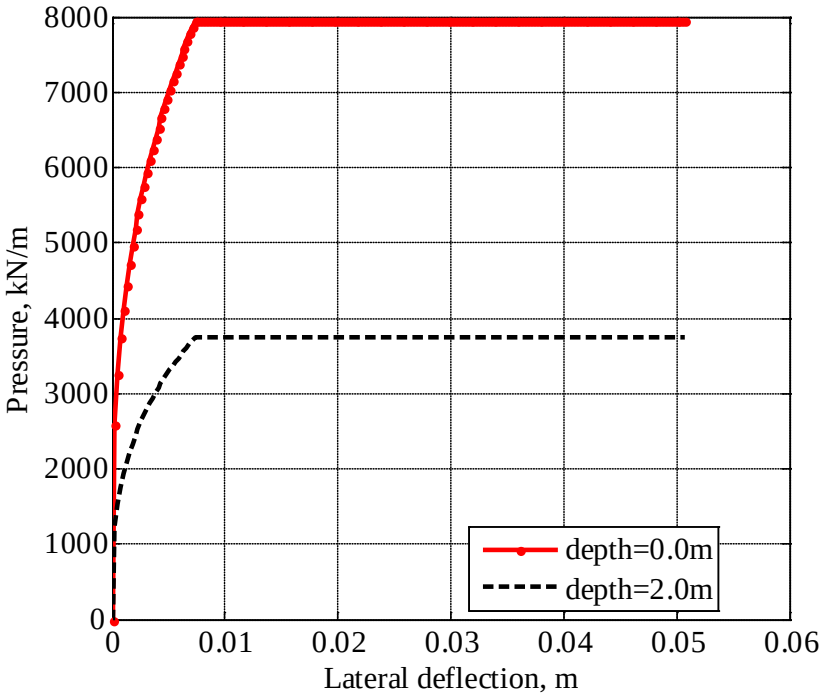

Figure 5.2. User-defined *p-y* curves for frozen silts

Soil lateral resistance reduction in the loose and medium dense sand layers due to full or partial liquefaction should be considered. In this analysis, p-multipliers, discussed in Section 3.3.1.3, were again used to approximate soil resistance reduction. Referring to Figure 4.8, excess pore pressure ratios (r_u) induced for the loose and medium dense sand layers and the dense sand layer are 70%–100% and 40%–50%, respectively. Loose and medium dense sand layers were assumed fully liquefied (i.e., r_u=100%), and a p-multiplier of 0.1 was used. The dense sand layer only underwent partial liquefaction, and a p-multiplier of 0.5 was selected. A sketch of the p-multiplier versus the pile depth is shown in Figure 5.3

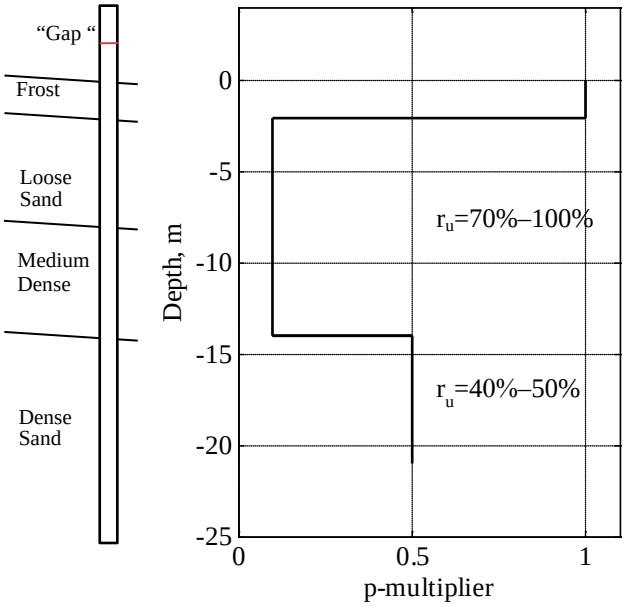

Figure 5.3. P-multipliers distribution along pile depth

5.2.3 Loading

The lateral spreading load was assumed constant in the frozen ground crust and linearly decreasing in the liquefied loose and medium sand layers. Figure 5.4 shows a sketch of the lateral spreading load. The far-field ground displacement obtained from the FE model, 1.43 m, was applied at the ground crust. Note that the far-field displacement does not stand for free-field displacement in this case due to pile pinning effects. In practice, the free-field displacement can be estimated using empirical or analytical methods, which will be discussed further.

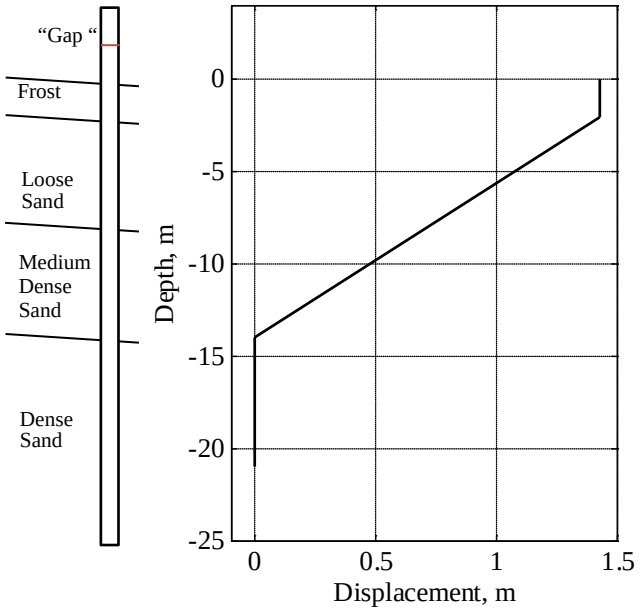

Figure 5.4. Imposed displacement loading

5.2.4 Boundary Conditions at the Pile Head

As mentioned in Chapter 4, the pile top is not allowed to rotate due to constraint of the cap beam. This was modeled by imposing a 0 rad angle on the pile top. The elastic spring simulating bridge deck constraint cannot be included in the LPILE model directly. The solution is to apply a constant constraint force (estimated as 1,500 kN by multiplying the spring stiffness and the final pile displacement) on the pile top in the counter-soil-movement direction.

5.3 Comparison with Solid-Fluid Coupled Finite Element Modeling

5.3.1 P-y Curves at Selected Depths

Figure 5.5 and Figure 5.6 show the *p-y* curves for frozen crust and sand layers, respectively. Comparing these figures, one can see that the frozen soil *p-y* curves are generally stronger than the unfrozen layers. Even though at a depth of -20 m, dense sand exhibits very high ultimate soil resistance ranging from 4,500 to 5,500 kN/m, the corresponding deflection value for ultimate resistance is much larger than for the frozen soil. Note that frozen soil resistance decreases with depth due to increasing temperature, while unfrozen sand resistance increases with depth due to increased effective confinement.

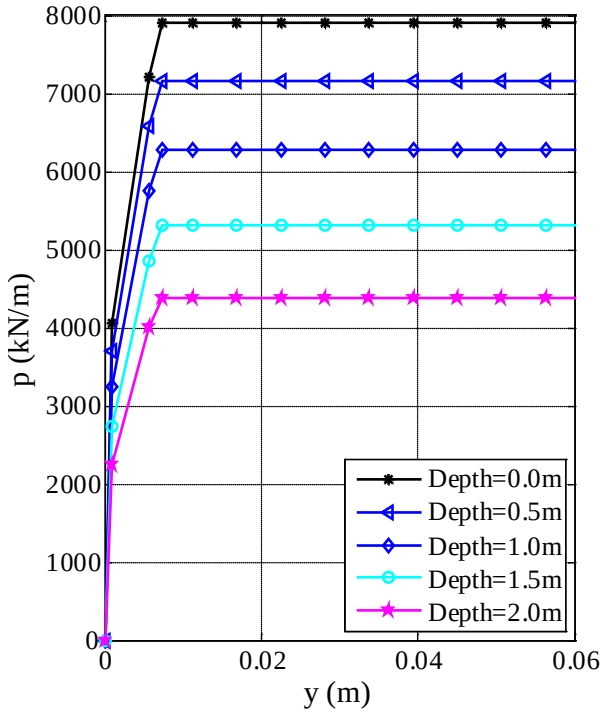

Figure 5.5. *P-y* curves for the frozen crust

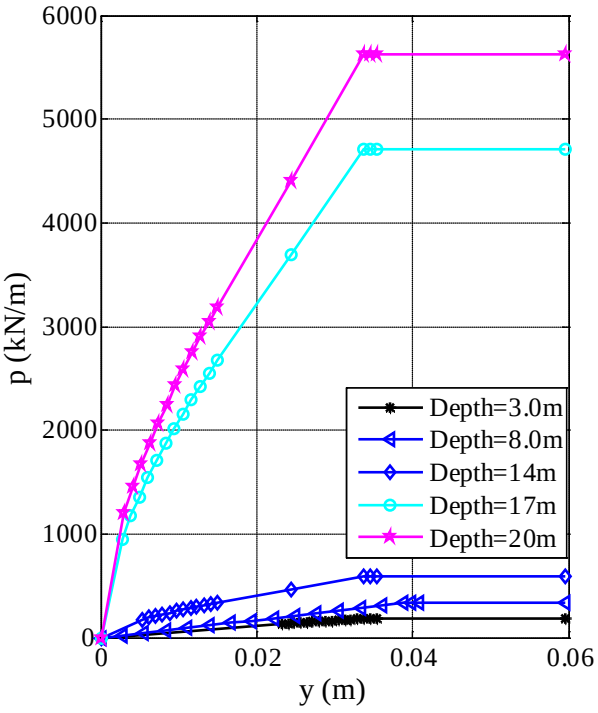

Figure 5.6. *P-y* curves for sand layers

5.3.2 Deflection, Rotation, Bending Moment, and Shear Force

Figure 5.7a to d shows the maximum deflection, rotation, bending moment, and shear force results obtained from the p-y approach. For comparison purposes, the maximum values of corresponding variables from solid-fluid coupled FE model are also shown.

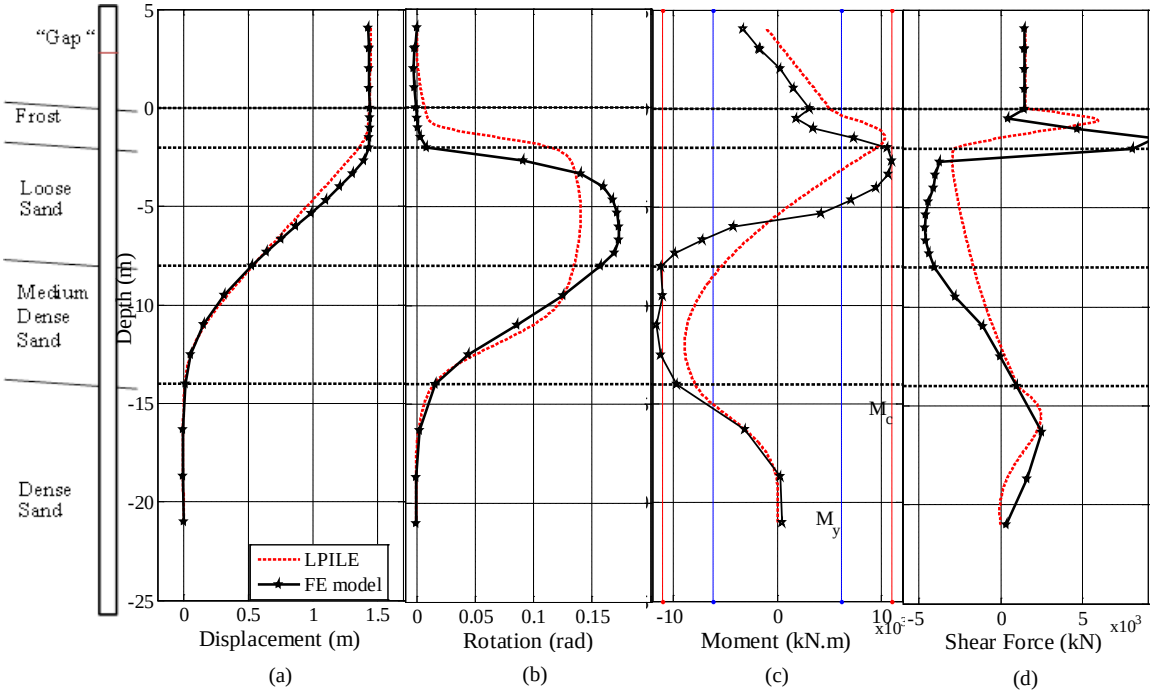

Figure 5.7. Comparison of pile performance predicted by the p-y approach and solid-fluid coupled FE model

The predicted deflection shape from LPILE analysis agrees well with that from FE modeling. However, the confinement effect of the frozen ground crust as modeled by LPILE seems to be smaller because the straight portion of the pile is shorter in the LPILE analysis. The difference of confinement effect is further shown by comparing the rotation of the pile shown in Figure 5.7b. In the FE model, a sharp rotation change of the pile occurs at the bottom of the frozen crust; a similar change in rotation occurs within the frozen crust layer in the LPILE model. These rotation changes imply that the *p-y* curves might be too soft.

Figure 5.7c shows the bending moment distribution along the pile depth. It is evident that prediction using the *p-y* approach compares favorably with that from FE modeling. The *p-y* approach is able to predict the formation of two plastic hinges at locations similar to those predicted by FE modeling. However, it is obvious that the peak bending moments at both plastic hinges are underpredicted by the *p-y* approach. The *p-y* approach predicts that the maximum

bending moment for the upper plastic hinge is 10,390 kN.m (11,060 kN.m by the FE model), and the maximum bending moment for the lower plastic hinge is 8,963 kN.m (11,620 kN.m by the FE model). The *p-y* approach underpredicts the maximum bending moment of the upper and lower plastic hinges by 6% and 23%, respectively. It is found that the maximum bending moment at the lower plastic hinge is sensitive to the p-multipliers and the prediction could be improved by using a different approach in selecting p-multipliers.

Figure 5.8 illustrates pile curvature profiles as predicted by the p-y approach and solid-fluid coupled FE model. Generally, the magnitude and location of the peak curvature in the upper plastic hinge from the p-y approach compares favorably with these from the FE model. However, the simplified model significantly underestimates the peak curvature at the lower plastic hinge when compared with the FE model, which again could be improved by using a different p-multipliers selection approach.

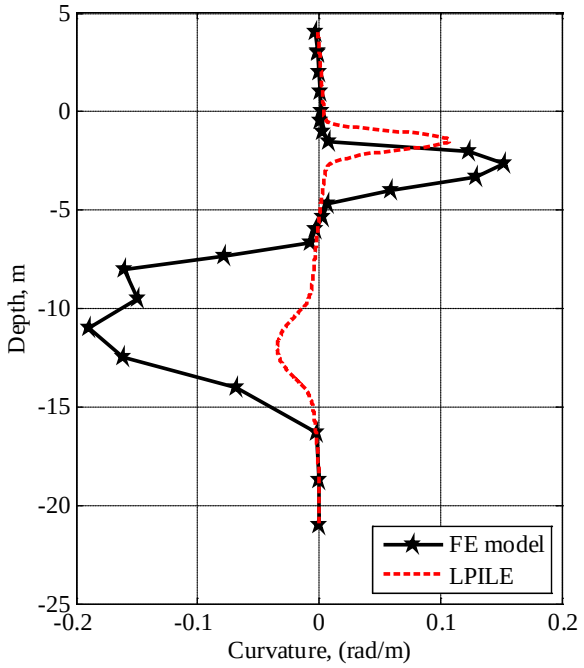

Figure 5.8. Comparison of results from the p-y approach and solid-fluid coupled FE model

Figure 5.7d shows the shear force distribution versus depth. With the *p-y* approach, shear force changes sharply in the frozen crust in a similar manner observed with the FE model. It changes slowly in loose and medium dense sand layers because of low soil resistance due to partial or full liquefaction. The *p-y* approach predicts that the maximum shear force in the frozen

crust is 5,987 kN.m (9,330 kN.m by the FE model). Again, this prediction suggests that the *p-y* curves used in this analysis are on the soft side.

5.4 Guidelines for Analyzing Pile Response by the *p-y* Approach

The *p-y* approach is effective in modeling the response of pile foundations subjected to laterally spreading frozen ground crust in liquefiable soils. To utilize this method in design practice, the following aspects must be treated with care, including obtaining free-field lateral spreading, selecting p-multipliers in fully or partially liquefied soils, constructing the *p-y* model for frozen soil, and modeling superstructure impact.

5.4.1 Estimating Lateral Spreading

5.4.1.1 Suggested Methods

In practice, the *p-y* approach would require free-field lateral displacement as the input. Empirical and semi-empirical procedures are available and commonly used to estimate free-field lateral spreading. We present two approaches for evaluating lateral spreading; their applicability in the case of frozen crust is not validated by field data.

Youd et al. (2002) proposed Equations 5.1 and 5.2 for evaluating lateral spreading:

$$\log D_H = -16.713 + 1.532M - 1.406\log R^* - 0.012R + 0.592\log W + 0.540T_{15} + 3.413\log(100 - F_{15}) - 0.795\log(D50_{15} + 0.1\text{mm}) \quad \text{(for a steep vertical face) (5\% } \le W \le 20\%) \tag{5.1}$$

$$\log D_H = -16.213 + 1.532M - 1.406\log R^* - 0.012R + 0.338\log S + 0.540\log T_{15} + 3.413\log(100 - F_{15}) - 0.795\log(D50_{15} + 0.1\text{mm}) \quad \text{(for gently sloping ground)} \tag{5.2}$$

where D_H is the horizontal displacement (m); M is the moment magnitude of the earthquake; R is the nearest distance (km) to the seismic energy source; T_{15} is the thickness (m) of saturated cohesionless soils (excluding soils deeper than 20 m or with more than 15% clay content) with $N_{1,60} \le 15$, where $N_{1,60}$ is the standardized SPT blow count corrected for overburden pressure and energy efficiency; F_{15} is the average fines content for granular material in T_{15}; W is the free-face ratio defined as the height of the free face divided by the distance from the base of the free face

to the point in question; S is the ground slope in percent; and $D50_{15}$ is the average D_{50} grain size (mm) in T_{15}. R^* is calculated by Equation 5.3:

$$R^* = 10^{(0.89M-5.64)} + R \quad 5.3$$

Zhang et al. (2012) proposed a simpler approach, which consists of Equations 5.4 and 5.5:

$$LD = (S + 0.2) \times LDI \text{ for } (0.2\%<S<3.5\%) \quad 5.4$$

$$LD = 6 \times (L/H)^2 \times LDI \text{ for } (4<L/H<40) \quad 5.5$$

where LDI is the lateral displacement index, which can be obtained by a set of plots proposed by Zhang et al. (2012); S is the ground slope; H is the free-face height; L is the distance to a free face; and LD is the estimated lateral displacement.

5.4.1.2 Example for Estimating Free-Field Lateral Spreading

Golder Associates Inc. (2010) and Alaska Department of Transportation and Public Facilities (2010) have documented detailed geotechnical and seismic investigation reports for the Brotherhood Bridge site in Juneau, Alaska. For example, the empirical equations in Youd et al. (2002) were used to estimate free-field lateral spreading. The process is presented in the following four steps:

Step 1: Obtain topographic parameters

Figure A. 1 in the appendix presents the topography map for the bridge site. No steep face exists at this site. A gentle slope can be observed from left-top corner to bottom-right corner, and a rough calculation shows the average ground slope S is 1%.

Step 2: Obtain geotechnical parameters

Figure A. 2 in the appendix presents the SPT blow count results for borehole TH-01 and TH-02. Only the data from TH-01 were used to demonstrate the process. Figure A. 3 and Figure A. 4 in the appendix present the particle-size distribution curves. According to these data and the definitions of each parameter, the following parameters are obtained by interpolation: T_{15} = 4.3 m, F_{15} = 11.3%, and $D50_{15}$ = 0.36 mm.

Step 3: Obtain seismic source parameters

The geologic and geometric characteristics of two main seismic sources are shown in Figure A. 5. The SE Denali fault was selected for the analysis because it has a slightly smaller moment magnitude and a much shorter distance to the bridge site. A M_w of 7.8 and an epicentral distance R of 25 km were used in this example. In practice, all credible source parameters should be considered.

Step 4: Calculate DH with the selected equation

Since no steep free face exists, Equation 5.2 should be used. By applying the appropriate topographic, geotechnical, and seismic parameters, Equation 5.2 yields a lateral displacement of 2.5 m.

5.4.2 Selecting P-multipliers

Applying the excess pore pressure (EPP) ratio data to acquire p-multipliers is not directly applicable in design practice due to lack of such data. In situ tests such as the SPT provide a possible solution for estimating p-multipliers. Ashford et al. (2011) suggest a method to estimate p-multipliers (m_p) based on the clean sand equivalent corrected blow count ($(N_1)_{60cs}$); it is presented in Table 5.2. However, more research is needed on how to properly select p-multipliers for better prediction results as noted in Section 5.3.2.

Table 5.2. P-multipliers (m_p) to account for liquefaction

$(N_1)_{60cs}$	m_p
<8	0.0 to 0.1
8-16	0.05 to 0.2
16-24	0.1 to 0.3
>24	0.2 to 0.5

5.4.3 Modeling Frozen Soil Resistance

The *p-y* curve proposed by Li (2011) is recommended for modeling frozen soil resistance. The frozen soil properties obtained by Yang et al. (2012) can be used in constructing the frozen soil *p-y* curves if the frozen soil conditions are similar.

5.4.4 Superstructure Interaction

Superstructure interaction includes translational and rotation constraints, and inertial force. Translational and rotation constraints are easily considered by defining appropriate boundary conditions on the pile top. The *p-y* approach is incapable of modeling the impact of inertial force that is time-dependent. In the case of foundations that may suffer from considerable superstructure inertial force, it is recommended that more sophisticated solid-fluid coupled FE modeling or other analyses be conducted.

5.5 Summary

In this chapter, a simplified approach, that is, the pseudo-static *p-y* approach, was used to model pile response subjected to frozen ground lateral spreading in liquefiable soils. Pile responses, including deflection, bending moment, and shear force profiles, were evaluated and compared with pile responses from FE modeling. The following conclusions were drawn:

1. Pile response results obtained from the *p-y* approach compare favorably with those from solid-fluid coupled FE modeling. The *p-y* approach predicted the formation of two plastic hinges and the maximum bending moment in the upper plastic hinge, but it underpredicted the maximum bending moment in the lower plastic hinge.
2. Overall, the *p-y* approach is effective in predicting the response of piles subjected to frozen ground crust lateral spreading in liquefiable soils.
3. The frozen soil *p-y* curve proposed by Li (2011) is quite effective in modeling frozen soil resistance in frozen soil-pile interaction.
4. Guidelines are proposed for practitioners who analyze the response of piles subjected to frozen ground crust lateral spreading in liquefiable soils by the *p-y* approach. These guidelines include how to obtain free-field displacement, select p-multipliers, model frozen soil resistance, and account for the effects of superstructure.

CHAPTER 6 SUMMARY AND RECOMMENDATIONS

6.1 Summary

Liquefaction and associated lateral spreading induce extensive ground failures and infrastructure damage around the world. One of the lessons learned from Alaska's major winter earthquakes is that frozen ground crust plays a crucial role in causing bridge foundation failures. From three aspects, this study analyzed the effect of ground crust on the seismic response of pile foundations: (1) A shake table experiment was conducted to gain an in-depth understanding of the impact of frozen ground crust on a model pile foundation, and the results were used in numerical model validation. (2) Loads imposed on pile foundations by the frozen crust were studied through solid-fluid coupled finite element (FE) analyses of a typical Alaska bridge foundation under two soil conditions—one an unfrozen crust and the other a frozen crust—and by the comparison of results obtained from these two cases. (3) The effectiveness of a simplified approach (i.e., the *p-y* approach) in predicting the response of piles subjected to frozen ground lateral spreading in liquefiable soils was evaluated by comparing the results of the *p-y* approach with those obtained from FE modeling.

The content and conclusions of this study are summarized below:

1. In the shake table experiment, laterally spreading frozen ground crust formed two plastic hinges: one near the frozen crust-loose sand interface and the other in the medium dense sand layer. The plastic hinge at the frozen crust-loose sand interface formed because of the large distributed load (soil resistance) induced by the frozen ground crust; the plastic hinge in the medium dense sand layer was the direct result of lateral spreading of the ground crust.
2. Two approaches—solid-fluid coupled FE modeling and the *p-y* approach—were used to model the shake table experiment. By comparing the results from numerical approaches with those from the experiment, both numerical approaches were confirmed effective in predicting the response of piles subjected to lateral spreading of a frozen ground crust, particularly the formation of plastic hinges at the frozen crust-loose sand interface and within the medium dense sand layer.
3. Solid-fluid coupled FE analysis was conducted for a full-size soil-pile system of both frozen (with a frozen active layer) and unfrozen (with an unfrozen active layer)

conditions, and lateral spreading with almost the same magnitude was induced in the ground crust for both cases.

4. Two plastic hinges were observed in both the frozen and unfrozen cases: one located near the frozen ground crust-loose sand layer interface (referred to as the upper plastic hinge) and the other within the medium dense sand layer (referred to as the lower plastic hinge).
5. For the frozen case, the maximum bending moments in these two plastic hinges exceeded the bending moment capacity of the pile; those in the unfrozen case did not reach bending moment capacity. The peak curvatures in both plastic hinges in the frozen case are 200% larger than that in the unfrozen case. This clearly indicates that the frozen crust will induce substantially larger hinge rotation and plastic deformation demand in the pile than will the unfrozen crust under similar seismic loading.
6. The p-y approach is effective in predicting the location and plastic deformation demand at the upper plastic hinge, and the location of the lower plastic hinge. It underestimates the plastic deformation demand in the lower plastic hinge. However, with further study, this could be improved by using a different p-multipliers selection approach.
7. Guidelines were proposed for practitioners who analyze the response of piles subjected to frozen ground lateral spreading in liquefiable soils by the *p-y* approach. These guidelines include how to obtain free-field displacement, select p-multipliers, model frozen soil resistance, and account for the effects of superstructure.

6.2 Suggestions for Future Research

The following topics or issues are recommended for future research:

1. Obtaining reliable free-field lateral spreading is one of the key issues that need to be resolved in applying the pseudo-static *p-y* approach. One could apply empirical methods in the literature to estimate free-field lateral spreading. However, it is recommended that field data, if available, be used to evaluate free-field lateral spreading. Two major winter earthquakes have occurred in Alaska. In particular, the 2002 Denali earthquake caused numerous cases of liquefaction and lateral spreading in Interior Alaska. Abundant data were collected through many site reconnaissance visits and satellite images. These data, if analyzed and synthesized for various sites, can be used to validate existing empirical

models or establish new or improved models that consider frozen crust cases, providing input for bridge design practices.

2. The shake table experiment and solid-fluid coupled FE modeling were performed for a single pile. In practice, pile groups, rather than single piles, are used as bridge substructures. It would be worthwhile to investigate how to extend the findings from this study to analysis of the performance of pile groups subjected to frozen ground crust lateral spreading in liquefied soils.
3. We found that the *p-y* approach tends to underpredict the maximum bending moments and peak curvatures of two plastic hinges. These results are quite sensitive to p-multipliers and frozen soil lateral resistance. The performance of the *p-y* approach could potentially be improved by conducting a sensitivity study of results to p-multipliers and frozen soil properties.
4. Further study is necessary to provide a more reliable prediction of lateral spread, including the reduction, if any, that is associated with pile pinning effects.

REFERENCES

Abate, G., Massimino, M.R., Maugeri, M., and Wood, D.M. (2010). “Numerical Modeling of a Shaking Table Test for Soil-Foundation-Superstructure Interaction by Means of a Soil Constitutive Model Implemented in a FEM Code.” Geotech. Geol. Eng, 28: 37–59.

Akili, W. (1971). “Stress-strain behavior of frozen fine-grained soils.” Highway Research Record: Frost Action and Drainage. No. 360: 1–8.

Alaska Department of Transportation and Public Facilities (2010). “Foundation geology report JNU Brotherhood Bridge widening.” Project No. 67987, State of Alaska.

American Petroleum Institute (API) (1987). “Recommended Practice for Planning, Designing and Constructing Fixed Offshore Platforms.” API Recommended Practice 2A(RP-2A), Washington, D.C, 17th edition.

Armstrong, R.J., Boulanger, R.W., Gulerce, U., Kutter, B.L., and Wilson, D.W. (2008). “Centrifuge modeling of pile pinning effects.” Geotechnical Earthquake Engineering and Soil Dynamics IV, D. Zeng, M. Manzari, and D. Hiltunen, eds., Geotechnical Special Publication No. 181, ASCE, NY.

Ashford, S.A, and Rollins, K.M. (2002). “The Treasure Island Liquefaction Test: FinalReport, Report”, SSRP-2001/17, Department of Structural Engineering, University of California, San Diego.

Ashford, S.A., Juirnarongrit, T., Sugano, T., and Hamada, M. (2006). “Soil-pile response to blast-induced lateral spreading. I: Field test.” Journal of Geotechnical and Geoenvironmental Engineering, ASCE, 132(2): 152–162.

Ashford et al. (2011). “Recommended design practice for pile foundations in laterally spreading ground”. PEER Report 2011/04.Baker, T.H.W., Jones, S.J. and Parameswaran, V.R. (1982). “Confined and Unconfined Compression Tests on Frozen Sands.” Proc. 4th Canadian Permafrost Conference, Roger J.E. Brown Memorial Vol., 387–393.

Boulanger, R.W., Wilson, D.W., Kutter, B.L., and Abghari, A. (1997). “Soil-pile-superstructure interaction in liquefiable sand.” Transportation Research Record No. 1569, TRB, NRC, National Academy Press, 55–64.

Boulanger, R.W., Curras, C.J., Kutter, B.L., Wilson, D.W., and Abghari, A. (1999). “Seismic soil-pile-structure interaction experiments and analyses.” Journal of Geotechnical and Geoenvironmental Engineering, 125(9): 750–759.

Boulanger, R.W., Kutter, B.L., Brandenberg, S.J., Singh, P., and Chang, D. (2003). “Pile foundations in liquefied and laterally spreading ground pile foundations in liquefied and laterally spreading ground during earthquakes: centrifuge experiments & analyses.” Report #UCD/CGM-03/01, Center for Geotechnical Modeling, University of California, Davis, September.

Brandenberg, S.J., and Boulanger, R.W. (2007). “Static pushover analyses of pile groups in liquefied and laterally spreading ground in centrifuge tests.” Journal of Geotechnical and Geoenvironmental Engineering, 133(9): 1055–1066.

Brandenberg, S.J., Boulanger, R.W., Kutter, B.L., and Chang, D. (2005). “Behavior of pile foundations in laterally spreading ground during centrifuge tests.” Journal of Geotechnical and Geoenvironmental Engineering, 131(11): 1378–1391.Cheng, Z., and Jeremic, B. (2009). “Numerical modeling and simulation of pile in liquefiable soil.” Soil Dynamics and Earthquake Engineering, 29:1405–1416.

Coe, C.J., Prevost, J.H., and Scanlan, R.H. (1985). “Dynamic stress wave reflections/attenuation earthquake simulation in centrifuge soil models.” Earthquake Engineering and Structural Dynamics, 13:109–128.

Crowther, G. S. (1990). “Analysis of laterally loaded piles embedded in layered frozen soil.” Journal of Geotechnical Engineering Vol. 116, No. 7.

Cubrinovski, M., Kokusho, T., and Ishihara, K. (2006). “Interpretation from large-scale shake table tests on piles undergoing lateral spreading in liquefied soils.” Soil Dynamics and Earthquake Engineering, 26(2–4): 275–286.

Cubrinovski, M., Uzuoka, R., Sugita, H., Tokimatsu, K., Sato, M., Ishihara, K., Tsukamoto, Y., and Kamata, T. (2008). “Prediction of pile response to lateral spreading by 3-D soil–water coupled dynamic analysis: Shaking in the direction of ground flow.” Soil Dynamics and Earthquake Engineering, 28: 421–435.

Dobry, R., and Abdoun, T. (2001). “Recent studies on seismic centrifuge modeling of liqefaction and its effect on deep foundations.” SOAP-3, Proc. 4th Intl. Conf. On Recent Advances in Geotechnical Earthquake Engrg. and Soil Dynamics, S. Prakash, ed, San Diego, CA.

Dobry, R., Taboada, V., and Liu, L. (1995). “Centrifuge modeling of liquefaction effects during earthquakes.” Proc., 1st Int. Conf. on Earthquake Geotechnical Engineering, K. Ishihara, ed., Vol. 3, Balkema/Rotterdam/The Netherlands, Tokyo, 1291–1324.Dobry, R., Abdoun, T., O’Rourke, T.D., and Goh, S.H. (2003). “Single piles in lateral spreads: field bending moment evaluation.” Journal of Geotechnical and Geoenvironmental. Engineering, 129(10): 879–889.

Elgamal, A., Yang, Z., and Parra, E., (2002). “Computational modeling of Cyclic Mobility and Post-Liquefaction Site Response.” Journal of Soil Dynamics and Earthquake Engineering, 22(4): 259–271.

Elgamal, A., Yang, Z., Parra, E., and Ragheb, A., (2003) "Modeling of Cyclic Mobility in Saturated Cohesionless Soils." , Int. J. Plasticity, 19, (6), 883-905.

Elgamal, A., Jinchi Lu, and Forcellini, D. (2009). “Mitigation of liquefaction-induced lateral deformation in a sloping stratum: Three-dimensional numerical simulation.” ASCE Journal of Geotechnical and Geoenvironmental Engineering, 135(11): 1672–1682.

Finn, W.D.L., and Fujita, N. (2002). “Piles in liquefiable soils: seismic analysis and design issues.” Soil Dynamics and Earthquake Engineering, 22: 731–742.

Fujii, S., Cubrinovski, M., Tokimatsu, K., and Hayashi, T. (1998). “Analyses of damaged and undamaged pile foundations in liquefied soils during the 1995 Kobe earthquake.” Geotechnical Earthquake Engineering and Soil Dynamics III, Geotechnical Special Publication No. 75, ASCE, 2: 1187–1198.

Golder Associates Inc, (2010), “Geotechnical investigation and liquefaction analysis, Juneau Brotherhood Bridge replacement, No. 737.” Project No. 67987, State of Alaska.

Haynes, F.D., and Karalius, J.A. (1977). “Effect of temperature on the strength of frozen silt.” CRREL Report 77-3, Cold Regions Research and Engineering Laboratory. Hanover, New Hampshire.

Horazdovsky, J.E. (2010). “Seasonal effects of frozen soil on the stiffness of bridge piles.” Master Thesis, University of Alaska Fairbanks, Aug.

Iwan, W.D. (1967). “On a class of models for the yielding behavior of continuous and composite systems.” Journal of Applied Mechanics, ASME, 34: 612–617.

JRA (2002). “Specifications for highway bridges.” Japan Road Association, Preliminary English Version, prepared by Public Works Research Institute (PWRI) and Civil Engineering Research Laboratory (CRL), Japan, November.

Kagawa, T., Taji, Y., Sato, M., and Minowa, C. (1997). “Soil-pile-structure interaction in liquefying sand from large scale shaking table tests and centrifuge tests.” Seismic Analysis and Design for Soil-Pile-Structure Interactions, Geotechnical Special Publication No. 70, ASCE: 69–84.

Karsan, I. D., and Jirsa, J. O. (1969). "Behavior of concrete under compressive loading." *Journal of Structural Division ASCE*, 95(ST12).

Kostadinov, M.V., and Yamazaki, F. (2001). “Detection of soil liquefaction from strong motion records.” Earthquake Engineering Structure Dynamics, 30(2): 173–93.

Lam, I., Arduino, P., and Mackenzie-Helnwein. P. (2009). “OpenSees Soil-Pile Interaction Study under Lateral Spread Loading.” International Foundation Congress & Equipment Expo ’09 (IFCEE’09), Orlando, FL, May 15–19.

Li, Qiang (2011). “Effect of frozen soils on the seismic behavior of highway bridge foundation.” M.S. Thesis, University of Alaska Anchorage, May.

Lu, J., Yang, Z., and Elgamal, A. (2006). “Openseespl three-dimensional lateral pile-ground interaction version 1.00 user’s manual.” Report No. SSRP-06/03, Department of Structural Engineering, University of California, San Diego.

Lu, J., Elgamal, A., Yan, L., Law, K.H., and Conte, J.P. (2011). “Large-scale numerical modeling in geotechnical earthquake engineering.” International Journal of Geomechanics, 11(6): 490–503.Matlock, H. (1970). “Correlations of design of laterally loaded piles in soft clay.” Proceeding of Offshore Technology Conference, Houston, 1: 577–594.

Mazzoni, S., McKenna, F., and Fenves, G.L. (2006). “Open System for Earthquake Engineering Simulation User Manual.” Pacific Earthquake Engineering Research Center, University of California, Berkeley, CA.

McGann, C.R., Arduino, P., and Mckenzie-Helnwein, P. (2011). “Applicability of conventional *p-y* relations to the analysis of piles in laterally spreading soil.” Journal of Geotechnical and Geoenvionmental Engineering, 137(6): 557–567.

Mroz, Z. (1967). “On the description of anisotropic work hardening.” Journal of Mechanics and Physics of Solids, 15: 163–175.

Naggar, M.H.El, Shayanfar, M.A., Kimiaei, M., and Aghakouchak, A.A. (2005), “Simplified BNWF model for nonlinear seismic response analysis of offshore piles with nonlinear input ground motion analysis.” Canadian Geotechnical Journal, 42: 365–380.

Parra, E. (1996). “Numerical modeling of liquefaction and lateral ground deformation including cyclic mobility and dilation response in soil systems.” Ph.D. Dissertation, Rensselaer Polytechnic Institute, Troy, NY.

Prevost, J.H. (1985). “A simple plasticity theory for frictional cohesionless soils.” Int. J. Soil Dynamics and Earthquake Engineering, 4(1): 9–17.

Reese, L.C., Cox, W.R., and Koop, F.D. (1974). “Analysis of laterally loaded piles in sand.” Proc., 6th Offshore Technology Conf., Vol. 2, Houston, 473–483.

Reese, L.C. (1997). “Analysis of laterally loaded piles in weak rock.” Journal of Geotechnical and Geoenvironmental Engineering, ASCE, 123(11) Nov., ASCE: 1010–1017.

Rollins, K.M., Gerber, T.M., Lane, J.D., and Ashford, S. (2005). “Lateral resistance of a full-scale pile group in liquefied sand.” Journal of Geotechnical and Geoenvironmental Engineering, 131(1): 115–125.

Ross, G.A, Seed, H.B., and Migliaccio, R.R. (1973). “Performance of highway bridge foundations.” The Great Alaska Earthquake of 1964 (Engineering), National Academy of Sciences, 190–242.

Shannon and Wilson Inc. (2002). “Documentation of geotechnical damages of the Magnitude 7.9 Denali Earthquake of Nov. 3, 2002.” http://clients.shanwil.net/project.php?projectid =Quake_2002. Retrieved on Feb. 27, 2009.

Shirato, M., Nonomura, Y., Fukui, J., and Nakatani, S. (2008). “Large-scale shake table experiment and numerical simulation on the nonlinear behavior of pile-groups subjected to large-scale earthquakes.” Soils and foundations, Japanese Geotechnical Society, 48 (3): 375–396.

Stevens, H.W., 1973. “Viscoelastic properties of frozen soil under vibratory loads.” North American Contribution to the Second International Conference on Permafrost. Yakutsk, Siverua, U.S.S.R., 400–409.

Tao, X., Kagawa, T., Minowa, C., and Abe, A. (1998). “Verification of dynamic soil-pile interaction.” Geotechnical Earthquake Engineering and Soil Dynamics III, Geotechnical Special Publication No. 75, ASCE, 2: 1199–1210.

Tokimatsu, K., Suzuki, H., and Suzuki, Y. (2001). “Back-calculated *p-y* relation of liquefied soils from large shaking table tests.” Fourth International Conference on Recent Advances in Geotechnical Earthquake Engineering and Soil Dynamics, S. Prakash, ed, University of Missouri – Rolla, paper 6.24.

Ueng, T.S. (2010). “Shaking table tests for studies of soil liquefaction and soil-pile interaction.” Geotechnical Engineering Journal of the SEAGS & AGSSEA, 41(1): 1–10.

Uzuoka, R., Cubrinovski, M., Sugita, H., Tokimatsu, K., Sento, N., Kazama, M., Zhang, F., Yashima, A., and Oka, F. (2008). “Prediction of pile response to lateral spreading by 3-D soil–water coupled dynamic analysis: Shaking in the direction of ground flow.” Soil Dynamics and Earthquake Engineering, 28: 436–452.

Vinson, T.S., Wilson, C.R., and Blonader, P. (1983). “Dynamic properties of naturally frozen silt.” National Academy Press, 1315–1320.

Weaver, T.J., Ashford, S.A., and Rollins, K.M. (2005), “Response of 0.6 m cast-in-steel-shell pile in liquefied soil under lateral spreading.” Journal of Geotechnical and Geoenvironmental Engineering, 131(1): 94–102.

Wilson, D.W. (1998). “Soil-pile-superstructure interaction at soft and liquefying soil sites.” Ph.D thesis, University of California, Davis, California.

Yang, Z. (2000). “Numerical modeling of earthquake site response including dilation and liquefaction.” Ph.D. Thesis, Department of Civil Engineering and Engineering Mechanics, Columbia University, New York, NY.

Yang, Z., and Elgamal, A. (2002). “Influence of permeability on liquefaction-induced shear deformation.” Journal of Engineering Mechanics, 128(7): 720–729.Yang, Z., and Jeremic, B. (2005). “Parametric study

into soil layering effects on the response of single piles to lateral loading." ASCE Journal of Geotechnical and Geoenvironmental Engineering, 131(6): 762–770

Yang, Z., Elgamal, A., and Parra, E. (2003). "Computational model for cyclic mobility and associated shear deformation." Journal of Geotechnical and Geoenvironmental Engineering, ASCE, 129(12): 1119–1127

Yang, Z., Ge, X., Still, B., and Paris, A. (2012). Frozen Soil Lateral Resistance for the Seismic Design of Highway Bridge Foundations. Draft Final Report, prepared for Alaska University Transportation Center and the State of Alaska Department of Transportation and Public Facilities, Dept. of Civil Engineering, University of Alaska Anchorage.

Yang, Z., Li, Q., Horazdovsky, J., Hulsey, J.L., and Marx, E. (2012). "Analysis of laterally loaded piles in frozen soils." State of the Art and Practice in Geotechnical Engineering (GeoCongress2012), Geotechnical Special Publication No. 225, 215–224.

Yao, S., Kobayashi, K., Yoshida, N., and Matsuo, H. (2004). "Interactive behavior of soil-pile-superstructure system in transient state to liquefaction by means of large shake table tests." Soil Dynamics and Earthquake Engineering, 24: 397–409.

Youd, T.L., Hansen, M.C. and Bartlett, F.S. (2002). "Revised multilinear regression equations for prediction of lateral spread displacement." ASCE J. of Geotech. and Geoenvironmental Engrg., Vol. 128, No. 12: 1007-1017

Zha, J. (2005). "Lateral spreading forces on bridge piles." Workshop on Piles in Liquefied and Lateral Spreading Ground, March 16–18, Davis, California.

Zhang, Yu (2009). "An investigation on cyclic resistance and dynamic characteristics of Mabel Creek silt." Ph.D. Dissertation, University of Alaska Fairbanks, Nov.

Zhang, X., Yang, Z., and Li, Q. (2012). "Analysis of laterally loaded piles in liquefiable soils with a frozen crust using *p-y* approach." Cold Regions Engineering 2012: Sustainable Infrastructure Development in a Challenging Cold Environment (Proc. 15th Int'l Specialty Conf. Cold Regions Engineering), eds. Brian Morse and Guy Dore, 456–466.

Zhu, Y., and Carbee, D.L. (1983). "Uniaxial compressive strength of frozen silt under constant deformation rates." Cold Regions Science and Technology, 9: 3–15.

APPENDIX

This appendix presents the geotechnical, topographical, and seismic investigation data for the Brotherhood Bridge site in Juneau, Alaska.

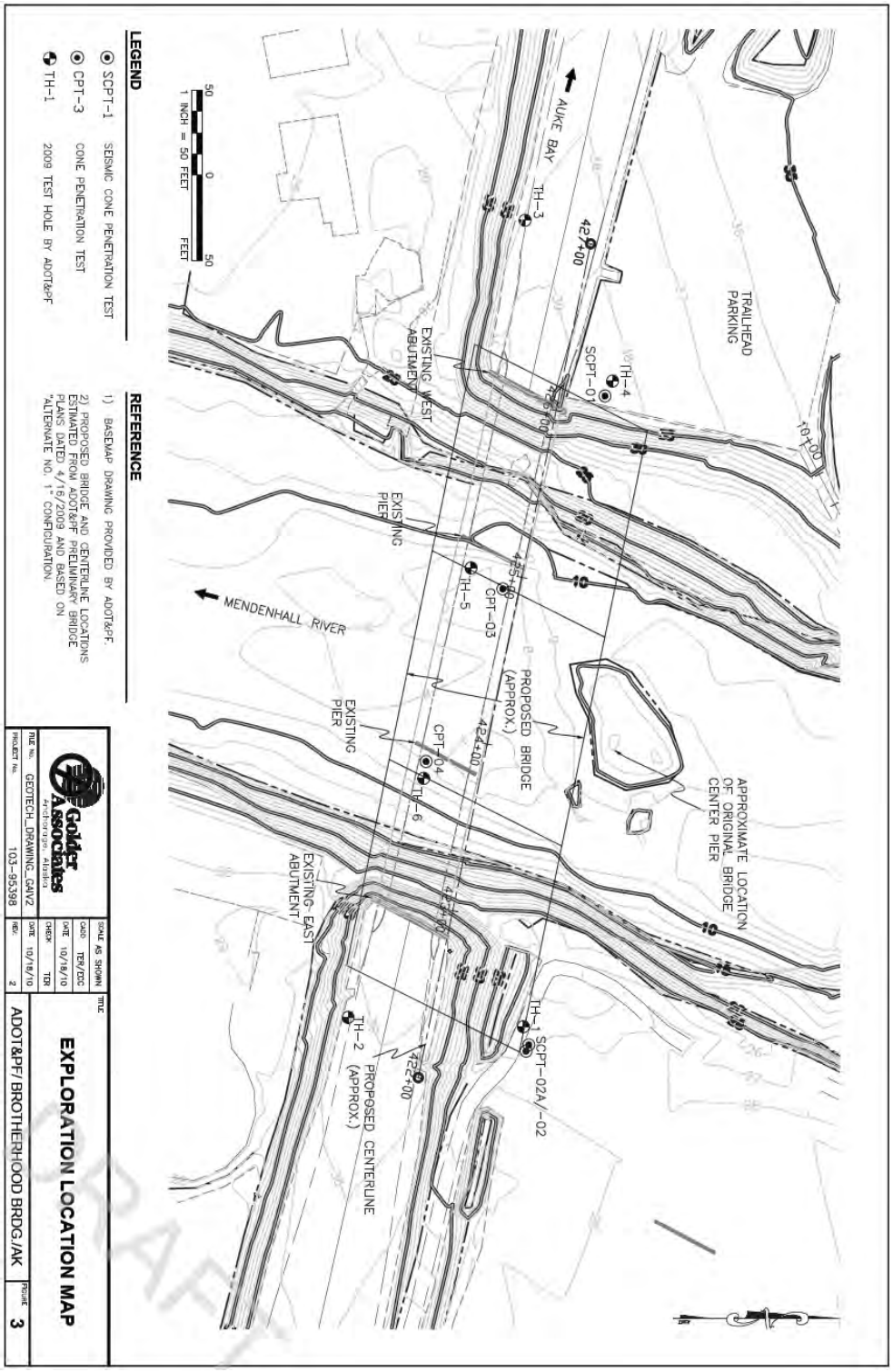

Figure A. 1. Exploration location map (Golder Associates, Inc. 2010)

Figure A. 2. SPT blow count corrections and liquefaction potential (Golder Associates, Inc. 2010)

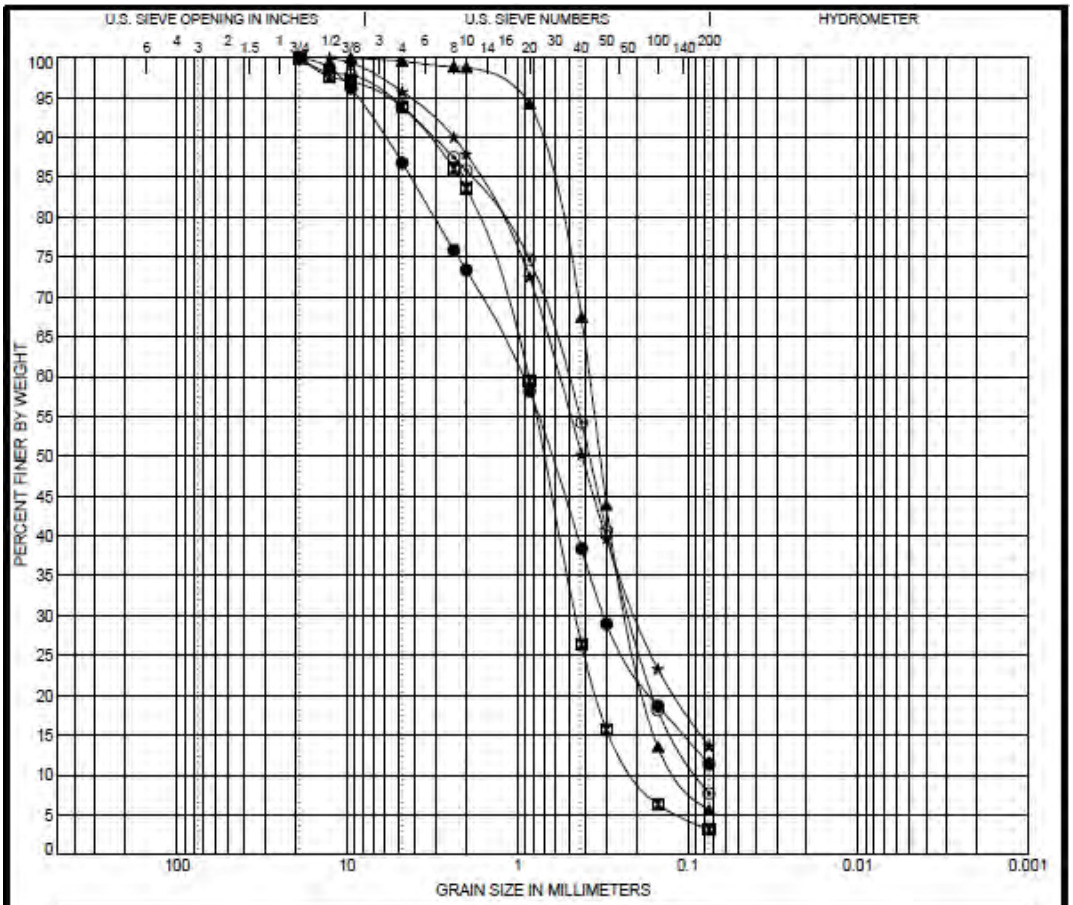

Sample # / Depth	Lab #	USCS Classification	%Org	% MC	SpG	LL	PL	PI
● TH-1-10 39.0	09C-298	WELL-GRADED SAND with SILT(SW-SM)		14.8		NV	NP	NP
⊠ TH-1-11 44.0	09C-299	POORLY GRADED SAND(SP)		16.2		NV	NP	NP
▲ TH-1-12 49.0	09C-300	POORLY GRADED SAND with SILT(SP-SM)		19.1		NV	NP	NP
★ TH-1-13 54.0	09C-301	SILTY SAND(SM)		15.9		NV	NP	NP
⊙ TH-1-14 59.0	09C-302	POORLY GRADED SAND with SILT(SP-SM)		13.4		NV	NP	NP

Sample # / Depth	Cc	Cu	D100	D60	D30	D10	%Gravel	%Sand	%Silt	%Clay	Frost Susceptible Soils (% finer 0.02mm)
● TH-1-10 39.0	1.57	14.29	19	0.94	0.311		13.2	75.5	11.4		
⊠ TH-1-11 44.0	1.21	4.40	19	0.864	0.453	0.197	6.2	90.6	3.2		
▲ TH-1-12 49.0	1.15	3.44	9.5	0.377	0.218	0.11	0.4	93.9	5.7		
★ TH-1-13 54.0			12.7	0.571	0.199		4.2	82.1	13.7		
⊙ TH-1-14 59.0	1.04	5.87	19	0.512	0.216	0.087	6.0	86.3	7.7		

Alaska D.O.T./P.F. Southeast Region
6860 Glacier Hwy.
Juneau, Ak 99801-7999
Telephone: (907) 465-4454
Fax: (907) 465-3506

SUBSURFACE DATA:: Results of Laboratory Testing Sheet 3 of 29

Location: Juneau

Project: Brotherhood Bridge Widening

Number: 67987

Figure A. 3. Particle size distribution – 1(State of Alaska Department of Transportation and Public Facilities 2010)

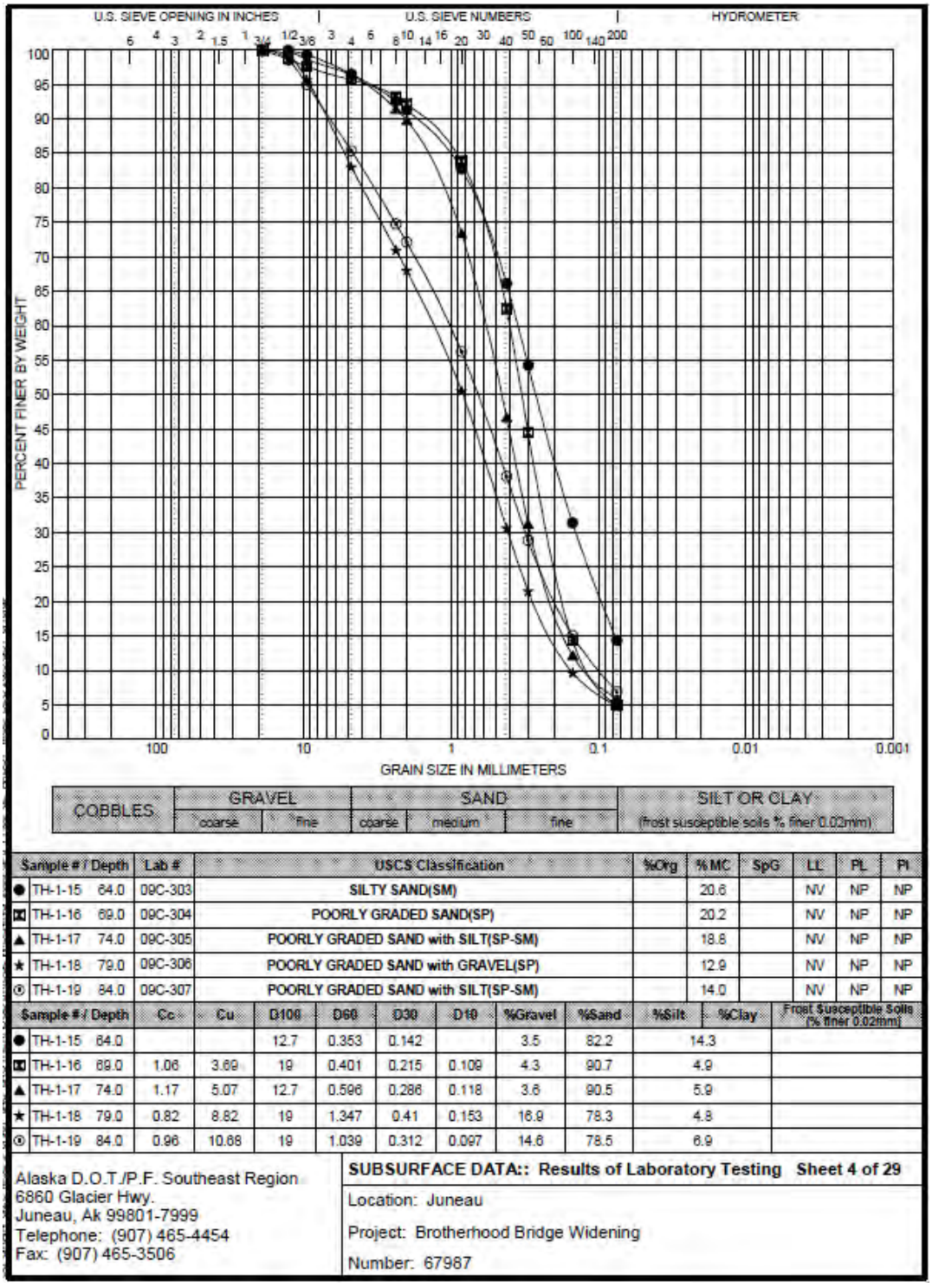

Sample # / Depth	Lab #	USCS Classification	%Org	% MC	SpG	LL	PL	PI
● TH-1-15 64.0	09C-303	SILTY SAND(SM)		20.6		NV	NP	NP
⊠ TH-1-16 69.0	09C-304	POORLY GRADED SAND(SP)		20.2		NV	NP	NP
▲ TH-1-17 74.0	09C-305	POORLY GRADED SAND with SILT(SP-SM)		18.8		NV	NP	NP
★ TH-1-18 79.0	09C-306	POORLY GRADED SAND with GRAVEL(SP)		12.9		NV	NP	NP
⊙ TH-1-19 84.0	09C-307	POORLY GRADED SAND with SILT(SP-SM)		14.0		NV	NP	NP

Sample # / Depth	Cc	Cu	D100	D60	D30	D10	%Gravel	%Sand	%Silt	%Clay	Frost Susceptible Soils (% finer 0.02mm)
● TH-1-15 64.0			12.7	0.353	0.142		3.5	82.2	14.3		
⊠ TH-1-16 69.0	1.06	3.69	19	0.401	0.215	0.109	4.3	90.7	4.9		
▲ TH-1-17 74.0	1.17	5.07	12.7	0.596	0.286	0.118	3.6	90.5	5.9		
★ TH-1-18 79.0	0.82	8.82	19	1.347	0.41	0.153	16.9	78.3	4.8		
⊙ TH-1-19 84.0	0.96	10.68	19	1.039	0.312	0.097	14.6	78.5	6.9		

Alaska D.O.T./P.F. Southeast Region
6860 Glacier Hwy.
Juneau, Ak 99801-7999
Telephone: (907) 465-4454
Fax: (907) 465-3506

SUBSURFACE DATA:: Results of Laboratory Testing **Sheet 4 of 29**

Location: Juneau

Project: Brotherhood Bridge Widening

Number: 67987

Figure A. 4. Particle size distribution – 2 (State of Alaska Department of Transportation and Public Facilities 2010)

Table 2
Estimated Fault Geologic and Geometric Characteristics

Fault (Type)	Distance to Site (km)	Rupture Length (km)	Rupture Area (km^2)	Slip Rate (mm/yr)	Range in Maximum Earthquake Magnitude (M_W)	Preferred Maximum Earthquake Magnitude (M_W)
SE Denali (strike-slip)	25	260-330	5,200-6,600	6-8	7.0-8.2	7.8
Fairweather-Queen Charlotte Islands (strike-slip)	135	400- 500	8,000-10,000	44-51	7.0-8.4	8.2

Figure A. 5. Estimated fault geologic and geometric characteristics (Golder Associates, Inc. 2010)